

Nematicity, magnetism and superconductivity in FeSe

Anna E Böhmer[‡]

Ames Laboratory, US DOE, Ames, IA 50011, USA

Andreas Kreisel

Institut für Theoretische Physik, Universität Leipzig, D-04103 Leipzig, Germany

Abstract. Iron-based superconductors are well known for their complex interplay between structure, magnetism and superconductivity. FeSe offers a particularly fascinating example. This material has been intensely discussed because of its extended nematic phase, whose relationship with magnetism is not obvious. Superconductivity in FeSe is highly tunable, with the superconducting transition temperature, T_c , ranging from 8 K in bulk single crystals at ambient pressure to almost 40 K under pressure or in intercalated systems, and to even higher temperatures in thin films. In this topical review, we present an overview of nematicity, magnetism and superconductivity, and discuss the interplay of these phases in FeSe. We focus on bulk FeSe and the effects of physical pressure and chemical substitutions as tuning parameters. The experimental results are discussed in the context of the well-studied iron-pnictide superconductors and interpretations from theoretical approaches are presented.

Contents

1	Introduction	2
1.1	Phase interplay in iron pnictides	2
1.2	FeSe and related systems	5
1.3	Outline	6
2	Nematicity	6
2.1	Orthorhombic lattice distortion	6
2.2	Electronic in-plane anisotropy	8
2.3	Nematic susceptibility	10
2.4	Electronic structure	11

[‡] Now at Institut für Festkörperphysik, Karlsruhe Institute of Technology, D-76021 Karlsruhe, Germany

<i>CONTENTS</i>	2
3 Magnetism	14
3.1 Magnetic fluctuations at ambient pressure	15
3.2 Pressure-temperature phase diagram	16
3.3 Magnetic order under pressure	18
4 Superconductivity	21
5 Effects of chemical substitutions in FeSe	24
6 Theoretical mechanisms	28
6.1 Nematicity and magnetic fluctuations in FeSe	30
6.2 Superconducting pairing in FeSe	32
7 Concluding remarks	35
8 References	36

1. Introduction

Unconventional superconductivity in strongly correlated materials often emerges close to phases characterized by magnetic, structural, orbital, or other types of order. A change of tuning parameters, like external pressure or the chemical composition, can impact these phases and induce transitions between them, resulting in complex phase diagrams. Iron-based superconductors are an ideal platform to study such interacting phases. These intriguing materials feature a complex interplay of high-temperature superconductivity, antiferromagnetic orders, structural distortions and orbital order. The large variety of available materials and suitable tuning parameters offers numerous possibilities for systematic and comparative studies. FeSe represents an unusual and particularly fascinating case of the interplay between structural, magnetic and electronic degrees of freedom.

1.1. Phase interplay in iron pnictides

Two distinctive features of iron-based materials are their complex phase interplay and a surprisingly large chemical variety. After the discovery of superconductivity in F-doped LaFeAsO[1], many related compounds were found. The materials are classified according to their stoichiometry into 1111-type, 122-type, 111-type, etc [2, 3, 4, 5], see Fig. 1 (a). The 122-type material family, with BaFe₂As₂ as its most prominent member, is arguably the most intensively studied. This is likely due to the relative ease of preparation of sizable single crystals and to an impressive variety of chemical substitutions that are capable of inducing superconductivity. These 122-type materials have shaped a picture of 'typical' interplay between orthorhombic distortion, nematicity, magnetism and superconductivity in iron-based materials (Fig. 1(b)), into which other compounds, like NaFeAs[6] or even the structurally very complex 10-3-8 system[7] also

fit well. The phase interplay of FeSe, however, does not seem to follow this pattern in several respects.

As also observed in many other unconventional superconductors, the superconducting instability in iron-based materials typically emerges when antiferromagnetic order is sufficiently reduced by modifying a tuning parameter. The superconducting transition temperature T_c has then a dome-like dependence on this tuning parameter[8]. A particularity of the iron-based materials is that their antiferromagnetism is (with few exceptions) “stripe type”, i.e., it distinguishes two perpendicular in-plane directions. In consequence, magnetic order is intimately coupled to a an orthorhombic lattice distortion, whereas the paramagnetic phase is typically tetragonal. Simultaneous magnetic and structural phase transitions occur, for example, in $(\text{Ba}_{1-x}\text{K}_x)\text{Fe}_2\text{As}_2$ [9] and $\text{Ba}(\text{Fe}_{1-x}\text{Ru}_x)_2\text{As}_2$ [10]. However, in a number of systems, the structural transition at T_s precedes the magnetic transition at T_N by several degrees upon cooling. Prominent examples are Co- or Ni-substituted BaFe_2As_2 [11, 12], LaFeAsO [13] and NaFeAs [6], which thus host a paramagnetic orthorhombic phase. This observation sparked the idea that the structural transition is related to a distinct, “nematic” electronic degree of freedom.

Nematicity has been a central theme in the study of iron-based materials[14]. The term nematic is borrowed from the field of liquid crystals, where it refers to a phase with broken rotational but preserved translational symmetry[15]. In the context of iron-based superconductors, “nematicity” and “nematic order” is often used synonymously to in-plane anisotropy, which means reduced rotational symmetry with respect to the tetragonal high-temperature phase. This electronic a - b anisotropy can be observed in various experiments, including electronic transport [16], optical reflectivity [17], angular-resolved photoemission spectroscopy (ARPES) [18], scanning tunneling microscopy (STM) [19], nuclear magnetic resonance (NMR) [20] and inelastic neutron scattering [21]. In general, a macroscopic crystal forms fine scale structural twins below T_s [22] such that the macroscopic response of the crystal is isotropic. In order to study the in-plane anisotropy associated with the nematic phase by macroscopic probes, samples need to be detwinned. Detwinning is often accomplished by the application of uniaxial stress [23]. Microscopic or local probes like NMR, ARPES, diffraction, or STM can resolve the domain structure or detect signals from the two types of domains separately without the need for detwinning.

By symmetry, all properties—be they structural, orbital or magnetic—acquire in-plane anisotropy in the orthorhombic phase, which complicates the determination of the microscopic origin of nematicity in iron-based materials[14]. This question may therefore only be solved by a combination of experiment and microscopic theories. Despite the separation of T_s and T_N , the two transitions follow each other rather closely as function of tuning parameters in most systems, suggesting their intimate coupling. Notably, the intensity of magnetic fluctuations in NMR[24, 25], as well as the spin-spin correlation length measured by neutron scattering[26] increase below T_s . Reciprocally, the magnitude of structural distortion increases below T_N [27]. This close coupling between structure and magnetism supports the idea that nematicity may be

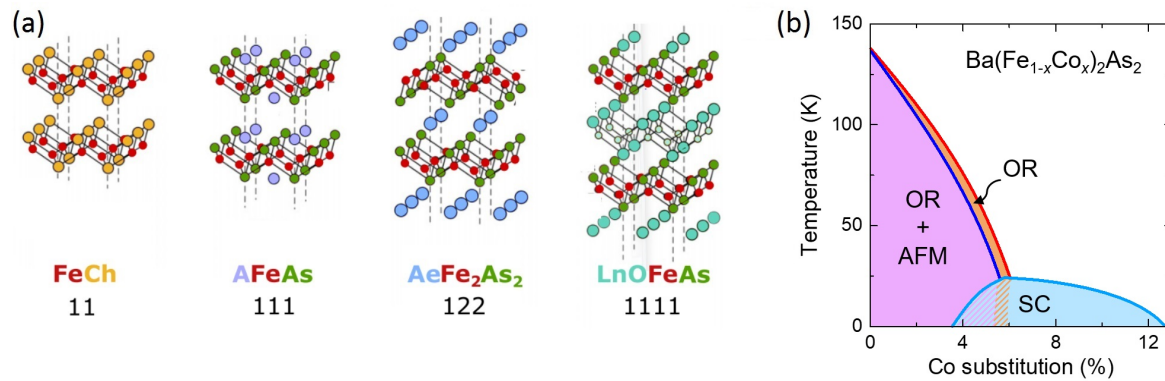


Figure 1. Crystal structures and typical phase diagram of iron-based superconductors. (a) Atomic structure of the four most common iron-based material families. In the 11-system, the chalcogenide atom Ch can be S, Se or Te. Representatives of the 111-type material family are LiFeAs and NaFeAs. In the 122-systems $AeFe_2As_2$, Ae stands for Ca, Sr, Ba or Eu. Numerous substitution series (e.g., Co, Ni, Ru, Rh, Pd, Pt or Ir for Fe; Na, K, Rb for A; or P for As) display superconductivity. In the 1111-system, Ln stands for a lanthanide ion, $Ln=La, Pr, Nd, Sm, Gd$ or Tb and a similarly wide variety of substitutions induces superconductivity. Partial substitution of O with F or H are particularly common. Reproduced with permission from [31]. © 2017 Wiley-VCH Verlag GmbH & Co. KGaA, Weinheim. (b) A schematic phase diagram of Co-substituted $BaFe_2As_2$, featuring an, orthorhombic (OR) and paramagnetic (nematic) region (orange), an orthorhombic and antiferromagnetic (AFM) region (rose) and a superconducting (SC) dome (blue).

consequence of magnetic interactions even when nematic order precedes magnetic order. In this so-called spin-nematic scenario [15], it is pointed out that stripe-type correlations between magnetic moments distinguish a direction in which the moments are primarily parallel from a direction in which they are antiparallel. These correlations, which break the tetragonal symmetry, can be long-range even if the magnetic moments themselves are not ordered. Thus, in this scenario, the tetragonal-to-orthorhombic transition can be induced by magnetic fluctuations at a temperature $T_s > T_N$.

Superconductivity is observed when the structural and magnetic transitions are sufficiently suppressed by a chemical substitution or pressure. It often coexists and competes with these phases in a part of the phase diagram (see Fig. 1(b)), as shown by a significant decrease in magnetic and structural (nematic) order parameters below T_c [28, 29]. Superconductivity is likely mediated by magnetic fluctuations [30].

Thus, in the general picture of phase interplay in iron-based materials, a stripe-type antiferromagnetic phase is intimately coupled to a nematic phase characterized by a sizable electronic a - b anisotropy and a structural orthorhombic distortion. Superconductivity competes with both nematic and magnetic order.

1.2. FeSe and related systems

FeSe is highly interesting in the context of phase interplay in iron-based materials because it hosts apparently very unusual interrelations between nematicity, magnetism and superconductivity. Bulk FeSe undergoes a tetragonal-to-orthorhombic transition at $T_s \approx 90$ K [32, 33, 34] similarly to the “nematic” transition of many other iron-based parent materials. However, no magnetic order is formed at ambient pressure [34, 35] and FeSe is superconducting below ~ 8 K [32]. Under the application of pressure, T_s decreases [36], a magnetically ordered phase emerges at ~ 1 GPa [35, 37] and T_c increases dramatically to a maximum of ≈ 37 K [38, 39, 40, 41, 42, 43] at ~ 6 GPa.

Chemical substitutions can be seen as tuning parameters for bulk FeSe having partially similar effects as external pressure. Te or S substitution for Se are most commonly studied [44]. The endmembers of these solid solutions, FeTe and FeS, are interesting materials in themselves [45, 46]. The structurally analogous $\text{FeTe}_{0.8}\text{S}_{0.2}$ material can even be tuned to superconductivity by simmering in alcoholic beverages [47]. Intercalation of FeSe is possible with various elements and molecules [48, 49] leading to an enhancement of T_c up to ~ 45 K. In addition, the superconducting phase in the K-Fe-Se system appears to be closely related and may be viewed as K-intercalated FeSe [50]. Finally, thin films of FeSe are an intriguing topic. The single-layer FeSe on SrTiO_3 [51, 52, 53] has surprised with the highest T_c of all iron-based materials, possibly reaching over 100 K [54]. Multilayer thin films, on the other hand, seem to have ‘conventional’ properties and resemble bulk FeSe [55].

Superconductivity in the layered PbO-type structure of FeSe (space group $P4/nmm$) was reported in 2008 [32] just two months after the report of superconductivity in the 122-type systems. However, the complex phase interplay in FeSe was only gradually revealed during the subsequent years. This is primarily due to difficulties in obtaining phase-pure and high-quality single crystals. Single-crystal growth of FeSe is made difficult by the complex binary Fe-Se composition-temperature phase diagram [56]. In particular, the superconducting tetragonal PbO-type and near-stoichiometric phase of FeSe has only a very narrow range of stability and undergoes a transformation to a hexagonal NiAs-type phase on warming above 457°C . In consequence, any preparation procedure above this temperature results in samples that have not formed in the tetragonal phase. They often have hexagonal morphology and consist of a mix of tetragonal and hexagonal phases [57], which inevitably leads to internal strains.

Early studies of FeSe used polycrystalline material prepared by solid state synthesis [32, 38, 58, 59, 40, 60], containing the hexagonal NiAs-type impurity phase. Furthermore, the tetragonal FeSe phase has a finite width of formation and the superconducting transition temperature is very sensitive to the exact stoichiometry [59]. Many early studies were performed on such polycrystalline, multi-phase material. There are also several early studies of the growth of tetragonal FeSe using Cl-salt-based flux techniques [61, 57, 62] and chemical vapor transport [63, 64]. A breakthrough came with the use of a eutectic mix of KCl and AlCl_3 salts with low melting temperature to

obtain FeSe directly in its tetragonal phase below 450°C [65, 66, 67]. This significantly improved the crystal quality, as shown by an up to ten-fold increase in residual resistivity ratio with respect to previously available samples [68]. A technique for flux-free growth of large crystals with preferential orientation is described in Ref. [69].

This topical review focuses on recent work using this 'new-generation' single crystals of FeSe and only occasionally refers to earlier results.

1.3. Outline

Early studies on iron-chalcogenide superconductors have been reviewed in Refs. [70, 71, 47, 72, 73]. Recently, the electronic structure of FeSe-related compounds has been reviewed in Refs. [74] (with a focus on the single-layer materials) and [75, 76]. The monolayer thin films are furthermore subject of the reviews [51, 52, 53].

This topical review discusses nematicity, magnetism and superconductivity and the interplay of these phases in bulk FeSe. The orthorhombic/nematic phase of FeSe at ambient pressure, which has received a lot of attention, is described in section 2. Magnetic fluctuations and the pressure-induced magnetic order are reviewed in section 3 and superconductivity is discussed in section 4. Chemically substituted FeSe is briefly discussed in section 5. The observed unusual interplay between structure, magnetism and superconductivity in FeSe has inspired a variety of theories, which will be reviewed in section 6. Furthermore, the theory of superconducting pairing in FeSe will be discussed in section 6. A summary and a comparison between FeSe and the archetypal 122-type iron-based systems will conclude this topical review.

2. Nematicity

FeSe undergoes a tetragonal-to-orthorhombic phase transition similarly to other iron-based systems on decreasing temperature, but, unlike many other iron-based materials, this transition is not followed by magnetic order. Therefore, the orthorhombic phase of FeSe has received great attention as an opportunity to study the purely nematic phase in an iron-based superconductor over a wide temperature range. However, it is still an open question whether nematicity in FeSe is of the same origin as, e.g., in 122-type systems.

2.1. Orthorhombic lattice distortion

The tetragonal-to-orthorhombic structural transition at T_s in FeSe was observed already at the time of the discovery of superconductivity in the material [32, 33] (Fig. 2 a). The structural deformation is analogous to the ubiquitous tetragonal-to-orthorhombic distortion in many 1111-, 122-, and 111-type iron-based materials. The nearest-neighbor Fe-Fe distances a and b – directed along the in-plane diagonal of the tetragonal unit cell – become inequivalent, resulting in a doubling and rotation of the tetragonal unit cell in the basal plane. The Fe-Se bond-lengths are not affected (Fig. 2 b).

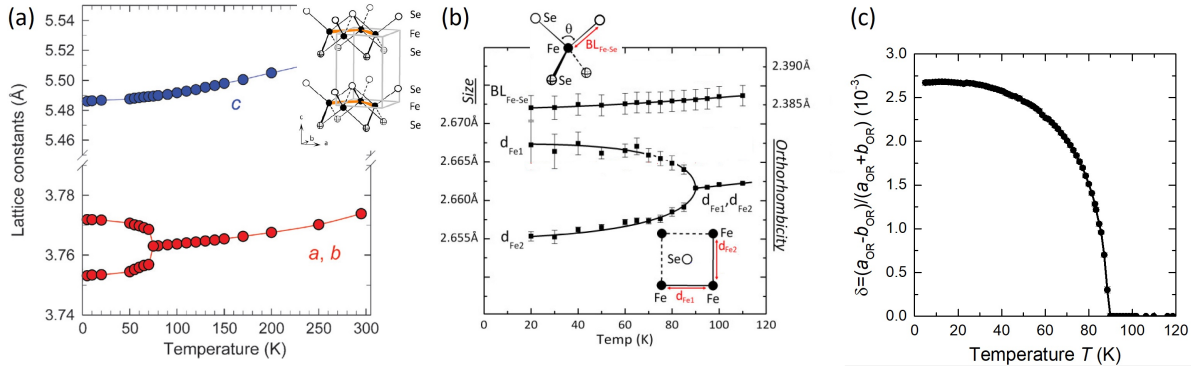


Figure 2. Temperature-dependent structural parameters of FeSe. (a) Temperature-dependent lattice parameters a , b and c of FeSe showing the tetragonal-to-orthorhombic transition in an early measurement using polycrystalline FeSe. (b) Fe-Se bond length and Fe-Fe distances as a function of temperature for a polycrystalline sample. Only the Fe-Fe distances are affected by the structural transition. (c) Temperature dependence of the orthorhombic distortion $\delta = (a - b)/(a + b)$ from high-energy x-ray diffraction on a single crystal. (a) Reproduced from Ref. [33] with permission of The Royal Society of Chemistry. (b) Reproduced with permission from [34], copyright 2009 American Physical Society. (c) Adapted from Ref. [77], licensed under a Creative Commons Attribution 4.0 International License.

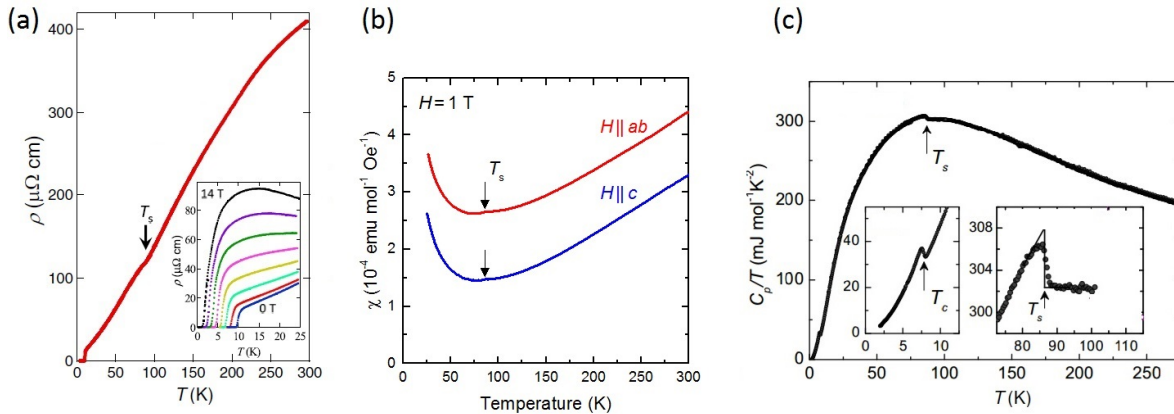


Figure 3. Signatures of the structural transition in standard transport and thermodynamic probes. (a) Resistivity of a high-quality FeSe single crystal with high residual resistivity ratio. The magneto-resistance reaches large values at low temperatures (inset). (b) Uniform magnetic susceptibility of an FeSe single crystal for revealing a subtle downward kink at T_s for both in-plane and out-of-plane external magnetic field[78]. (c) Heat capacity divided by temperature of an FeSe single crystal. Insets show magnification of the data close to T_s and T_c revealing clear second-order phase transitions. (a) Reproduced from Ref. [68]. (c) Reproduced with permission from Ref. [79], copyright 2015 American Physical Society.

The temperature dependence of the orthorhombic distortion $\delta = (a - b)/(a + b)$ indicates a continuous (second-order) phase transition at $T_s = 90$ K. At low temperatures, $\delta \approx 2.7 \times 10^{-3}$ [77] (see Fig. 2c). This value is very similar to the orthorhombic distortion of BaFe_2As_2 ($\delta(T = 0) = 4 \times 10^{-3}$ [80]) when accounting for the different transition temperature, $T_s \approx 140$ K. In fact, the ratio $\delta(T = 0)/T_s$ is practically identical in the two systems. Intriguingly, the onset of superconductivity does not measurably change the orthorhombic distortion (Fig. 2c), in strong contrast to 122-type iron-based superconductors[66].

The structural transition of FeSe is also visible in standard transport and thermodynamic probes (Fig. 3). Resistivity shows a slight upward kink on decreasing temperature through T_s . This anomaly is more pronounced in single crystals and was sometimes overlooked in polycrystalline material. The uniform magnetic susceptibility has a slight downward kink at T_s . The specific heat shows a clear second-order type jump at T_s of $\Delta C_p/T_s \approx 6$ mJ mol⁻¹ K⁻²[79, 81], as expected for a continuous phase transition. Interestingly, the size of the specific-heat anomaly is very similar to the low-temperature Sommerfeld coefficient of $\sim 6 - 7$ mJ mol⁻¹, suggesting an electronic phase transition[81].

2.2. Electronic in-plane anisotropy

The observation of a large in-plane resistivity anisotropy in detwinned samples of Co-doped BaFe_2As_2 [84, 16] was a starting point for the investigation of electronic nematicity in the iron-based systems. FeSe single crystals are easily damaged by uniaxial force, which makes the mechanical detwinning necessary for a measurement of this in-plane anisotropy difficult. Only measurements of the resistivity anisotropy under tensile uniaxial stress in a 'horseshoe device' have succeeded so far[82] (Fig. 4 (a),(b)). A small resistivity anisotropy with $\rho_a > \rho_b$ was found. The sign of $\rho_a - \rho_b$ is opposite to (electron-doped) BaFe_2As_2 . Furthermore, a significant fraction of the observed anisotropy was shown to be induced by the applied uniaxial stress. Subtraction of this elastoresistive effect from the measured $\rho_a - \rho_b$ indicates an anisotropy of $\rho_a - \rho_b \leq 3 \mu\Omega\text{cm}$ in the limit of zero external force, which is only about 4% of the in-plane average resistivity; a small value compared to $\text{Ba}(\text{Fe}_{1-x}\text{Co}_x)_2\text{As}_2$ [85] (Fig. 4 (c)).

Nuclear magnetic resonance (NMR) as a local probe allows to distinctly study the two types of orthorhombic domains[20] without the need for detwinning. ⁷⁷Se is an NMR active nucleus and ⁷⁷Se NMR has played an important role in the study of FeSe [86, 87, 42, 79, 83, 88, 89]. Under a given direction of in-plane applied magnetic field, the two types of orthorhombic domains show distinctly different NMR spectral shifts, \mathcal{K} . This difference, $\Delta\mathcal{K}$ arises because the magnetic field is directed along the a -axis of one type and along the b -axis of the other type of domains [79, 83, 89] [Fig. 4 (d-f)]. The value of the NMR spectral shift (Knight shift) is determined by the local magnetic susceptibility at the Se site and the hyperfine coupling constant. In Ref. [83], it was argued that the observed significant line splitting cannot be a

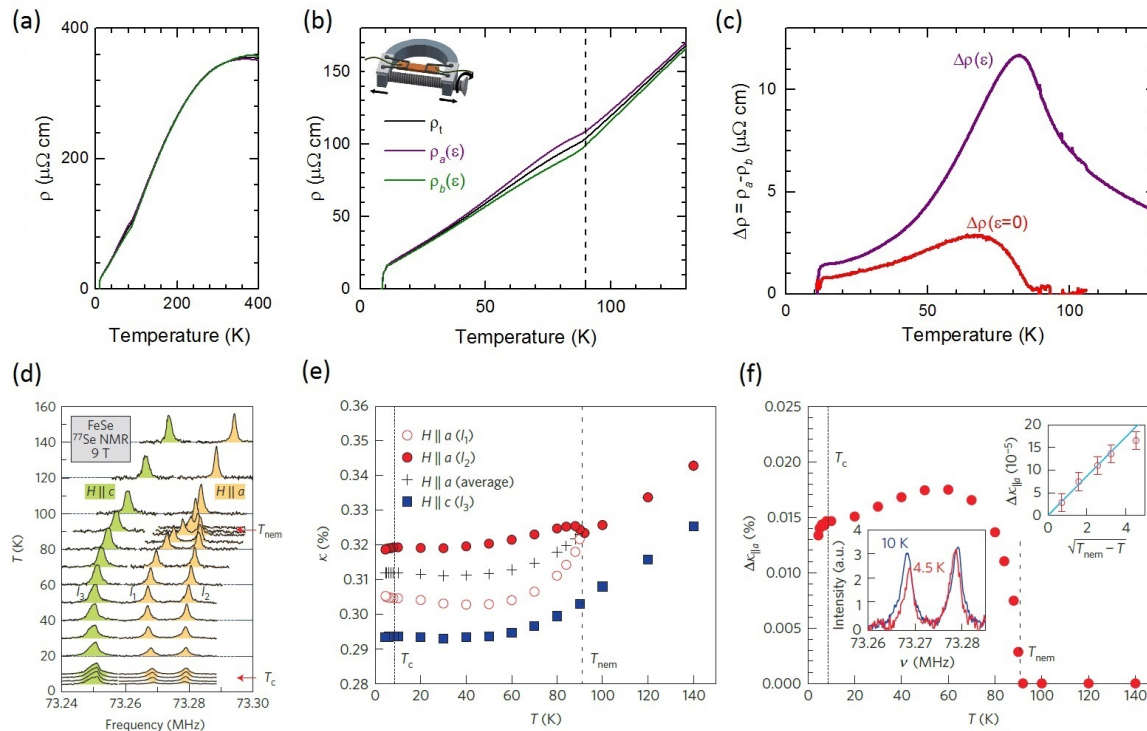


Figure 4. In-plane anisotropy of electronic properties of FeSe. (a), (b) In-plane resistivity of twinned (ρ_t) and detwinned (ρ_a , ρ_b) FeSe. Samples were detwinned by applying tensile strain, ε , via a 'horseshoe device' [inset in (b)], and ρ_b was calculated from the two measurements[82]. (c) The measured resistivity anisotropy $\Delta\rho = \rho_a - \rho_b$ at finite applied strain (purple line) consists of an 'intrinsic' a - b anisotropy of $\leq 3 \mu\Omega\text{cm}$ (red line) and a larger strain-induced contribution [82]. (d) NMR spectra of an FeSe single crystal, revealing a significant different NMR spectral shift for the two types of orthorhombic domains below T_s for a given field direction as a line splitting. (e) Temperature dependent NMR spectral shift. (f) The difference of the two in-plane NMR lines, showing an order-parameter-like temperature dependence close to T_s and a slight decrease below T_c [83]. (a)-(c) Reproduced with permission from Ref. [82], copyright 2016 American Physical Society. (d)-(f) Reprinted by permission from Macmillan Publishers Ltd: Nature Materials, Ref. [83], copyright 2015.

'simple' consequence changing atomic distances following the small orthorhombic lattice distortion. Moreover, $\Delta\mathcal{K}$ decreases below the superconducting transition, in contrast to the structural distortion. For these reasons, the anisotropy $\Delta\mathcal{K}$ has been associated with an electronic nematic order parameter[83]. From the absence of a strong response of spin fluctuations to the nematic transition, it was argued that nematicity in FeSe is likely of orbital origin[83]. In Ref. [79], it was shown that the signature of spin fluctuations in NMR sets in at T_s , but is absent at higher temperatures. From this observation, the driving force of the structural transition in FeSe was also argued to be non-magnetic. However, later inelastic neutron scattering showed the presence of magnetic fluctuations at all temperatures (see section 3), as well as a feedback effect between spin-fluctuations and orthorhombic distortion[90, 91], indicating that nematicity in FeSe may have an intimate relation with magnetism after all.

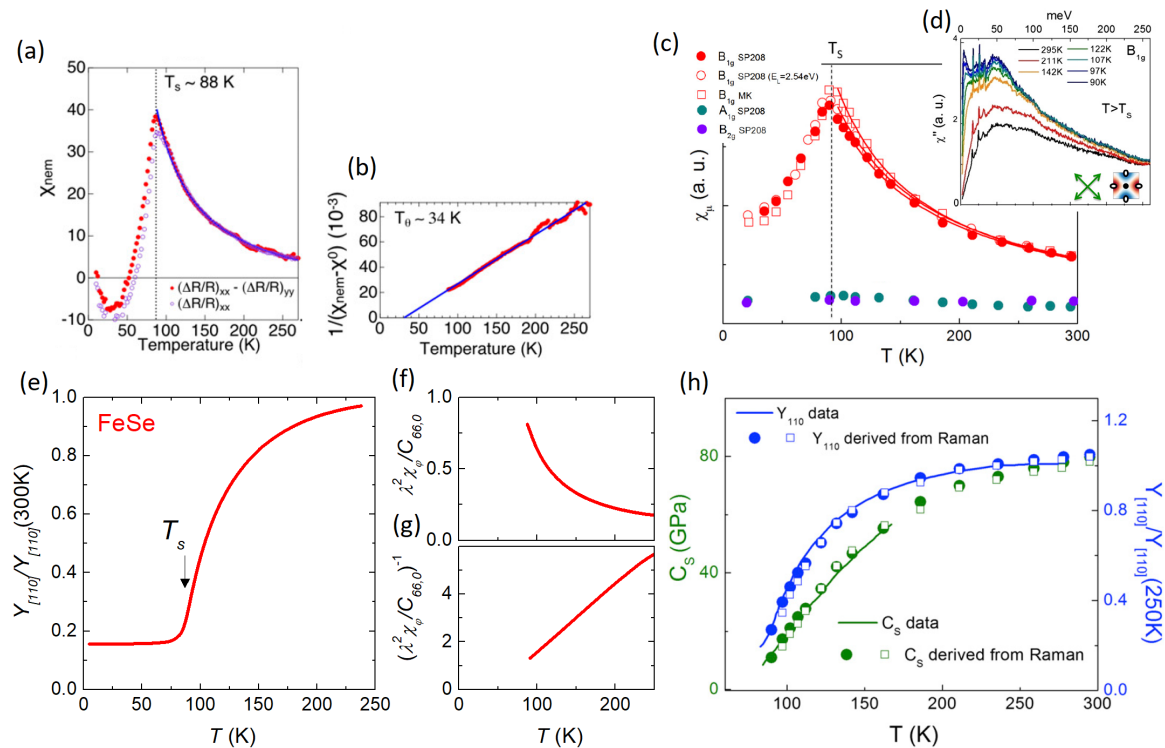


Figure 5. Nematic susceptibility of FeSe. (a) Nematic susceptibility χ_{nem} of FeSe as measured by the elastoresistivity coefficient m_{66} and (b), a Curie-Weiss plot of the same quantity[95]. (c) Charge nematic susceptibility from electronic Raman scattering, diverging on approaching T_s [96]. (d) shows the a selection of the corresponding Raman spectra. (e) Normalized Young's modulus $Y_{[110]}$ of FeSe, dominated by the elastic shear modulus C_s , obtained by three-point bending[97]. Assuming the existence of a distinct nematic order parameter, the nematic susceptibility can be inferred from the shear modulus as $C_s/C_{s,0} = 1 - \lambda^2 \chi_{\text{nem}}$ ($C_{s,0}$ is bare value of the shear modulus and λ is a coupling constant), and is shown in (f), (g). (h) Under the same assumption, the charge nematic susceptibility in (c) is perfectly consistent with $Y_{[110]}$ and C_s [96]. (a), (b) Reproduced from Ref. [95]. (c), (d), (h) Reproduced from Ref. [96]. (e)-(g) Adapted from Ref. [97].

The electronic in-plane anisotropy of FeSe was also revealed and studied using optical methods, namely in the optical reflectivity in the mid-infrared spectral range[92], in the optical birefringence [82], and in polarized ultrafast spectroscopy in a pump-probe experiment [93]. Recently, the in-plane anisotropy in the nematic state and associated fluctuations were studied using resistance, uniform magnetic susceptibility and magnetostriction measurements of single crystals strained via a substrate [94].

2.3. Nematic susceptibility

The nematic susceptibility has been one of the key properties in the study of iron-based systems. This quantity describes the tendency of the material to develop a - b anisotropy under uniaxial strain. It can be determined as the in-plane anisotropy of a physical

quantity, e.g., resistivity, that is induced by elastic deformation of the sample [98]. The nematic susceptibility defined in this way tends to a divergence at a temperature $T_0 < T_s$, which would be the nematic transition in the absence of the coupling to the crystal lattice. The “real” nematic susceptibility, however, is renormalized by this coupling to the lattice so that it diverges as expected when nematic order sets in at T_s [98, 97].

The elastoresistivity coefficient, $2m_{66} = \frac{1}{\rho} \frac{d(\Delta\rho)}{d(\varepsilon_a - \varepsilon_b)}$, describes the relative change of the resistance anisotropy $\Delta\rho = \rho_a - \rho_b$ with respect to orthorhombic strain and is frequently used as a measure of the nematic susceptibility[98, 99, 100]. It is found to diverge upon approaching T_s in FeSe [101, 95, 82] [Fig. 5(a),(b)], consistent with an electronically driven nematic transition. The magnitude of $2m_{66}$ is comparable to BaFe₂As₂ in two reports[82, 95] but its sign is opposite to BaFe₂As₂. The temperature dependence of $2m_{66}$ follows approximately a Curie-Weiss law $\sim \frac{1}{T-T_0}$ and the inferred Curie temperature T_0 ranges from 34 K to 83 K in the different reports [101, 95, 82].

The elastic shear modulus related to the structural transition of FeSe, C_s , softens (decreases) significantly on approaching T_s from above [102, 79], Fig. 5(e). This is expected for a second order structural transition regardless of its origin. In the case of an electronic nematic phase transition, the bare shear modulus $C_{s,0}$ is renormalized by the nematic susceptibility χ_{nem} , according to $C_s = C_{s,0} - \lambda^2 \chi_{\text{nem}}$ [103, 104]. The inferred χ_{nem} follows a perfect Curie-Weiss law and is consistent with the elastoresistivity measurements (Fig. 5(f),(g)).

The electronic charge susceptibility in the symmetry channel that is associated with the nematic transition can be obtained from electronic Raman scattering [105, 106] (Fig. 5(d)). Notably, the thus inferred nematic susceptibility of FeSe, χ_{B1g} , also shows a clear divergence [96] (Fig. 5(c)). The χ_{B1g} -data can be used to explain the elastic shear modulus via $C_s = C_{s,0} - \lambda^2 \chi_{\text{nem}}$. The experimental data[102, 79, 96] are in perfect agreement (Fig. 5(h)), which has been interpreted as evidence for charge-induced nematicity in FeSe[96].

2.4. Electronic structure

The electronic structure of FeSe is complex and has been studied in detail via magnetotransport, quantum oscillations, ARPES and STM. The magneto-resistance of FeSe increases sharply below T_s [110, 111]. Detailed analysis of magneto-transport data in multiband models indicates the reduction of total carrier density and the emergence of a small number of high-mobility carriers[110, 112, 113, 114, 115, 116] in the orthorhombic phase.

A number of ARPES studies have investigated the electronic structure of FeSe in great detail and have recently been reviewed in [74, 75, 76]. Here, a short summary is presented, with a focus on the changes of the electronic structure related to the nematic transition (Fig. 6).

The electronic structure of FeSe is broadly similar to other iron-based

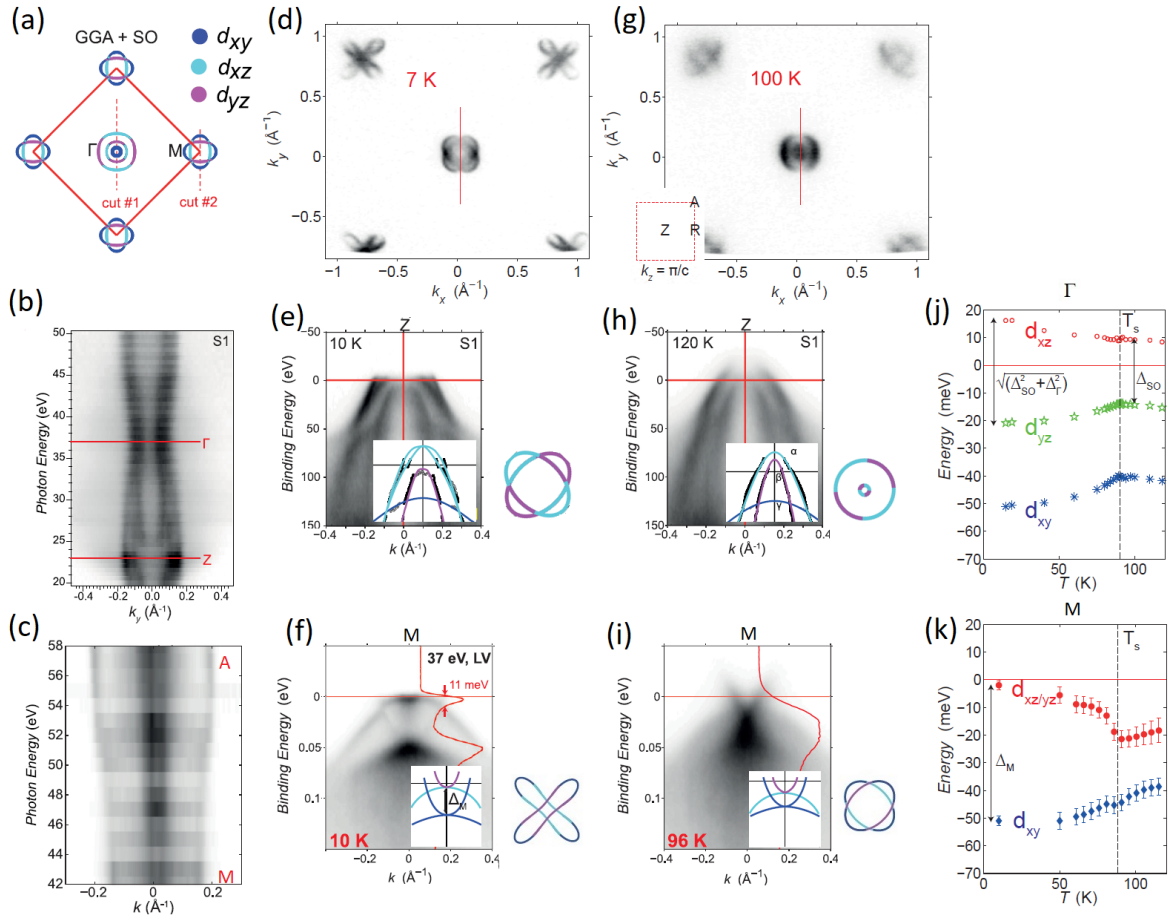


Figure 6. High-resolution ARPES data on twinned FeSe[101, 107, 76]. (a) Fermi surfaces according to DFT calculations predict hole cylinders around the zone center and electron cylinders in the zone corners with orbital contents as indicated. (b), (c) Measured k_z dispersion of the Fermi surface cylinders close to the zone center and the zone corner, respectively. (d)-(f) Fermi surface map and cuts across the Z and M points above T_s . A schematic representation of the dispersions and the Fermi surfaces are indicated. (g)-(i) Fermi surface map and cuts across the Z and M points below T_s . A schematic representation of the dispersions and the Fermi surfaces are indicated. Two ellipses corresponding to two types of orthorhombic domains are visible. (j) Temperature dependence of the position of d_{xz} , d_{yz} and d_{xy} bands at the Γ point. The splitting between the bands of d_{xz} and d_{yz} character above T_s arises from spin-orbit coupling. (k) Temperature dependence of the position of d_{xz} , d_{yz} and d_{xy} bands at the M point. No splitting between d_{xz} and d_{yz} is resolved. (a), (b), (e), (h) Reproduced with permission from Ref. [101], copyright 2015 American Physical Society. (c), (d), (f), (g), (i), (k) Reproduced from Ref. [107], Creative Commons Attribution 3.0 licence. (j) Reproduced with permission from Ref. [76].

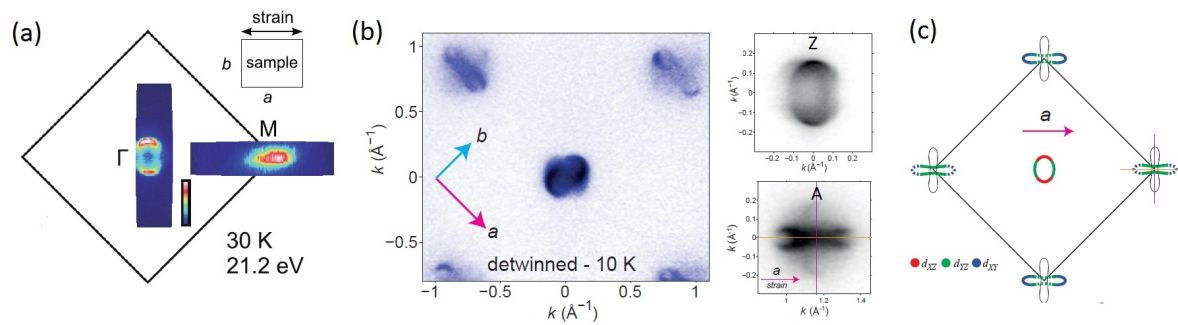


Figure 7. ARPES data on detwinned FeSe (a) Low-temperature Fermi surface map obtained by ARPES on detwinned crystals of FeSe, showing hole and electron pockets elongated in opposite directions. The schematic drawing illustrates the orientation of the sample axes with respect to the applied strain. (b) High-resolution Fermi surface map of $\sim 80\%$ detwinned FeSe and details around the hole and electron pockets. Most surprisingly, a selection rule appears to prevent observation of one of the two “peanut”-shaped pockets in the zone corner. (c) Schematic illustration of the Fermi surface of the majority domain (colored lines, indicating orbital content) and contribution of the minority domain (thin black line). (a) Reproduced with permission from Ref. [108], copyright 2015 American Physical Society. (b), (c) Reproduced from Ref. [109], Creative Commons Attribution 3.0 licence.

superconductors and the Fermi surface consists of quasi two-dimensional hole cylinders around the Brillouin zone center and electron cylinders around Brillouin zone corners, seen in ARPES (Fig. 6 (b)-(e)). The size of the observed Fermi surfaces is significantly reduced with respect to band-structure calculations in the tetragonal state (Fig. 6(a)), especially at low temperatures[117, 118]. Quantum oscillation measurements [119, 115, 120] are consistent with these results.

Three bands are close to the Fermi level in the Brillouin zone center (Fig. 6(f)). The α -band crosses the Fermi level and forms a hole-type Fermi surface cylinder with a mild k_z dispersion (Fig. 6(b)). The β -band crosses the Fermi level only close to the Z point and thus forms a three-dimensional pocket [101, 121]. The α and β bands are of d_{xz}/d_{yz} character and are split by 20 meV at Γ , via spin-orbit interaction[122, 123]. Additionally, there is a d_{xy} -type γ band lying entirely below the Fermi energy. It displays a particularly strong mass renormalization of ~ 9 .

Close to the Brillouin zone center, there are only subtle changes of the band structure associated with the structural transition. On entering the orthorhombic phase, the splitting between α and β bands increases (Fig. 6(j)) so that the β band is pushed entirely below the Fermi energy. In addition, there is an elliptical distortion of the remaining hole Fermi surface. The superposition of two types of orthorhombic domains leads to the observed crossed ellipses at the center of the Brillouin zone, Fig. 6 (e),(g) [101], though this scenario was questioned in Ref. [75]. Measurements on detwinned crystals (see Fig. 7) have indicated that orbital energy of the d_{xz} orbital is higher than the energy related to the d_{yz} orbital, $E_{xz} > E_{yz}$, in the Brillouin-zone center[108]. The difference was estimated to $\sim 10\text{meV}$ [108] (15 meV in Refs. [107, 124]).

The situation at the Brillouin-zone corner is more complex. Two elliptical, quasi two-dimensional electron pockets are observed at the M-point (Fig. 6 (d), (e), (h), (i)). A large splitting of 50 meV between two bands at the M point at low temperatures was initially associated with the difference between orbital energies E_{xz} and E_{yz} in the orthorhombic phase [125, 126, 101]. This appears consistent with recent data presented in Ref. [127]. This large value of 50 meV, which cannot be reproduced by band-structure calculations of orthorhombic FeSe, has been taken as evidence for the presence of electronic nematic order in the material (e.g., Ref. [125]). The measurements on detwinned crystals indicate that $E_{xz} < E_{yz}$ [125, 108], i.e., the sign of orbital order at the M point is opposite to the Γ -point [108].

New high-resolution data on twinned and detwinned samples along with a reinterpretation of the band splitting at the M point have been reported recently [107, 124, 109]. According to this interpretation, the band splitting of 50 meV at the M point does not arise from nematic order and is present at high temperatures already (Fig. 6 (k)). On the other hand, a splitting between d_{xz} and d_{yz} associated with nematic order of only ~ 10 meV at the lowest temperature was suggested [124]. Notably, it was pointed out in Ref. [124] that this splitting of 10 meV at the M point is entirely consistent with band structure calculations in the orthorhombic state and no additional electronic nematic order is required to explain it. Only the orbital anisotropy at the Brillouin-zone center is not predicted by these calculations. The implication is that the electronic nematic order is of a type that affects only the orbital energies close to the center of the Brillouin zone. A candidate, unidirectional nematic bond ordering, has been proposed in Ref. [107].

The recent high-resolution ARPES measurements on detwinned crystals [109] (Fig. 7(b),(c)) reveal that, as an unexpected dramatic consequence of nematicity, only one of the two crossed “peanut-shaped” electron pockets can be observed when a single orthorhombic domain is studied. It was suggested that this might be due to a selection rule specific to ARPES, whose origin is unknown. Similarly, in recent Bogoliubov quasiparticle interference experiments, only one electron pockets was observed, which was ascribed to a significantly reduced coherence of the second pocket [128]. The relation between this “one-peanut” observation and nematic order is a fascinating open question.

3. Magnetism

At ambient pressure, bulk FeSe does not order magnetically, but significant magnetic fluctuations with a complex temperature and momentum dependence are observed. The application of hydrostatic pressure induces a dome of magnetic order with a maximum transition temperature $T_N \approx 45$ K.

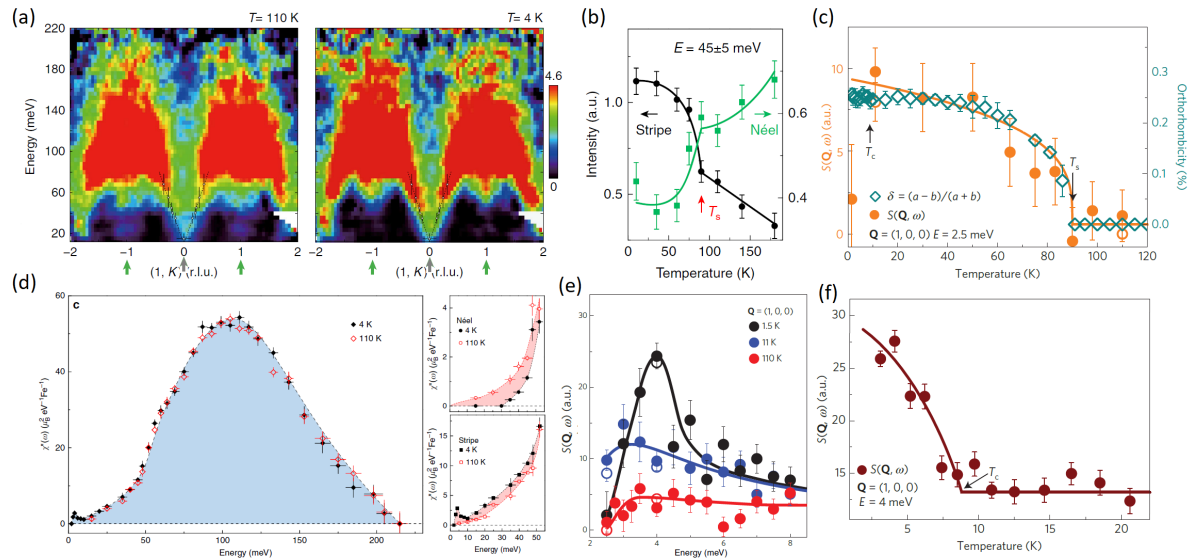


Figure 8. Inelastic neutron scattering results from coaligned sets of FeSe single crystals [90, 129]. (a) Dispersion of spin fluctuations in FeSe at $T = 110$ K and 4 K, showing intensity both around the stripe-type wave vector and the Néel-type wave vector $[(1,0)$ and $(1,1)$, respectively, in this notation]. (b) Temperature dependence of the intensity around the stripe-type and Néel-type wave vectors. (c) Temperature dependence of the low-energy dynamic spin correlation $S(Q, \omega)$, around the stripe-type wave vector (yellow circles), which correlates with the orthorhombic structural distortion (teal diamonds). (d) Energy dependence of the dynamic susceptibility at 4 and 110 K, corresponding to the data in (a) and the energy dependence of the Néel-type and stripe-type fluctuations. (e) Energy dependence of the dynamic spin correlation at low temperatures, revealing a superconducting resonance at the stripe-type wave vector. (f) Temperature dependence of the low-energy dynamic spin correlation around the stripe-type wave vector enhanced by the resonance below T_c . (a),(b),(d) Reproduced from Ref. [129], Creative Commons Attribution 4.0 International License. (c),(e),(f) Reprinted by permission from Macmillan Publishers Ltd: Nature Materials, Ref. [90], copyright 2015.

3.1. Magnetic fluctuations at ambient pressure

An early review[130] discussed magnetic excitations in FeSe from NMR and inelastic neutron scattering experiments. The early NMR measurements on polycrystalline FeSe[87] show an enhancement of the spin-lattice relaxation rate divided by temperature $1/T_1T$ arising from an increase in low-energy spin fluctuations around $T^* \approx 100$ K. Subsequent measurements on single crystals showed that the onset of this enhancement occurs very close to T_s [79] at ambient pressure, suggesting a coupling of magnetic fluctuations and nematic order.

Recently, the magnetic fluctuations of FeSe at ambient pressure have been studied in detail using inelastic neutron scattering[131, 90, 129, 132] revealing their complex dependence on temperature and wave vector (Fig. 8). Magnetic fluctuations are present both around the stripe-type wave vector and around the Néel-type wave vector over a broad energy range[129] (Fig. 8 (a)). They were found to have a smaller bandwidth than

in 122-type systems. A large corresponding total fluctuating moment of $\sim 5.1 \mu_B^2/\text{Fe}$ (effective spin of $S \sim 0.74$) was estimated [129]. At very low energies, magnetic fluctuations have negligible spectral weight for $T > T_s$ but acquire spectral weight below T_s [90] (Fig. 8(c)), consistent with the NMR data [133]. On decreasing temperature through T_s , spectral weight is transferred from the checkerboard-type to the stripe-type fluctuations for energies $\lesssim 60$ meV [129] (Fig. 8(b),(d)). Very recently, electronic Raman spectra have been interpreted as arising from a frustrated spin-1 system with competition between stripe-type and Néel-type magnetic ordering vectors [134], consistent with the neutron results. On the other hand, recent Raman data on FeSe and FeSe $_{1-x}$ S $_x$ in Ref. [135] have been taken as evidence for the formation of stripe-type quadrupolar order, i.e., a wave of quadrupole moment without charge or spin modulation, in the nematic phase of FeSe.

The presence of spin fluctuations in FeSe at ambient pressure indicates the proximity to a magnetically ordered state. However, the complexity of the fluctuation spectrum may indicate magnetic frustration, which is a possible explanation for the absence of magnetic ordering in FeSe at ambient pressure[136]. The clear impact of the structural transition on the magnetic fluctuation spectrum demonstrates the coupling between magnetic and structural properties in FeSe [90, 129].

In the superconducting state, a clear spin-resonance is observed around the stripe-type wave vector[90] (Fig. 8(e),(f)), consistent with a spin-fluctuation-mediated superconducting pairing mechanism. Polarized inelastic neutron scattering has revealed that spin-orbit coupling is important and that the low-energy magnetic fluctuations, including the superconducting resonance, are mainly *c*-axis polarized[132].

3.2. Pressure-temperature phase diagram

Although FeSe does not order magnetically at ambient pressure [39, 34, 35], magnetic order is induced by pressures exceeding ~ 0.8 GPa. The detailed determination of the pressure-temperature phase diagram is the result of several years of effort by a number of groups (Figs. 9, 10, 11). Surprisingly, the structural transition at $T_s = 90$ K at ambient pressure decreases under pressure[36], whereas the magnetic transition temperature T_N increases[35, 37, 137, 138]. These opposing trends are highly unusual for iron-based systems. The resistance data as shown in Fig. 10 allows to follow this evolution rather well. The structural transition results in a small kink in the resistance, whereas the signature of the magnetic transition is an upward jump at low pressures and a downward jump at higher pressures. Ultimately, the magnetic order has a dome-like pressure dependence with a maximum of ~ 45 K around 4 GPa[138] (Fig. 9(e)).

High-resolution x-ray diffraction under pressure combined with time-domain Mössbauer spectroscopy showed that structural and magnetic phase transition lines actually merge around 1.6 GPa into a joint magneto-structural transition at higher pressures [77] (Fig. 9(f)). NMR similarly demonstrates the decrease of T_s under pressure until structural and magnetic phase transitions merge into a combined first-order

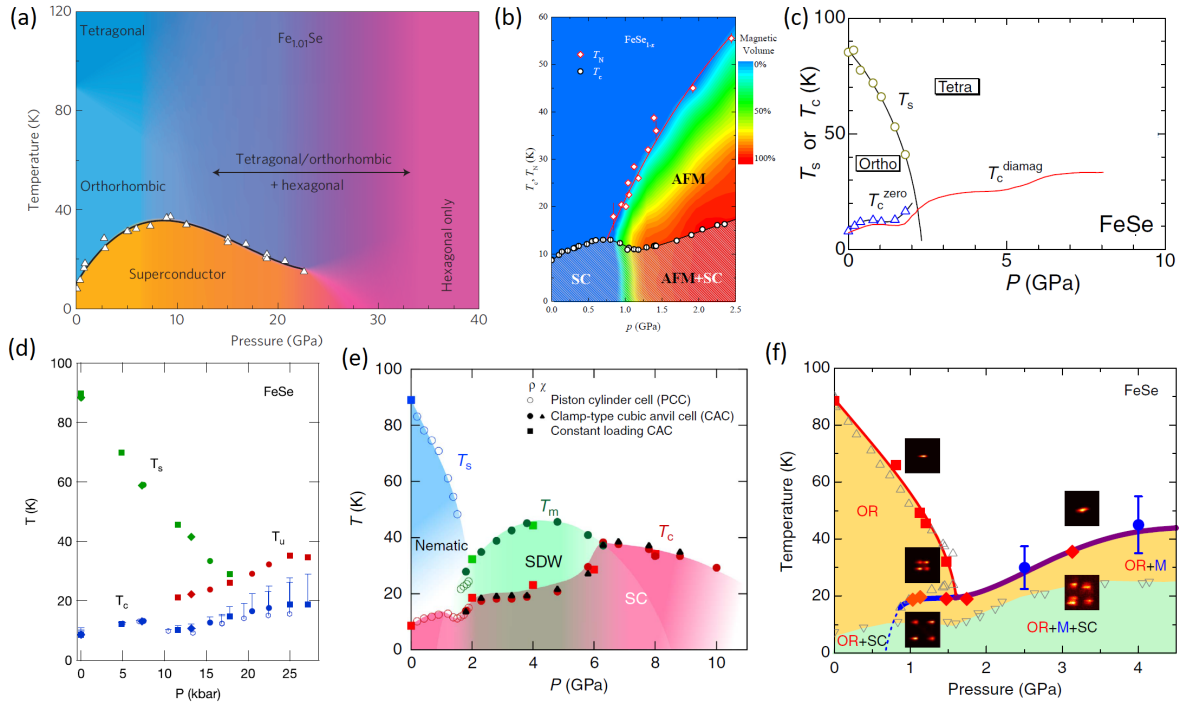


Figure 9. Experimental pressure-temperature phase diagrams of FeSe. (a) Early temperature-pressure phase diagram for polycrystalline FeSe, extending to high pressures. The huge enhancement of T_c under pressure and the transformation to a different crystallographic phase at high pressures is shown. (b) Phase diagram obtained from μ SR measurements on the polycrystalline material, showing the emergence of magnetic order. (c) Phase diagram obtained from resistivity and magnetization measurements on single crystals, showing the suppression of T_s under pressure for the first time and detailing the “three-step”-like enhancement of T_c under pressure. (d) Phase diagram obtained from resistivity and susceptibility measurements on high-quality single crystals revealing for the first time both structural and magnetic phase transitions in the same experiment. (e) Phase diagram obtained from resistivity measurements on high-quality single crystals over a large pressure range (see Fig. 10), showing a dome-shaped region of magnetic order. (f) Phase diagram obtained using x-ray diffraction and Mössbauer spectroscopy on single crystals under pressure, revealing that structural and magnetic phase lines merge into a joint magneto-structural transition under pressure. (a) Reprinted by permission from Macmillan Publishers Ltd: Nature Materials, Ref. [39], copyright 2009. (b) Reproduced with permission from Ref. [37], copyright 2012 American Physical Society. (c) Reproduced with permission from Ref. [36], article copyrighted by JPS ©2014, The Physical Society of Japan. (d) Reproduced from Ref. [137], Creative Commons Attribution 4.0 License. (e) Reproduced from Ref. [138], Creative Commons Attribution 4.0 International License. (f) Reproduced from Ref. [77], Creative Commons Attribution 4.0 International License.

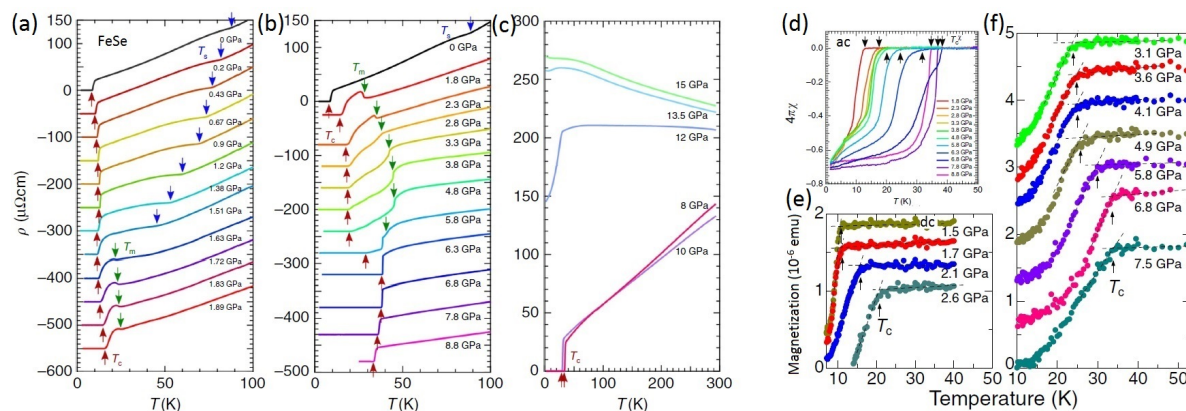


Figure 10. Resistance and magnetization data of single crystalline FeSe under pressure. (a)-(c) Resistivity data over a wide pressure range. A kink indicates the structural transition which is suppressed under pressure and an upturn (downturn at higher pressures) indicates the onset of magnetic order. At the highest pressures, the resistivity increases abruptly indicating the transition to the high-pressure orthorhombic phase. (d) AC susceptibility and (e), (f) DC magnetic susceptibility [36] showing a clear diamagnetic signal related to superconductivity over the whole pressure range. (a)-(d) Reproduced from Ref. [138], Creative Commons Attribution 4.0 International License. (e), (f) Reproduced with permission from Ref. [36], article copyrighted by JPS ©2014, The Physical Society of Japan.

transition around 2 GPa[89]. An important question is whether the magnetically ordered phase in FeSe is analogous to the stripe-type phase in other iron-based superconductors, as suggested by the merging of structural and magnetic transitions. This question will be discussed in section 3.3.

The evolution of the superconducting transition in FeSe under hydrostatic pressure appears to be closely related to the pressure dependence of nematic and magnetic orders. T_c of FeSe under pressure exhibits a complex three-step-like increase (Fig. 9(c),(e)), as revealed by transport as well as by magnetization measurements [36, 138]. T_c initially increases under pressure and reaches a local maximum with $T_c \approx 13$ K at 0.8 GPa, the pressure at which magnetic order sets in. Subsequently, $T_c(p)$ shows a local minimum around 1.2 GPa and a plateau at $\sim 2 - 5$ GPa. T_c reaches its maximum of 38.3 K close to 6 GPa, when magnetic order is suppressed [138]. Further application of pressure reduces T_c . At pressures $\gtrsim 7-10$ GPa, tetragonal FeSe irreversibly transforms into a new crystallographic structure, identified as orthorhombic[60, 139, 40] (previously sometimes as hexagonal[57, 39]) with significantly reduced unit cell volume. This transformation likely leads to a loss of superconductivity[138].

3.3. Magnetic order under pressure

Magnetotransport[114] and quantum oscillation[140] experiments under pressure demonstrate a significant reconstruction of the Fermi surface in the magnetic state, as expected for the onset of antiferromagnetic order. The most direct microscopic

probe for the nature of magnetic order would be neutron diffraction. However, neutron experiments on FeSe under pressure have so far not succeeded to resolve magnetic signals. This is likely due to the small ordered magnetic moment. From the early μ SR data (Fig. 11(a)-(d)) an ordered moment of only $\sim 0.2\mu_B$ [35, 37] is inferred at 2.5 GPa. Similarly, time-domain Mössbauer spectroscopy[77] is consistent with a small value of the ordered moment of the order of $\sim 0.2 \mu_B/\text{Fe}$ at $p = 4$ GPa (Fig. 11(e)).

High-resolution x-ray diffraction [77] demonstrates that the tetragonal symmetry is broken in the magnetic state, as is the case for stripe-type magnetic order in other iron-based systems. Moreover, an abrupt increase of the orthorhombic distortion in decreasing temperature through T_N is observed, reminiscent of the behavior of Co- and Rh-doped BaFe_2As_2 [27] and a sign of cooperative coupling of the two types of order. ^{77}Se NMR study of single crystalline FeSe under pressure[89] likewise suggests stripe-type antiferromagnetic order. In particular, the observed c -axis oriented magnetic hyperfine field at the Se site (Fig. 11(f),(g)) is consistent with stripe-type ordering and Fe-moments pointing along the a -axis[89], as in the 122-type iron-based materials. In addition, the in-plane/out-of-plane anisotropy of the spin-lattice relaxation rate of 1.5 has been taken as an indication of stripe-type magnetic fluctuations above T_N [89]. However, observed changes of spectral weight might indicate a broad distribution of magnetic moments, or phase inhomogeneity in the magnetic state[89]. A μ SR study on a crystal 'with preferred orientation' under pressure [141] is also consistent with stripe-type antiferromagnetic order.

An interaction between magnetic order and superconductivity is observed only in the low-pressure range. Upon decreasing the temperature below T_c , a decrease of the magnetic hyperfine field and volume fraction are observed in μ SR on polycrystalline samples for $p \leq 1.4$ GPa [35, 37] (Fig. 11(a)-(d)).

The temperature evolution of the spin-lattice relaxation rate divided by temperature $1/T_1T$ in NMR under pressure (Fig. 12) allows to study magnetic fluctuations and the evolution of the character of the magnetic transition under pressure as well. Measurable magnetic fluctuations onset below a temperature T^* that is essentially pressure independent[52, 142], strongly suggesting that the coincidence of T^* and T_s at ambient pressure is accidental. Interestingly, the onset of these low-energy spin fluctuations correlates with the onset of local static nematicity, suggesting their cooperative interplay[142]. This extended region of static inhomogeneous nematicity in the temperature-pressure phase diagram of FeSe was also reported in Ref. [143]. On decreasing temperature at intermediate pressures, $1/T_1T$ shows a clear divergence, indicative of a second-order transition at T_N when $T_s > T_N$. However, this divergence is absent at higher pressures, indicating a first-order magneto-structural transition at $T_s = T_N$ [89].

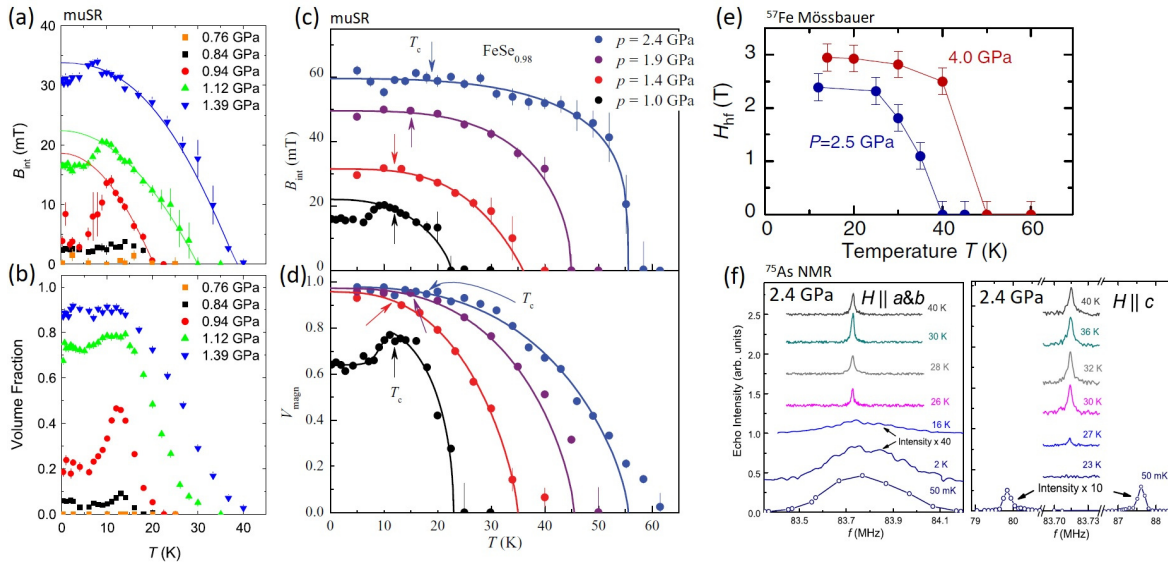


Figure 11. Magnetic order in FeSe under pressure. (a),(b) Temperature dependence of the internal magnetic field at the muon site and the magnetic volume fraction vs. temperature, respectively, at various pressures up to 1.39 GPa. (c),(d) Internal magnetic field at the muon site and magnetic volume fraction at pressures up to 2.4 GPa, respectively. (e) Temperature dependence of the magnetic hyperfine field at the iron-site at 2.5 GPa and 4.0 GPa. (f) ^{75}As NMR spectra of single-crystalline FeSe at 2.4 GPa under in-plane and c -axis magnetic fields. A hyperfine field at the As-site of 0.48 T oriented along the c -axis is revealed. (a), (b) Reproduced with permission from Ref. [35], copyright 2010 American Physical Society. (c), (d) Reproduced with permission from Ref. [37], copyright 2012 American Physical Society. (e) Adapted from Ref. [77], Creative Commons Attribution 4.0 International License. (f) Reproduced with permission from Ref. [89], copyright 2016 American Physical Society.

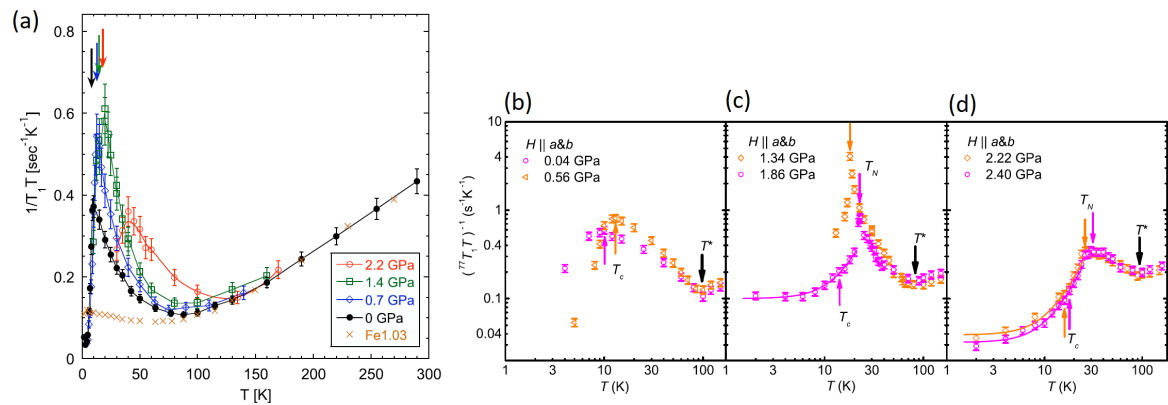


Figure 12. The ^{77}Se spin-lattice relaxation rate under pressure. (a) ^{77}Se spin-lattice relaxation rate divided by temperature, $1/T_1T$, of polycrystalline FeSe under pressure. The upturn below $T^* \sim 100$ K is associated with the emergence of low-energy spin fluctuations. (b)-(d) $1/T_1T$ at various pressures, indicating a first-order magnetic transition at high pressures. The onset of enhanced relaxation rate, T^* , is nearly pressure independent. (a) Reproduced with permission from Ref. [87], copyright 2009 American Physical Society. (b)-(d) Reproduced with permission from Ref. [89], copyright 2016 American Physical Society.

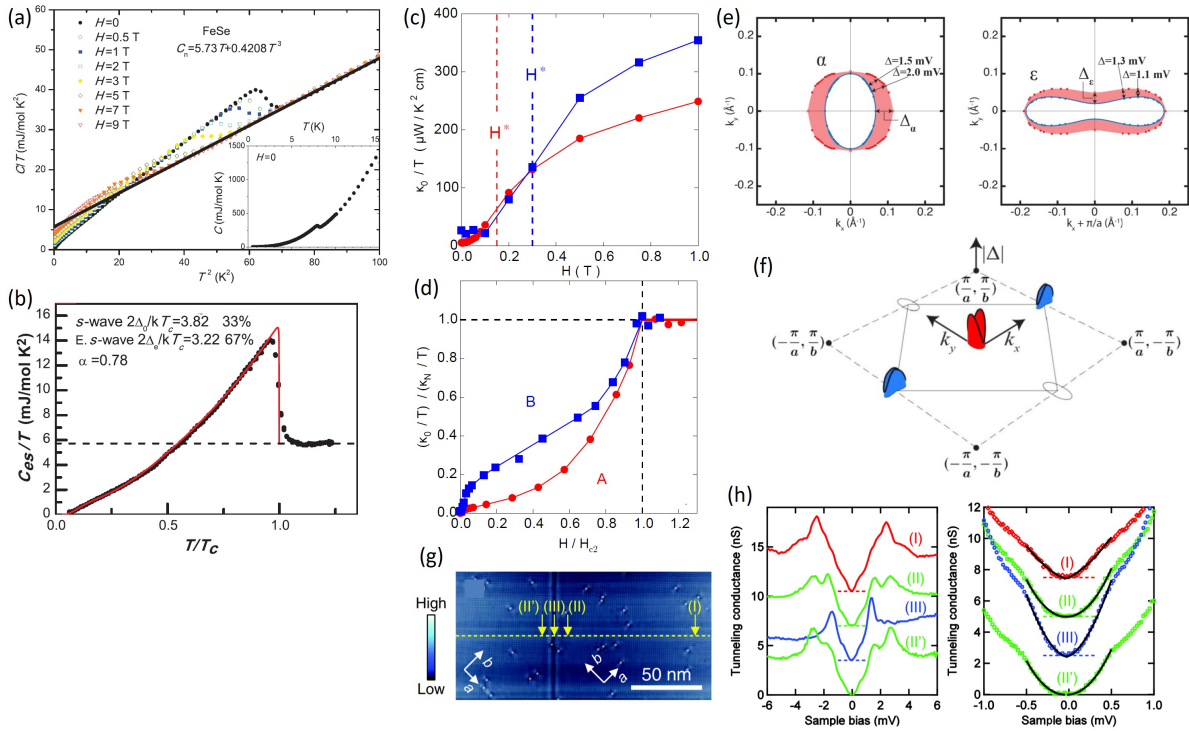


Figure 13. Experimental results concerning the superconducting gap structure of FeSe. (a) Specific heat of single-crystalline FeSe. (b) Electronic specific heat of FeSe and fitted BCS-type model consisting of a sum of an isotropic s -wave gap and a nodeless anisotropic (extended s -wave) gap. (c), (d) Thermal conductivity of two samples of FeSe indicating the absence of nodes. (e) Gap structure of the central hole and elongated electron pockets of FeSe as determined by Bogoliubov quasiparticle interference. A pronounced two-fold anisotropy of the gap is observed for the electron pocket. (f) Illustration of this gap structure; the color-code indicates the sign change between the Fermi surface pockets [128]. (g) STM image of a domain boundary of FeSe. (h) Tunneling spectra taken at several points across this domain boundary as indicated in (g). The low-energy part of the tunneling spectra suggests possible changes of the gap structure as a function of position. (a), (b) Reproduced with permission from Ref. [144], copyright 2011 American Physical Society. (c), (d) Reproduced with permission from Ref. [145], copyright 2016 American Physical Society. (e), (f) From Ref. [128]. Reprinted with permission from AAAS. (g), (h) Reproduced from Ref. [146], Creative Commons Attribution 3.0 License.

4. Superconductivity

Superconductivity in FeSe has many intriguing and complex features. The superconducting transition temperature of bulk FeSe at ambient pressure is about 8 – 9 K, which is modest for iron-based superconductors. However, there are numerous ways to increase this T_c significantly. Application of hydrostatic pressure or intercalation of ions or molecules increases T_c to 35-45 K [38, 39, 40, 49, 147, 148]. In monolayer thin films of FeSe on SrTiO₃, T_c can reach 60-80 K [149], and by some accounts even more than 100 K [54], as recently reviewed in Refs. [51, 52, 53].

The enormous tunability of T_c of FeSe hints at an unconventional origin of

superconductivity in the compound. The observation of a spin-resonance mode (Fig. 8(e),(f)) is consistent with a spin-fluctuation-mediated sign-changing pairing mechanism [90]. Furthermore, the analysis of STM data[128] with a phase sensitive method[150, 151] found evidence for a sign change of superconducting gap between electron and hole Fermi surfaces, the presence of in-gap resonances at impurities was interpreted with the same conclusion[152]. Recently, a strong electron-phonon interaction in FeSe was deduced from a pump-probe experiment and the importance of a cooperative interplay between electron-electron and electron-phonon interactions for superconductivity in FeSe was suggested[153].

The extremely small Fermi-surfaces of FeSe together with the 'typical' values for the superconducting gaps of 2-3 meV mean that the ratio of Δ to E_F in FeSe is as high as 0.1 – 1. This places FeSe into the regime of a (multiband) BCS-BEC crossover, which has been intensively discussed[68, 154, 155]. In particular, strong superconducting fluctuations associated with preformed Cooper pairs have been reported [154]. Fe(Se,Te) with $\sim 40\% - 60\%$ Te content appears to be in a similar regime [156, 157].

The superconducting gap structure of FeSe has been subject of intense study; some recent results are summarized in Fig. 13. Signatures of multigap superconductivity are generally observed [144, 158, 145, 159, 160]. The dimensionless specific heat jump at T_c of $\Delta C/\gamma_n T_c = 1.65$ indicates moderately or strong coupling superconductivity [144]. Early specific heat data in single crystals are consistent with the absence of nodes in the superconducting gap[144]. However, from STM data on thin films[161, 162] and on single crystals[68], it was suggested that clean FeSe is a nodal superconductor. Other more recent studies including STM[128, 163], specific heat[163], thermal conductivity[145, 155] and the London penetration depth[164, 165] indicate, however, that FeSe is fully gapped superconductor, albeit with deep gap minima. The specific-heat data in Refs. [166] and [167] are consistent with nodal superconductivity or deep gap minima. A recent detailed study of the field-angle dependent specific heat of FeSe[160] proposes three distinct superconducting gaps, of which the two smallest ones are anisotropic, and the smallest possibly nodal.

It is likely that small modifications in sample preparation, leading to a change of the precise Fe:Se ratio, or to internal stresses can induce variations of the gap structure from nodal to nodeless with deep minima of the gaps. It was shown that changes in sample preparation can have a significant impact on T_c , which can vary between 3 – 9 K for samples prepared with slightly different starting compositions and temperature profiles [97]. Effects of impurity scattering can explain the variation of T_c and at the same time the filling in of low-energy density of states. Indeed, a proton irradiation study concludes that if there are gap nodes in FeSe, these are "symmetry-unprotected"[168]. Furthermore, the superconducting gap appears to also become "more" nodeless close to an orthorhombic domain boundary[146]. Thus, it might be possible that nodal and nodeless spatial regions coexist in a bulk sample.

Very interesting is the pronounced two-fold anisotropy of the superconducting properties in FeSe. A sizable in-plane anisotropy of the superconducting coherence

lengths, as shown by the spatial extent of the vortex cores, was observed early in thin films[169] and confirmed by measurements on bulk single crystals [146]. A clear two-fold anisotropy of the superconducting gaps was demonstrated by high-resolution Bogoliubov quasiparticle interference [128]. ARPES on lightly S-doped FeSe likewise revealed a significant 2-fold anisotropy of the superconducting gap[170].

The pronounced two-fold anisotropy of the superconducting gap structure, given that the crystal structure is distorted only very slightly from tetragonal, suggests a strong link between nematicity and superconductivity in FeSe. In the prototypical 122-type superconductors, the interaction between superconductivity and stripe-type magnetic order leads to a sizeable decrease of orthorhombic distortion and ordered magnetic moment below T_c [29, 28]. In contrast, the relation between orthorhombic lattice distortion and superconductivity in FeSe is very subtle. The small changes of the lattice parameters at T_c were studied using high-resolution dilatometry in Ref. [66]. It was found that the a and b axes change in a very similar manner at the superconducting transition, so that the effect of T_c on the orthorhombic distortion is only a slight curvature change[66]. As can be inferred via a thermodynamic relation, this indicates that T_c is unaffected by small changes of δ . Interestingly, in lightly S-doped FeSe, the same method indicates that superconductivity couples *cooperatively* with orthorhombic distortion[166]. This means that an increase of δ would result in an increase of T_c , a behavior not seen in any other iron-based superconductor so far.

In contrast to the structural distortion, the in-plane anisotropy of the NMR spectra at ambient pressure actually decreases slightly below T_c [83, 142]. This was proposed to be a sign of competition between electronic nematicity and superconductivity [83]. Interestingly, no such competition is visible in the lattice parameters[66].

Interestingly, T_c appears to be generally suppressed by presence of the pressure-induced magnetic order in FeSe. In particular, $T_c(p)$ exhibits a local maximum at $p \sim 0.8$ GPa (the point of emergence of magnetic order) and a global maximum at $p \sim 6$ GPa, when T_N is reduced to below T_c . However, in the pressure range $\sim 2 - 6$ GPa, both T_c and T_N appear to increase under pressure, which is unexpected if magnetic order and superconductivity compete strongly. A decrease of magnetic hyperfine field below the superconducting transition has been demonstrated only in the low pressure range $p \sim 0.8 - 1.4$ GPa[35, 37]. Furthermore, no change of orthorhombic distortion at T_c is resolved at any pressure [77]. These observations may indicate a much weaker interaction between superconductivity and magnetic order than in other iron-based systems. Experimental studies of the superconducting gap structure under pressure are exceedingly difficult and have not been reported to date.

There is a possibility that superconductivity in FeSe does not even coexist microscopically with magnetic order above a certain pressure value, which would explain why no signature of T_c is observed in the lattice parameters and hyperfine fields. The transport and magnetic signatures of superconductivity under pressure may arise from only a small volume fraction of the sample. This was suggested based on NMR data which do not find any change of the spin-lattice relaxation rate $1/T_1$ below T_c

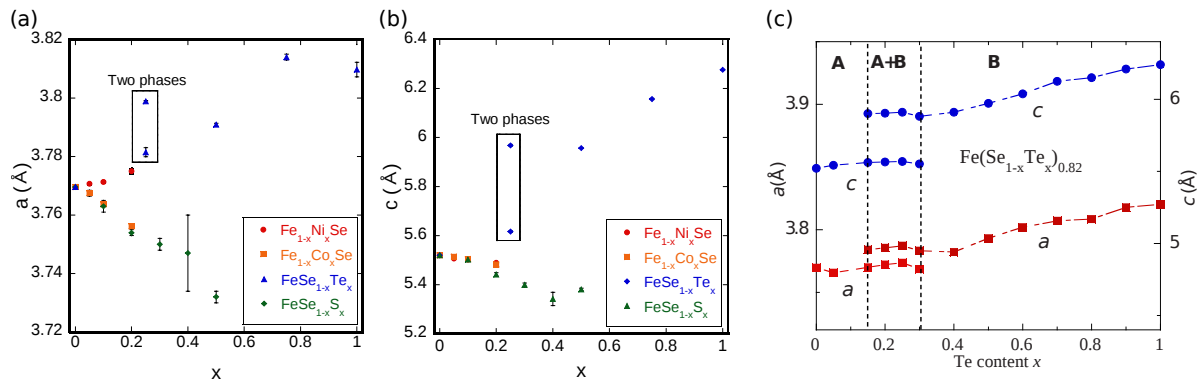


Figure 14. Evolution of the lattice parameters of substituted FeSe. (a), (b) a - and c -lattice parameter, respectively, of polycrystalline FeSe as a function of Ni, Co, Te, and S. A two-phase region in the Fe(Se,Te) series is indicated. (c) Evolution of lattice parameters in the Fe(Se,Te) series showing the two-phase region between $\sim 10 - 30\%$ Te content. (a), (b) Reproduced with permission from Ref. [44], articles copyrighted by JPS ©2009 The Physical Society of Japan. (c) Reproduced with permission from Ref. [173], copyright 2008 American Physical Society.

under pressure [89]. Note that in 122-type materials with a strong first-order magneto-structural transition like $\text{Ca}(\text{Fe}_{1-x}\text{Co}_x)_2\text{As}_2$, microscopic coexistence between magnetic order and superconductivity is not observed either [171]. Recently, the absence of bulk superconductivity in the magnetically ordered part of the phase diagram has indeed been indicated by AC magnetic susceptibility in slightly sulfur-substituted FeSe[172]. Future experimental studies are needed to reveal to which extent superconductivity can coexist with magnetic order in FeSe under pressure.

5. Effects of chemical substitutions in FeSe

Chemical substitutions are a common way of tuning iron-based materials[12]. However, the variety of successful chemical substitution in FeSe is rather limited as compared to many other iron-based systems. Initially, substitution of Te and S for Se, and of Co and Ni for Fe have been studied in some detail using polycrystalline samples and the Fe(Se,Te) system has received particular attention[44], see Fig. 14 (a), (b). A tetragonal-to-orthorhombic structural transition appears at a reduced $T_s = 40$ K in $\text{Fe}_{1.03}\text{Se}_{0.57}\text{Te}_{0.43}$ [176]. The superconducting transition temperature reaches a maximum of $T_c = 14$ K at approximately 50% Te content[71]. The FeTe endmember of the series orders antiferromagnetically, but with a double-stripe structure—different from most iron-based systems[45]. This system is complex due to a significant amount of excess Fe leading to a rich $\text{Fe}_{1+\delta}\text{Te}$ phase diagram[177, 178]. Furthermore, the Se and Te ions occupy the same Wyckoff position in the lattice, but have different heights above the iron plane, entailing a significant amount of structural disorder [179]. A miscibility gap between 10% and 30% Te content has been demonstrated [173], see Fig.14 (c). Fe(Se,Te) has been reviewed previously[180] and will not be discussed in further detail

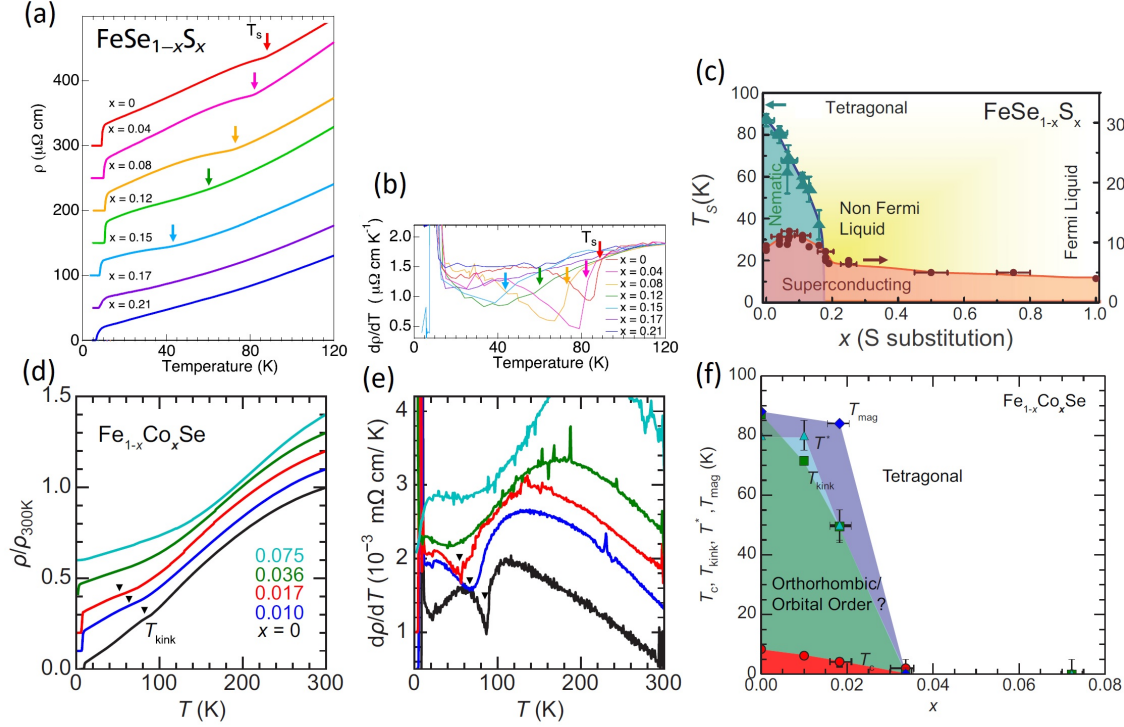


Figure 15. Electrical resistance and phase diagrams of Co- and S-substituted FeSe single crystals. (a), (b) Resistance and temperature derivative of the resistance of S-substituted FeSe, respectively. Data in (a) are offset vertically. (c) Phase diagram of $\text{FeSe}_{1-x}\text{S}_x$. Note that T_s and T_c are plotted on the left and right temperature axis, respectively. (d), (e) Resistance and temperature derivative of the resistance of Co-substituted FeSe, respectively. Data in are offset vertically. (f) Phase diagrams of Co-substituted FeSe. (a), (b) Reproduced from Ref. [95]. (c) Reproduced with permission from Ref. [174], copyright 2017 American Physical Society. (d)-(f) Reproduced with permission from Ref. [175], copyright 2016 American Physical Society.

here. Attempts to grow Te-substituted single crystals of FeSe using vapor transport have failed[81] and the miscibility gap at low Te content[173] makes connecting the Fe(Se,Te) series with pure FeSe difficult.

For vapor-grown single crystals, the two main kinds of substitution are S for Se and Co for Fe. Sulfur substitution is considered to act as chemical pressure, since it leads to a decrease of the lattice parameters[181] and sulfur is isovalent to Se, see Fig. 14. Cobalt substitution is more likely to introduce additional charge carriers. Nevertheless, both Co and S substitution suppress the structural transition at T_s [175, 182, 183, 95, 184]. The critical concentrations, at which T_s is completely suppressed, are approximately 16% S content and only 3% Co content[175], see Fig. 15. T_c initially increases with S substitution and reaches a broad maximum of 11 – 12 K at $\approx 8\%$ S content[95, 184, 185, 174], well inside the orthorhombic phase. Further S substitution decreases T_c moderately to ≈ 6 K at 20% S content. Co substitution, conversely, decreases T_c monotonically and superconductivity is completely suppressed

concomitantly with T_s at about 3% Co content[175]. No sign of magnetic order is observed at ambient pressure for either kind of substitution. Early NMR work has demonstrated the suppression of the low-temperature magnetic fluctuations at 10% Co substitution[130].

Since the orthorhombic phase of FeSe is a rare example of a nematic phase without magnetic order in the iron-based systems, suppressing T_s allows for the study of a pure nematic quantum critical point (QCP) [95]. Indeed, a Fermi-liquid-like T^2 behavior of resistivity is observed only at high sulfur concentrations, whereas the resistivity at intermediate sulfur concentrations suggests non-Fermi-liquid behavior close to the endpoint of the nematic phase[174], see Fig. 15. This strongly resembles the behavior of the resistivity in $\text{BaFe}_2(\text{As}_{1-x}\text{P}_x)_2$ [186], which has been discussed in terms of a quantum criticality [186, 187, 188, 189, 190]. However, in both S and Co substituted FeSe, T_c is not maximum at the QCP, in contrast to $\text{BaFe}_2(\text{As}_{1-x}\text{P}_x)_2$.

The nematic susceptibility, as probed by the strain-dependence of the resistivity, was studied across the possible nematic quantum critical point in the Fe(Se,S) system[95]. The nematic susceptibility was found to diverge with an approximate Curie-Weiss law for all compositions and the Weiss temperature changes sign at the critical concentration of $\approx 15\%$ S content. Notably, the amplitude of elastoresistivity is strongly enhanced close to this critical point. This behavior is strongly reminiscent of the behavior of $\text{Ba}(\text{Fe}_{1-x}\text{Co}_x)_2\text{As}_2$ and has been discussed as a signature of a nematic quantum critical point[98].

The evolution of the electronic structure of FeSe with S substitution has been studied in detail using ARPES[184, 174], quantum oscillations[185] and STM[191]. The distortion of the electron Fermi-surfaces was shown to be reduced by increasing S content as the orthorhombicity is gradually suppressed[184]. Furthermore, the Fermi surfaces generally become larger upon S substitution [185] and electronic correlations weaken[174]. The pronounced two-fold anisotropy of the superconducting gap of FeSe is clearly related to its orthorhombic crystal structure. Therefore, it is interesting to study the evolution of the superconducting gap in $\text{FeSe}_{1-x}\text{S}_x$, when the ground state evolves from orthorhombic to tetragonal. An analysis of specific heat and thermal conductivity found that even in tetragonal $\text{FeSe}_{1-x}\text{S}_x$ the superconducting gap is still highly anisotropic and possibly nodal[192]. However, the recent STM study found evidence for two distinct superconducting pairing states in the orthorhombic and tetragonal samples, respectively[191].

Pure FeS with the same PbO-type tetragonal crystal structure as FeSe is a superconductor with $T_c = 5$ K[46]. This crystallographic phase is, however, only stable below 200 – 250°C[193]. FeS has not been grown out of the vapor phase, but either by hydrothermal synthesis from iron powder and sulfide solution[46, 194] or by deintercalation of K-Fe-S[193]. Likely due to this challenge, the complete series Fe(Se,S) could not yet be studied. The normal and superconducting properties of the multiband system FeS were studied in detail[195, 196, 197, 198], indicating nodal superconductivity[197, 198]. The superconducting transition temperature is

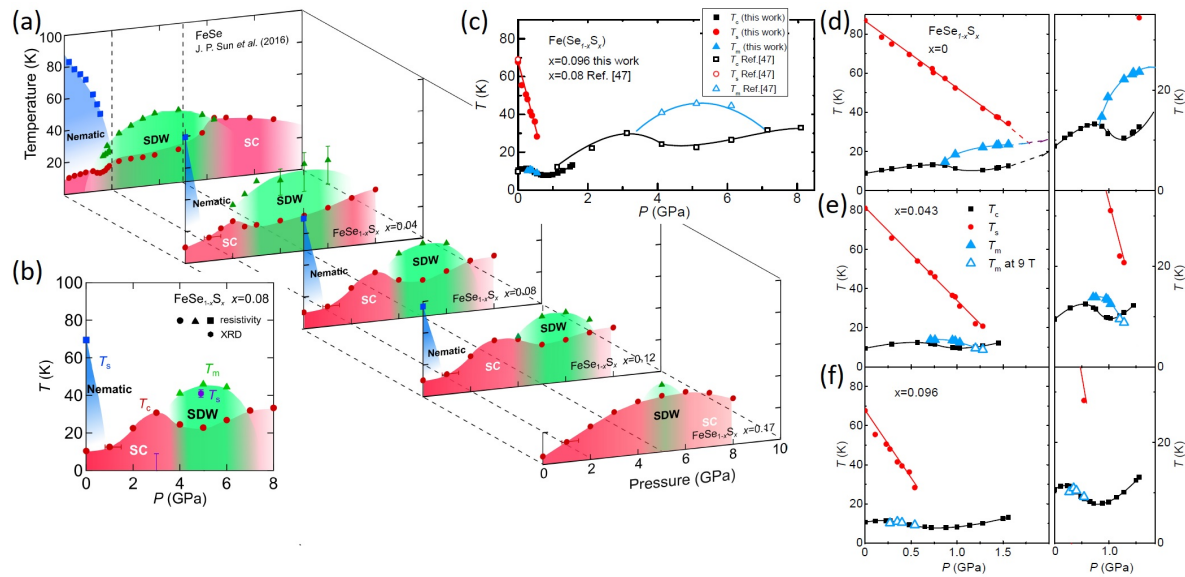


Figure 16. Phase diagram of FeSe with combined S substitution and applied pressure (a) Pressure-temperature phase diagrams of $\text{Fe}(\text{Se}_{1-x}\text{S}_x)$ for $0 \leq x \leq 0.17$ showing the shrinking of the pressure-induced magnetic dome and its detaching from the nematic phase with increased sulfur content x . (b) View of the pressure-temperature phase diagram of $\text{FeSe}_{0.92}\text{S}_{0.08}$. T_c is maximized in the absence of magnetic and nematic order. (d)-(f) Temperature pressure phase diagrams of $\text{Fe}(\text{Se}_{1-x}\text{S}_x)$ for small $0 \leq x \leq 0.096$ in the low-pressure range. The presence of a small dome of magnetic order at low pressures, that is rapidly suppressed for increasing x , is suggested. (c) Combination of data from Ref. [181] (labeled “Ref. [47]”) and [201] (labeled “this work”) to a detailed $p - T$ phase diagram of $\text{Fe}(\text{Se}_{1-x}\text{S}_x)$ for $x \approx 0.09$. (a), (b) Reproduced from Ref. [181], Creative Commons Attribution 4.0 International License. (c)-(f) Reproduced with permission from Ref. [201], copyright 2017 American Physical Society.

monotonically suppressed under pressure[199]. A recent comprehensive inelastic neutron diffraction, quantum oscillations and elastoresistivity study[200] suggested FeS to be a weakly correlated analogue to FeSe.

The combination of chemical pressure induced by sulfur substitution and physical pressure leads to particularly interesting phase diagrams (Fig. 16), which may further elucidate the phase interplay in FeSe. The structural transition at T_s is gradually suppressed by both chemical and physical pressure. In contrast, the pressure range over which magnetic order occurs is reduced on increasing the sulfur content, but the maximum T_N changes only slightly. In consequence, for a certain range of sulfur content, nematic order and magnetic order occur in detached parts of the temperature-pressure phase diagram of $\text{Fe}(\text{Se,S})$ (Fig. 16 (a)-(c)). Furthermore, samples with low sulfur content $< 10\%$ exhibit an additional small dome of likely magnetic order in the low pressure range (Fig. 16 (e),(f)) [201]. This phase remains below T_s on increasing sulfur content and its emergence under pressure coincides with the local maximum of T_c (that occurs at 0.8 GPa in pure FeSe) for all studied compositions of $\text{Fe}(\text{Se,S})$

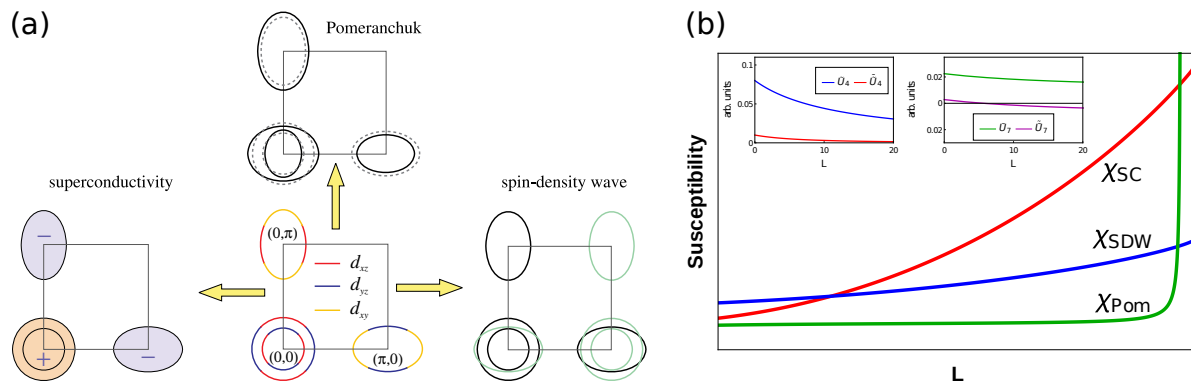


Figure 17. Potential instabilities at low energies as revealed by RG analysis. (a) The Fermi surface topology of Fe-based superconductors (orbital content plotted in color) allows for three electronic instabilities as indicated in the pictures on the left (s_{\pm} superconductivity), right (stripe SDW magnetism) and top (nematicity, breaking of C_4 lattice rotational symmetry). (b) The flow of the susceptibilities of the 3 instabilities as function of the RG parameter L . While the susceptibilities in the superconducting channel and the Pomeranchuk channel diverge, thus leading to such an order, the one in the SDW channel increases, but remains finite as L approaches the scale L_0 where the flow has to stop (slightly outside the plot range). Insets: Representative RG flow of some of 10 decoupled interactions as worked out in Ref. [204]; some of them flow to zero (\tilde{U}_4 and \tilde{U}_4), others flow to small but finite values (\tilde{U}_7 and \tilde{U}_7). (a) Reproduced from Ref. [205], Creative Commons Attribution 3.0 License. (b) Reproduced with permission from Ref. [204], copyright 2017 American Physical Society.

[201]. The superconducting upper critical field, H_{c2} , displays an anomaly at this point[201], similar to the anomaly of H_{c2} at the emergence of magnetic order in pure FeSe[202, 203]. Notably, T_c is of the order of 30-35 K whenever superconductivity sets in within a tetragonal, paramagnetic phase [181]. This observation supports the picture of competing superconductivity and magnetic order.

6. Theoretical mechanisms

Immediately after the discovery of the iron-based superconductors, ab-initio methods were applied to calculate the basic properties of their electronic structure[206, 207, 208]. The general topology of the expected Fermi surface sheets and the nature of the low-energy electronic states as Fe-d states are in agreement with experimental observations[2, 209, 101]. However, discrepancies between the results from DFT investigations and experimental results are particularly pronounced in the case of FeSe: In contrast to the theoretical results, the experimental Fermi surface sheets in FeSe are extremely small[209]. Furthermore, obtaining a stable orthorhombic crystal structure with DFT approaches requires imposing finite magnetic order[136] which is (at zero pressure) experimentally absent.

The electronic structure of the iron-based superconductors was found to be only moderately correlated; much less than, for example, in the cuprates. Therefore,

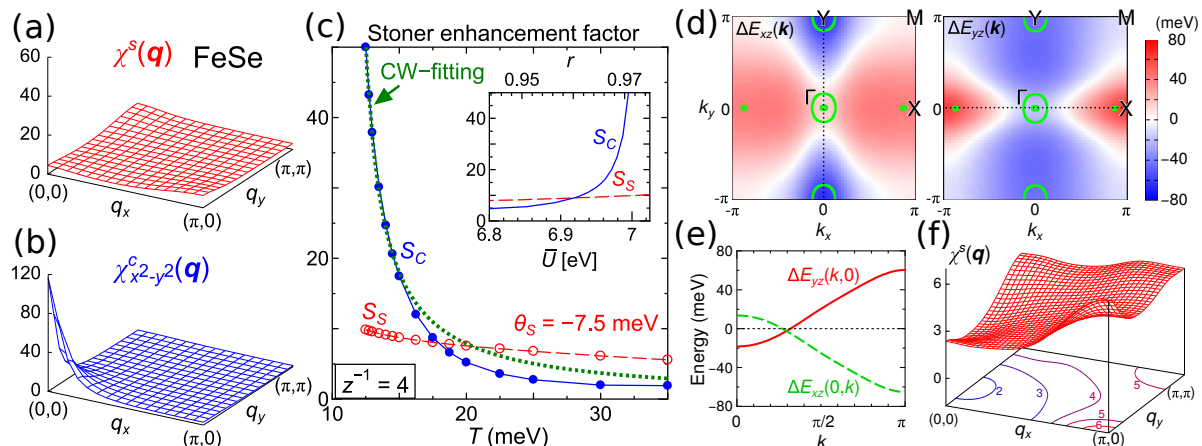


Figure 18. Nematic order in FeSe as found from a strong-coupling effect when working out the self-consistent vertex correction approach. (a) Spin susceptibility $\chi^s(q)$ as calculated with quasiparticle mass renormalization $z = 1$ and interaction strength $r = 0.25$. (b) Charge susceptibility $\chi^c(q)$ for the same parameters as in (a) exhibiting a large peak at $q = (0, 0)$. (c) Stoner enhancement factors for the ferro-orbital order S_C and the antiferromagnetic order S_S which drive the respective order once becoming large. Setting the quasiparticle mass renormalization $z^{-1} = 4$, S_C becomes diverging. Inset: Enhancement factors as function of r showing a divergence close to $r = 0.97$. (d) Self-consistent solution of the orbital polarization, i.e. the orbital shifts $\Delta E_{xz}(k)$ and $\Delta E_{yz}(k)$ plotted in the Brillouin zone. The model exhibits an orbital order at $T = 50$ meV yielding a C_2 symmetric shape of the Fermi surface. (e) The orbital polarization ΔE_{yz} (ΔE_{xz}) plotted along the k_x (k_y) axis making the sign change of the orbital order evident. (f) The spin susceptibility $\chi^s(q)$ becomes C_2 symmetric in the orbital ordered state. Adapted from Ref.[217], Creative Commons Attribution 3.0 License.

DMFT methods are a suitable approach to calculate electronic properties of iron-based superconductors. These methods have been applied to FeSe early on[210]. The general trend of band shifts at the Γ and the M-point (red/blue shift) relative to the DFT result was obtained. It makes the Fermi surface sheets smaller, thus closer to the experimentally observed sizes[211]. For a review on ab-initio perspectives see Ref. [212]. For FeSe in particular, such a DMFT based approach can account for the correct crystallographic z_{Se} position when relaxing the structure[213], and finds the so-called lower Hubbard-bands which have been observed in ARPES measurements [214, 215].

Features of the magnetic fluctuations have been calculated as well[216], but the nematic order and the resulting orthorhombic crystal structure are difficult to obtain from ab-initio based methods. This is also true for the extremely small Fermi surface sheets in FeSe[209, 215]. Thus, various aspects of the material in the normal state and the superconducting state have been examined by model-based calculations where the specific choice of the parameters needs to be motivated.

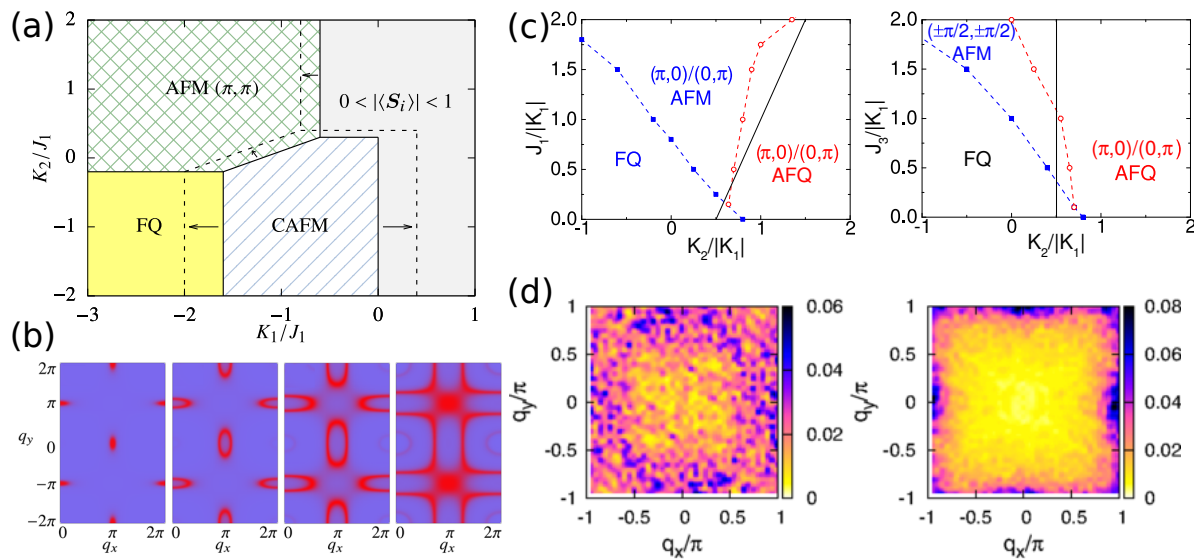


Figure 19. Ferroquadrupolar order and antiferroquadrupolar order as source for nematicity in FeSe. (a) Variational mean-field phase diagram of an Hamiltonian of localized $S = 1$ spins with bilinear Heisenberg interactions J_i and biquadratic interactions K_i showing a ferroquadrupolar order (FQ), antiferromagnetic Néel order (AFM) and a columnar antiferromagnetic order (CAFM). The phase boundaries shift when breaking the C_4 symmetry of the model Hamiltonian by hand. (b) Expected dynamical structure factor in the FQ phase at energies $\omega/J_1 = \{2, 4, 6, 8\}$ (left to right). (c) Classical phase diagram of a bilinear-biquadratic Heisenberg model with antiferroquadrupolar order. The calculation is at finite temperature $T/|K_1| = 0.01$ and the dashed lines show the crossovers between different orders (AFQ: antiferroquadrupolar order). (d) Expected momentum distribution of the dipolar magnetic structure factor in the presence of quadrupolar order for $K_2 = -1$ (left) and $K_2 = 1.5$ (right) with $J_1 = J_2 = 1$ and $K_1 = -1$ as calculated within a classical Monte Carlo approach at $T/|K_1| = 0.01$. (a), (b) Reproduced with permission from Ref. [218], copyright 2016 American Physical Society. (c), (d) Reproduced with permission from Ref. [219], copyright 2015 American Physical Society.

6.1. Nematicity and magnetic fluctuations in FeSe

Upon lowering temperature, many solid state systems undergo transitions to phases with lower symmetries. FeSe, specifically, undergoes a transition to a nematic state $T_s \sim 90$ K. However, unlike other iron based superconductors, FeSe does not develop magnetic order at low temperatures, which led to a strong debate concerning the origin of nematic order in FeSe. Possible sources for the nematic order could be lattice vibrations, spin fluctuations or orbital fluctuations[14]. In the case of FeSe, there are no experimental evidences for a lattice driven instability, but the other two scenarios have been proposed for various reasons. The absence of strong spin fluctuations around T_s led to the conclusion of orbitally driven nematicity[83]. Recent investigations on the spin excitations via inelastic neutron scattering[90] put further constraints to theoretical models, namely, the transfer of spectral weight from Néel to stripe fluctuations and the emergence of low-energy spin fluctuations upon lowering the temperature.

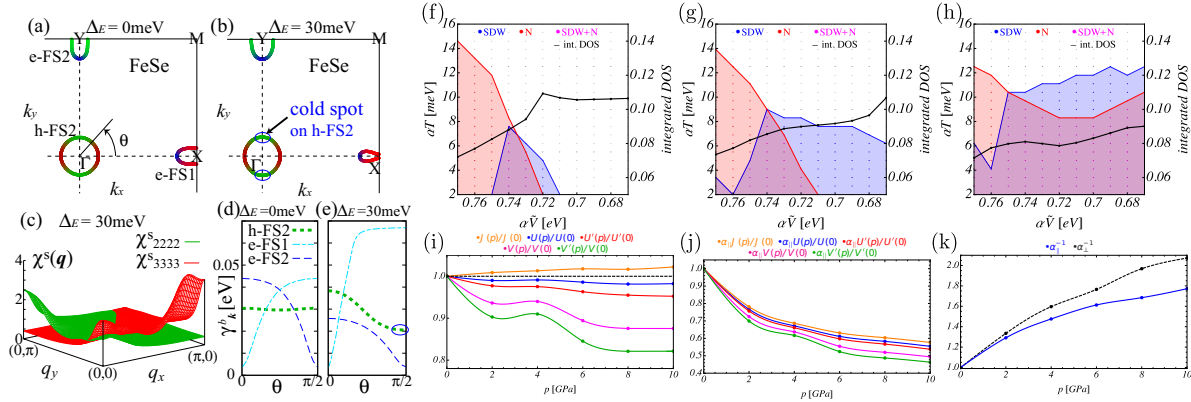


Figure 20. Transport anisotropy in FeSe [220] and orbital order from nearest neighbor Coulomb interactions [221] (a) Fermi surface of a model for FeSe without orbital order and (b) Fermi surface of the same model with a shift of $\Delta E = 30$ meV where the Fermi surface at the X-point has the bowtie shape and the Fermi surface at the Γ point exhibits cold spots at positions where few spin-fluctuations produce a damping of the quasiparticles. (c) Momentum structure of the spin-susceptibilities of the d_{xz} and d_{yz} orbitals with orbital order. (d) Quasiparticle damping γ_k^b from a self-consistent calculation of the self-energy as a function of angle [see (a)] around the Fermi surfaces without orbital order and (e) the same with orbital order exhibiting a pronounced minimum at $\pi/2$ for the holelike Fermi surface, thus a cold spot [see (b)]. (f-h) Phase diagram for FeSe as calculated from a mean field approach including nearest neighbor Coulomb interactions[221]. Shown are the nematic “N” and magnetic “SDW” phases as function of temperature T and interaction strength $\alpha\tilde{V}$ which decreases as function of pressure. The magnetic instability becomes stronger on increasing the rescaled Hund’s coupling αJ : (f) $\alpha J = 0.325$, (g) $\alpha J = 0.35$, (h) $\alpha J = 0.375$. The increase of the integrated density of states is consistent with the increase of the critical temperature for the superconducting instability as function of pressure as seen experimentally[39, 38, 40]. (i) Pressure-induced renormalization of on-site interactions (U, U', J) and extended Coulomb interactions (V, V') extracted from DFT calculations relative to the values at ambient pressure[221]. The Hund’s coupling J increases with pressure, while all other interactions show a downward trend. (j) The rescaled couplings with respect to the renormalization of the hoppings $\alpha_{||}^{-1}$ (k) allows us to connect the rescaled interactions $\alpha\tilde{V}$ with the pressure in the phase diagrams (f-h). (a)-(d) Reproduced with permission from Ref. [220], copyright 2017 American Physical Society. (f)-(k) Reproduced with permission from Ref. [221], copyright 2017 American Physical Society.

Despite the fact that FeSe is a metal, Heisenberg models of localized spins have been applied to understand its properties. Ab initio studies suggest that the electronic structure of FeSe leads to various competing magnetic states and ultimately does not allow for long range magnetic order. As a result, pure nematic order can be realized down to low temperatures[136, 222, 223]. This scenario of competing magnetic state is also consistent with the pinned stripe-type charge ordering found in thin films of FeSe[224].

In other approaches to calculate the magnetic spectrum, the effects of band renormalizations are taken into account by starting from electronic structure models

consistent with experimentally measured eigenenergies[225, 226] (Fig. 21). The magnetic fluctuations have also been calculated by ab initio methods in conjunction with DMFT[216, 227], see Fig. 22 (a-b). Including further neighbor interactions for localized spins, it has been argued that the nematic state is realized from quantum paramagnetic phase[91]. When biquadratic interactions are considered in a scenario driven by localized spins, the nematic properties of FeSe and spin-fluctuations seen in inelastic neutron scattering experiments were explained by a quadrupolar phase[91, 219, 218, 228, 229] and have signatures of dipolar fluctuations, see Fig. 19.

The phase diagram of FeSe has been analyzed theoretically with mean-field approaches [136], field-theoretical methods[91] and numerical methods [219, 230, 228, 218, 229]. A complementary microscopic approach starts from an itinerant model including a multiorbital electronic structure together with a Hubbard-Hund interaction. A variety of possible sources for nematic order in FeSe are revealed. A renormalization group analysis reveals that interaction parameters of different orbital components scale differently. Thus, magnetic fluctuations that lead to a superconducting instability also promote nematic order without leading to a magnetically ordered state[231, 205, 204, 232, 233], see Fig. 17. Spin-fluctuations together with orbital mismatch of the electron and hole Fermi surfaces may also be at the origin of nematicity [234]. Experimental evidence obtained by electronic Raman scattering suggests a Pomeranchuk instability [96, 106]. Finally, orbital fluctuations due to vertex corrections, as illustrated in Fig. 18, have been proposed [217, 235]. Furthermore, the transport anisotropy in the nematic phase has been argued to be due to the positions of cold spots on the Fermi surface which are determined by the spin fluctuations, see Fig. 20(a-e)[220].

In the orbital-order scenarios for nematicity, various types of order can be ruled out because their symmetries are not compatible with common experimental investigations[236] such that a bond order parameter seems essential to describe observed band splittings. The experimentally observed sign change of the orbital polarization[108] has been argued to be due to the positive feedback between the nematic orbital order and the spin susceptibility and calculated in a self-consistent approach[237]. Interatomic Coulomb interactions were found to renormalize the band structure and also lead to such an order parameter[238, 230]. In addition, the increase of the superconducting transition temperature together with a reduction of the tendency towards nematicity as function of pressure can be understood in the same scenario, by using a combination of model-based calculations with input from ab-initio approaches[221], see Fig. 20(f-k).

6.2. Superconducting pairing in FeSe

Similar to the microscopic models for nematicity, two general starting points seem reasonable for the description of the superconducting pairing glue in iron-based superconductors. Localized spin models generally lead to a sign changing order parameter via spin-fluctuations, whereas itinerant models can take advantage of fluctuations of various kinds to support the superconducting instability. Orbital

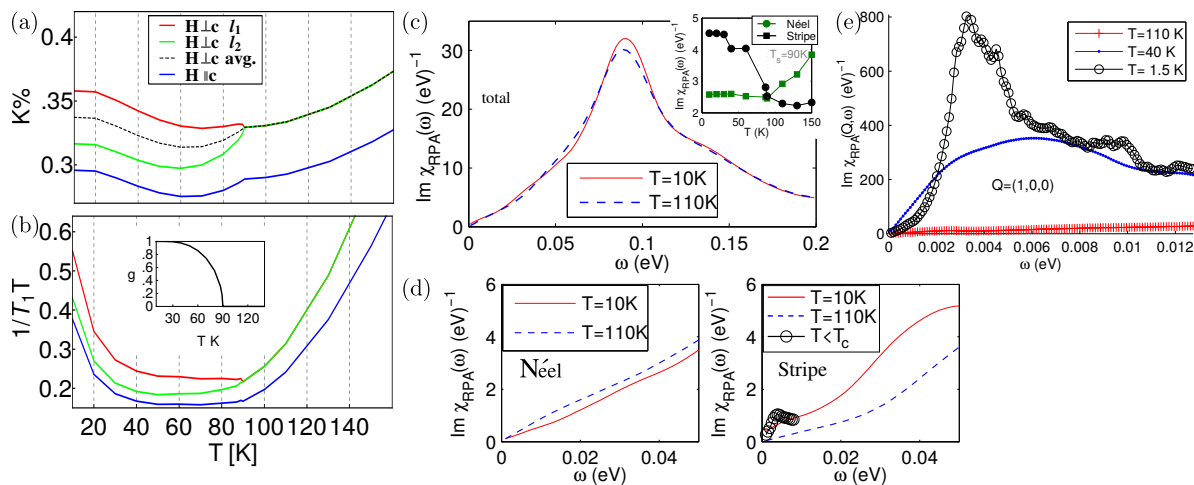


Figure 21. Spin fluctuations in FeSe from an itinerant model (a) Calculation of the Knight shift as expected in an orbital order scenario, (b) expected temperature dependence of the low energy spin fluctuations as measured in an NMR experiment via the spin-lattice relaxation rate divided by temperature $1/T_1T$. (c) The local susceptibility $\chi(\omega)$ is almost unchanged when entering the nematic phase, while the relative weight of the stripe and Néel fluctuations is reversed (inset) as seen experimentally[90, 91], see Fig. 8. (d) Integrated spin fluctuations of Néel type and stripe type at low energies from an itinerant model with orbital order. (e) Calculated spin resonance from sign-changing superconducting order parameter. (a), (b) Reproduced with permission from Ref. [226], copyright 2015 American Physical Society. (c)-(e) Reproduced with permission from Ref. [225], copyright 2015 American Physical Society.

fluctuations supposedly lead to an order parameter without sign change that may account for the slow suppression of the critical temperature upon isoelectronic substitution[175]. Pairing arising from a nematic quantum spin liquid has been used to calculate the superconducting order parameter recently[240].

For a superconducting instability in presence of nematicity (i.e. in a orthorhombic system), the common symmetry classification in s-wave and d-wave instabilities is not valid anymore; this is a consequence which is independent of the underlying pairing interaction. The resulting order parameter is of lower symmetry as well and can lead to accidental nodes in presence of a sign-changing order parameter[225, 226]. The role of the nematic order parameter for the pairing interaction is still under debate. Under the assumption that both instabilities compete, the critical temperature should increase when nematicity is suppressed[83, 184]. It turns out that nematic fluctuations are capable of pairing electrons[241]. Finally, it is possible that more than one single pairing mechanism is responsible for the various properties as it has been suggested by the observation of a double dome in doped FeSe films[242].

Electronic correlations play an important role in iron-based superconductors in general and are supposed to be large in FeSe in particular[209, 101, 107, 211]. As already discussed in many respects for iron-based superconductors, electronic states dominated by some orbitals are more strongly correlated than states dominated by other

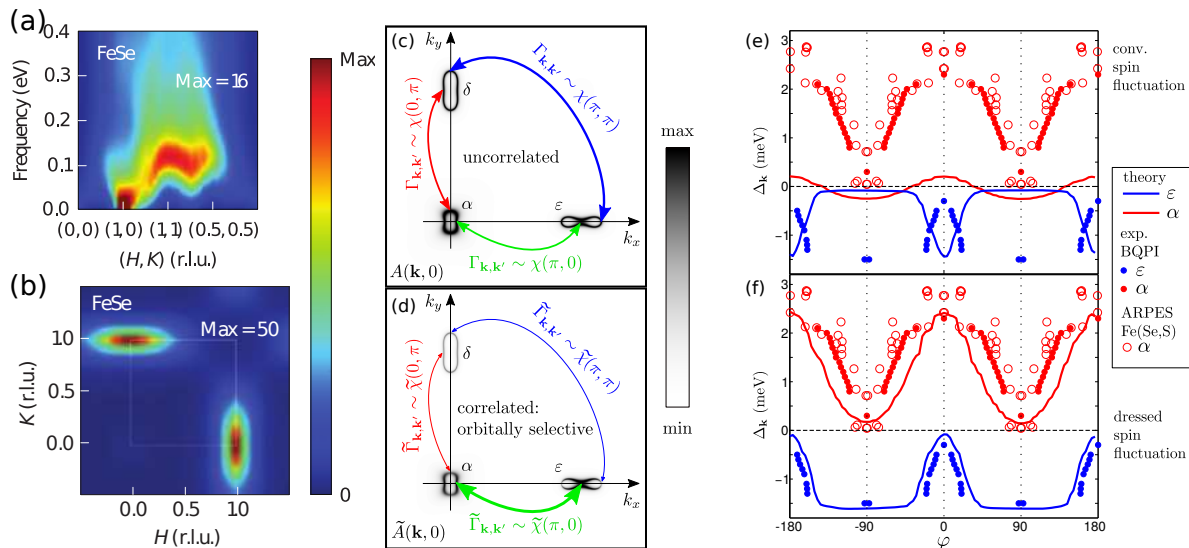


Figure 22. Spin fluctuations from a DMFT approach and superconducting pairing with orbital selective mechanism (a) Dynamic spin structure factor $S(q, \omega)$ calculated using DFT+DMFT, plotted along high symmetry directions. (b) Dynamic structure factor in the 2D plane (H, K) at $k_z = \pi$. (c) Spectral function $A(k, \omega)$ of a fully coherent electronic structure for FeSe. A superconducting pairing from spin-fluctuations in this uncorrelated model leads to 3 almost equally dominant pairing interactions in the d_{xy} orbital (blue), the d_{xz} orbital (red) and the d_{yz} orbital (blue). (d) Imposing orbital selectivity within modified quasiparticle weights changes the spectral function $\tilde{A}(k, \omega)$ such that the δ pocket at $(0, \pi)$ becomes almost invisible and strongly suppresses the pairing in two orbitals leaving the dominating pairing glue $\tilde{\Gamma}_{k, k'}$ from the d_{yz} orbital (thick, green arrow). (e) A conventional spin-fluctuation pairing mechanism with the model from (c) leads to a superconducting gap incompatible with experimental observations. (f) Including correlations via reduced quasiparticle weights and a splitting of those due to nematicity makes the pairing in the d_{yz} orbital dominant[239] and can account for the experimentally observed anisotropy[128]. (a), (b) Reprinted by permission from Macmillan Publishers Ltd: Nature Physics, Ref. [216], copyright 2014. (c)-(f) Reproduced with permission from Ref. [239], copyright 2017 American Physical Society.

orbitals. Describing the electronic structure within a Fermi-liquid picture, this leads to substantial differences in quasiparticle weights and interactions. This orbital selectivity influences properties of the magnetism and allows for orbital ordering[243, 244, 245, 211, 246, 247, 248]. Indeed, the Cooper pairing itself can also become orbital-selective, thus electrons of a specific orbital character form Cooper pairs of the superconductor yielding a highly anisotropic superconducting energy gap [249, 250]. The consequences of these orbital selective electronic correlations for superconductivity in FeSe were discussed recently[128, 239]. Implementing this idea in a phenomenological approach describes the experimentally observed variations of the superconducting energy gap in FeSe quite well when assuming a spin-fluctuation driven pairing interaction[128, 239] [Fig. 22(c-f)]. At the same time, also properties of the scattering on native impurities and trends in the magnetic fluctuation spectrum can be understood.

7. Concluding remarks

FeSe is host to a complex phase interplay between nematicity, magnetism and superconductivity, that at first sight appears very different from “typical” iron-based superconductors.

The orthorhombic phase of FeSe that occurs over a wide temperature range, resembles the nematic phase that is found only in a narrow temperature range in many iron-pnictides. In both cases, this phase is reached via a second-order phase transition from the tetragonal high-temperature phase. The signatures at T_s in magnetic susceptibility, resistivity and specific heat in FeSe are reminiscent of the respective anomalies at T_s in those electron-doped BaFe_2As_2 systems that show a split between T_s and T_N . Similarly, the nematic susceptibility, as inferred by various probes, behaves in a similar manner in FeSe and typical 122-type iron-arsenides. The elastic shear modulus and the electronic Raman responses are very similar as well. However, momentum-resolved probes show some possible differences in the nematic phase between the two types of systems. The magnetic fluctuation spectrum in FeSe is notably more complex than in many 122-type superconductors, with both stripe-type and checkerboard-type low-energy magnetic fluctuations. In addition, the change of the electronic band structure in crossing T_s might be more complex in FeSe than in the 122's, necessitating 'bond-type' nematic order for its explanation. Though they are often assumed to be equivalent, the relation between the nematic phase in FeSe and in 122-systems appears to be a central open question. Its resolution is complicated by the small temperature extent of the nematic phase in systems other than FeSe.

Magnetic order in FeSe has been found only under applied pressure. The coupling of orthorhombic lattice distortion and magnetic order is, however, similar in FeSe and doped 122-type materials. When magnetic order sets in with $T_N < T_s$, the orthorhombic distortion increases abruptly in the magnetic phase, not dissimilar to the behavior of lightly Co- and Rh-doped BaFe_2As_2 . Moreover, the enhancement of stripe-type magnetic fluctuations in the orthorhombic phase is reminiscent of the familiar iron-arsenide systems. Finally, magnetic order and orthorhombic distortion set in as a joint first-order phase transition in pressurized FeSe, similar to the case in many (hole-doped or isovalently substituted) 122-type iron-based superconductors.

Whereas structure and magnetism in substituted BaFe_2As_2 and pressurized FeSe appear analogous, the coupling between superconductivity and nematic/magnetic order remains enigmatic in FeSe. The onset of superconductivity has only a minor effect on nematicity in FeSe, whereas in sulfur-substituted FeSe, superconductivity even appears to favor a larger orthorhombic distortion - in contrast to all other known iron-based systems. Finally, it remains an open question whether superconductivity coexists with the pressure-induced magnetic order.

The realization of a nematic state in FeSe allows to test and possibly falsify theoretical scenarios and mechanisms for nematicity and its interplay with other phases in this system. Itinerant models of the electronic structure and models of localized

magnetic moments have been starting points for theoretical investigations. Ab-initio based methods are able to calculate important quantities, but model-based calculations are still needed to understand the basic principles and put FeSe and its properties in the context of other iron-based materials. These approaches need input from experimental investigations and/or first-principle investigations to justify the theoretical starting point. For the superconducting state it seems that new mechanisms are required to explain the exotic properties of FeSe at ambient pressure and understand the phase interplay in pressurized FeSe.

The study of FeSe has revealed a fascinating variant of the interplay between structure, magnetism and superconductivity in iron-based systems. In particular, the orthorhombic distortion, or nematicity, has been firmly established as an independent player that may be distinct from magnetism. Future surprising discoveries, possibly in doped or intercalated FeSe-based systems seem likely. The complexity of the FeSe phase diagram when chemical and physical pressure are combined may be a hint at yet undiscovered phenomena.

Acknowledgments: We would like to thank Brian M. Andersen, Andreas Kreyssig, William R. Meier and Aashish Sapkota for interesting and useful discussions. The work at Ames Laboratory was supported by the US Department of Energy under DE-AC02-07CH11358.

8. References

- [1] Yoichi Kamihara, Takumi Watanabe, Masahiro Hirano, and Hideo Hosono. Iron-based layered superconductor $\text{La}[\text{O}_{1-x}\text{F}_x]\text{FeAs}$ ($x = 0.05 - 0.12$) with $T_c = 26$ K. *Journal of the American Chemical Society*, 130(11):3296–3297, 2008.
- [2] J. Paglione and R. L. Greene. High-temperature superconductivity in iron-based materials. *Nature Physics*, 6:645–658, 2010.
- [3] David C. Johnston. The puzzle of high temperature superconductivity in layered iron pnictides and chalcogenides. *Advances in Physics*, 59(6):803–1061, 2010.
- [4] G. R. Stewart. Superconductivity in iron compounds. *Rev. Mod. Phys.*, 83:1589–1652, Dec 2011.
- [5] Hideo Hosono and Kazuhiko Kuroki. Iron-based superconductors: Current status of materials and pairing mechanism. *Physica C: Superconductivity and its Applications*, 514:399 – 422, 2015. Superconducting Materials: Conventional, Unconventional and Undetermined.
- [6] Dinah R. Parker, Matthew J. P. Smith, Tom Lancaster, Andrew J. Steele, Isabel Franke, Peter J. Baker, Francis L. Pratt, Michael J. Pitcher, Stephen J. Blundell, and Simon J. Clarke. Control of the competition between a magnetic phase and a superconducting phase in cobalt-doped and nickel-doped NaFeAs using electron count. *Phys. Rev. Lett.*, 104:057007, Feb 2010.
- [7] A. Sapkota, G. S. Tucker, M. Ramazanoglu, W. Tian, N. Ni, R. J. Cava, R. J. McQueeney, A. I. Goldman, and A. Kreyssig. Lattice distortion and stripelike antiferromagnetic order in $\text{Ca}_{10}(\text{Pt}_3\text{As}_8)(\text{Fe}_2\text{As}_2)_5$. *Phys. Rev. B*, 90:100504, Sep 2014.
- [8] Yasutomo J. Uemura. Superconductivity: Commonalities in phase and mode. *Nature Materials*, 8:253–255, 2009.
- [9] S. Avci, O. Chmaissem, D. Y. Chung, S. Rosenkranz, E. A. Goremychkin, J. P. Castellán, I. S. Todorov, J. A. Schlueter, H. Claus, A. Daoud-Aladine, D. D. Khalyavin, M. G. Kanatzidis, and R. Osborn. Phase diagram of $\text{Ba}_{1-x}\text{K}_x\text{Fe}_2\text{As}_2$. *Phys. Rev. B*, 85:184507, May 2012.
- [10] A. Thaler, N. Ni, A. Kracher, J. Q. Yan, S. L. Bud’ko, and P. C. Canfield. Physical and magnetic properties of $\text{Ba}(\text{Fe}_{1-x}\text{Ru}_x)_2\text{As}_2$ single crystals. *Phys. Rev. B*, 82:014534, Jul 2010.

- [11] N. Ni, A. Thaler, A. Kracher, J. Q. Yan, S. L. Bud'ko, and P. C. Canfield. Phase diagrams of $\text{Ba}(\text{Fe}_{1-x}\text{M}_x)_2\text{As}_2$ single crystals ($M=\text{Rh}$ and Pd). *Phys. Rev. B*, 80:024511, Jul 2009.
- [12] Paul C. Canfield and Sergey L. Bud'ko. FeAs-based superconductivity: A case study of the effects of transition metal doping on BaFe_2As_2 . *Annual Review of Condensed Matter Physics*, 1(1):27–50, 2010.
- [13] Clarina de la Cruz, Q. Huang, J. W. Lynn, Jiying Li, W. Ratcliff II, J. L. Zarestky, H. A. Mook, G. F. Chen, J. L. Luo, N. L. Wang, and Pengcheng Dai. Magnetic order close to superconductivity in the iron-based layered $\text{LaO}_{1-x}\text{F}_x\text{FeAs}$ systems. *Nature*, 453:899–902, 2008.
- [14] R. M. Fernandes, A. V. Chubukov, and J. Schmalian. What drives nematic order in iron-based superconductors? *Nature Physics*, 10:97–104, 2014.
- [15] Rafael M. Fernandes and Jörg Schmalian. Manifestations of nematic degrees of freedom in the magnetic, elastic, and superconducting properties of the iron pnictides. *Superconductor Science and Technology*, 25(8):084005, 2012.
- [16] Jiun-Haw Chu, James G. Analytis, Kristiaan De Greve, Peter L. McMahon, Zahirul Islam, Yoshihisa Yamamoto, and Ian R. Fisher. In-plane resistivity anisotropy in an underdoped iron arsenide superconductor. *Science*, 329(5993):824–826, 2010.
- [17] A. Dusza, A. Lucarelli, F. Pfuner, J.-H. Chu, I. R. Fisher, and L. Degiorgi. Anisotropic charge dynamics in detwinned $\text{Ba}(\text{Fe}_{1-x}\text{Co}_x)_2\text{As}_2$. *EPL (Europhysics Letters)*, 93(3):37002, 2011.
- [18] Ming Yi, Donghui Lu, Jiun-Haw Chu, James G. Analytis, Adam P. Sorini, Alexander F. Kemper, Brian Moritz, Sung-Kwan Mo, Rob G. Moore, Makoto Hashimoto, Wei-Sheng Lee, Zahid Hussain, Thomas P. Devereaux, Ian R. Fisher, and Zhi-Xun Shen. Symmetry-breaking orbital anisotropy observed for detwinned $\text{Ba}(\text{Fe}_{1-x}\text{Co}_x)_2\text{As}_2$ above the spin density wave transition. *Proceedings of the National Academy of Sciences*, 108(17):6878–6883, 2011.
- [19] T.-M. Chuang, M. P. Allan, J. Lee, Y. Xie, N. Ni, S. L. Bud'ko, G. S. Boebinger, P. C. Canfield, and J. C. Davis. Nematic electronic structure in the “parent” state of the iron-based superconductor $\text{Ca}(\text{Fe}_{1-x}\text{Co}_x)_2\text{As}_2$. *Science*, 327:181, 2010.
- [20] M. Fu, D. A. Torchetti, T. Imai, F. L. Ning, J.-Q. Yan, and A. S. Sefat. NMR search for the spin nematic state in a LaFeAsO single crystal. *Phys. Rev. Lett.*, 109:247001, Dec 2012.
- [21] Xingye Lu, J. T. Park, Rui Zhang, Huiqian Luo, Andriy H. Nevidomskyy, Qimiao Si, and Pengcheng Dai. Nematic spin correlations in the tetragonal state of uniaxial-strained $\text{BaFe}_{2-x}\text{Ni}_x\text{As}_2$. *Science*, 345(6197):657–660, 2014.
- [22] M. A. Tanatar, A. Kreyssig, S. Nandi, N. Ni, S. L. Bud'ko, P. C. Canfield, A. I. Goldman, and R. Prozorov. Direct imaging of the structural domains in the iron pnictides AFe_2As_2 ($A=\text{Ca}$, Sr , Ba). *Phys. Rev. B*, 79:180508, May 2009.
- [23] I. R. Fisher, L. Degiorgi, and Z. X. Shen. In-plane electronic anisotropy of underdoped '122' Fe-arsenide superconductors revealed by measurements of detwinned single crystals. *Reports on Progress in Physics*, 74(12):124506, 2011.
- [24] L. Ma, G. F. Chen, Dao-Xin Yao, J. Zhang, S. Zhang, T.-L. Xia, and Weiqiang Yu. ^{23}Na and ^{75}As NMR study of antiferromagnetism and spin fluctuations in NaFeAs single crystals. *Phys. Rev. B*, 83:132501, Apr 2011.
- [25] F. L. Ning, M. Fu, D. A. Torchetti, T. Imai, A. S. Sefat, P. Cheng, B. Shen, and H.-H. Wen. Critical behavior of the spin density wave transition in underdoped $\text{Ba}(\text{Fe}_{1-x}\text{Co}_x)_2\text{As}_2$ ($x \leq 0.05$): ^{75}As NMR investigation. *Phys. Rev. B*, 89:214511, Jun 2014.
- [26] Qiang Zhang, Rafael M. Fernandes, Jagat Lamsal, Jiaqiang Yan, Songxue Chi, Gregory S. Tucker, Daniel K. Pratt, Jeffrey W. Lynn, R. W. McCallum, Paul C. Canfield, Thomas A. Lograsso, Alan I. Goldman, David Vakhnin, and Robert J. McQueeney. Neutron-scattering measurements of spin excitations in LaFeAsO and $\text{Ba}(\text{Fe}_{0.953}\text{Co}_{0.047})_2\text{As}_2$: Evidence for a sharp enhancement of spin fluctuations by nematic order. *Phys. Rev. Lett.*, 114:057001, Feb 2015.
- [27] M. G. Kim, R. M. Fernandes, A. Kreyssig, J. W. Kim, A. Thaler, S. L. Bud'ko, P. C. Canfield, R. J. McQueeney, J. Schmalian, and A. I. Goldman. Character of the structural and magnetic phase

- transitions in the parent and electron-doped BaFe_2As_2 compounds. *Phys. Rev. B*, 83:134522, Apr 2011.
- [28] Rafael M. Fernandes, Daniel K. Pratt, Wei Tian, Jerel Zarestky, Andreas Kreyssig, Shibabrata Nandi, Min Gyu Kim, Alex Thaler, Ni Ni, Paul C. Canfield, Robert J. McQueeney, Jörg Schmalian, and Alan I. Goldman. Unconventional pairing in the iron arsenide superconductors. *Phys. Rev. B*, 81:140501, Apr 2010.
- [29] S. Nandi, M. G. Kim, A. Kreyssig, R. M. Fernandes, D. K. Pratt, A. Thaler, N. Ni, S. L. Bud'ko, P. C. Canfield, J. Schmalian, R. J. McQueeney, and A. I. Goldman. Anomalous suppression of the orthorhombic lattice distortion in superconducting $\text{Ba}(\text{Fe}_{1-x}\text{Co}_x)_2\text{As}_2$ single crystals. *Phys. Rev. Lett.*, 104:057006, Feb 2010.
- [30] I.I. Mazin and J. Schmalian. Pairing symmetry and pairing state in ferropnictides: Theoretical overview. *Physica C: Superconductivity*, 469(9-12):614 – 627, 2009. Superconductivity in Iron-Pnictides.
- [31] Anna Böhmer and Andreas Kreyssig. Eisenbasierte Vielfalt. *Physik in unserer Zeit*, 48(2):70–77, 2017.
- [32] Fong-Chi Hsu, Jiu-Yong Luo, Kuo-Wei Yeh, Ta-Kun Chen, Tzu-Wen Huang, Phillip M. Wu, Yong-Chi Lee, Yi-Lin Huang, Yan-Yi Chu, Der-Chung Yan, and Maw-Kuen Wu. Superconductivity in the PbO-type structure α -FeSe. *Proceedings of the National Academy of Sciences*, 105(38):14262–14264, 2008.
- [33] Serena Margadonna, Yasuhiro Takabayashi, Martin T. McDonald, Karolina Kasperkiewicz, Yoshikazu Mizuguchi, Yoshihiko Takano, Andrew N. Fitch, Emmanuelle Suard, and Kosmas Prassides. Crystal structure of the new FeSe_{1-x} superconductor. *Chem. Commun.*, pages 5607–5609, 2008.
- [34] T. M. McQueen, A. J. Williams, P. W. Stephens, J. Tao, Y. Zhu, V. Ksenofontov, F. Casper, C. Felser, and R. J. Cava. Tetragonal-to-orthorhombic structural phase transition at 90 K in the superconductor $\text{Fe}_{1.01}\text{Se}$. *Phys. Rev. Lett.*, 103:057002, Jul 2009.
- [35] M. Bendele, A. Amato, K. Conder, M. Elender, H. Keller, H.-H. Klauss, H. Luetkens, E. Pomjakushina, A. Raselli, and R. Khasanov. Pressure induced static magnetic order in superconducting FeSe_{1-x} . *Phys. Rev. Lett.*, 104:087003, Feb 2010.
- [36] Kiyotaka Miyoshi, Koh Morishita, Eriko Mutou, Masatoshi Kondo, Osamu Seida, Kenji Fujiwara, Jun Takeuchi, and Shijo Nishigori. Enhanced superconductivity on the tetragonal lattice in FeSe under hydrostatic pressure. *Journal of the Physical Society of Japan*, 83(1):013702, 2014.
- [37] M. Bendele, A. Ichsanow, Yu. Pashkevich, L. Keller, Th. Strässle, A. Gusev, E. Pomjakushina, K. Conder, R. Khasanov, and H. Keller. Coexistence of superconductivity and magnetism in FeSe_{1-x} under pressure. *Phys. Rev. B*, 85:064517, Feb 2012.
- [38] Yoshikazu Mizuguchi, Fumiaki Tomioka, Shunsuke Tsuda, Takahide Yamaguchi, and Yoshihiko Takano. Superconductivity at 27 K in tetragonal FeSe under high pressure. *Applied Physics Letters*, 93(15):152505, 2008.
- [39] S. Medvedev, T. M. McQueen, I. A. Troyan, T. Palasyuk, M. I. Erements, R. J. Cava, S. Naghavi, F. Casper, V. Ksenofontov, G. Wortmann, and C. Felser. Electronic and magnetic phase diagram of β - $\text{Fe}_{1.01}$ with superconductivity at 36.7 K under pressure. *Nature Mat.*, 8:630–633, 2009.
- [40] S. Margadonna, Y. Takabayashi, Y. Ohishi, Y. Mizuguchi, Y. Takano, T. Kagayama, T. Nakagawa, M. Takata, and K. Prassides. Pressure evolution of the low-temperature crystal structure and bonding of the superconductor FeSe ($T_c = 37$ K). *Phys. Rev. B*, 80:064506, Aug 2009.
- [41] G. Garbarino, A. Sow, P. Lejay, A. Sulpice, P. Toulemonde, M. Mezouar, and M. Nú nez Regueiro. High-temperature superconductivity (T_c onset at 34 K) in the high-pressure orthorhombic phase of FeSe. *EPL (Europhysics Letters)*, 86(2):27001, 2009.
- [42] Satoru Masaki, Hisashi Kotegawa, Yudai Hara, Hideki Tou, Keizo Murata, Yoshikazu Mizuguchi, and Yoshihiko Takano. Precise pressure dependence of the superconducting transition

- temperature of FeSe: Resistivity and ^{77}Se -NMR study. *Journal of the Physical Society of Japan*, 78(6):063704, 2009.
- [43] H. Okabe, N. Takeshita, K. Horigane, T. Muranaka, and J. Akimitsu. Pressure-induced high- T_c superconducting phase in FeSe: Correlation between anion height and T_c . *Phys. Rev. B*, 81:205119, May 2010.
- [44] Yoshikazu Mizuguchi, Fumiaki Tomioka, Shunsuke Tsuda, Takahide Yamaguchi, and Yoshihiko Takano. Substitution effects on FeSe superconductor. *Journal of the Physical Society of Japan*, 78(7):074712, 2009.
- [45] Wei Bao, Y. Qiu, Q. Huang, M. A. Green, P. Zajdel, M. R. Fitzsimmons, M. Zhernenkov, S. Chang, Minghu Fang, B. Qian, E. K. Vehstedt, Jinhu Yang, H. M. Pham, L. Spinu, and Z. Q. Mao. Tunable $(\delta\pi, \delta\pi)$ -type antiferromagnetic order in α -Fe(Te,Se) superconductors. *Phys. Rev. Lett.*, 102:247001, Jun 2009.
- [46] Xiaofang Lai, Hui Zhang, Yingqi Wang, Xin Wang, Xian Zhang, Jianhua Lin, and Fuqiang Huang. Observation of superconductivity in tetragonal FeS. *Journal of the American Chemical Society*, 137(32):10148–10151, 2015. PMID: 26244711.
- [47] Keita Deguchi, Yoshihiko Takano, and Yoshikazu Mizuguchi. Physics and chemistry of layered chalcogenide superconductors. *Science and Technology of Advanced Materials*, 13(5):054303, 2012.
- [48] Matthew Burrard-Lucas, David G. Free, Stefan J. Sedlmaier, Jack D. Wright, Simon J. Cassidy, Yoshiaki Hara, Alex J. Corkett, Tom Lancaster, Peter J. Baker, Stephen J. Blundell, and Simon J. Clarke. Enhancement of the superconducting transition temperature of FeSe by intercalation of a molecular spacer layer. *Nature Materials*, 12:15–19, 2013.
- [49] T. P. Ying, X. L. Chen, G. Wang, S. F. Jin, T. T. Zhou, X. F. Lai, H. Zhang, and W. Y. Wang. Observation of superconductivity at 30 ~ 46 K in $A_x\text{Fe}_2\text{Se}_2$ ($A = \text{Li, Na, Ba, Sr, Ca, Yb, and Eu}$). *Scientific Reports*, 2:426, 2012.
- [50] A. Krzton-Maziopa, V. Svitlyk, E. Pomjakushina, R. Puzniak, and K. Conder. Superconductivity in alkali metal intercalated iron selenides. *Journal of Physics: Condensed Matter*, 28(29):293002, 2016.
- [51] M V Sadvovskii. High-temperature superconductivity in FeSe monolayers. *Physics-Uspekhi*, 59(10):947, 2016.
- [52] Ziqiao Wang, Chaofei Liu, Yi Liu, and Jian Wang. High-temperature superconductivity in one-unit-cell FeSe films. *Journal of Physics: Condensed Matter*, 29(15):153001, 2017.
- [53] Dennis Huang and Jennifer E. Hoffman. Monolayer FeSe on SrTiO_3 . *Annual Review of Condensed Matter Physics*, 8(1):311–336, 2017.
- [54] Jian-Feng Ge, Zhi-Long Liu, Canhua Liu, Chun-Lei Gao, Dong Qian, Qi-Kun Xue, Ying Liu, and Jin-Feng Jia. Superconductivity above 100 K in single-layer FeSe films on doped SrTiO_3 . *Nature Materials*, 14:285–289, 2015.
- [55] Can-Li Song, Yi-Lin Wang, Ye-Ping Jiang, Zhi Li, Lili Wang, Ke He, Xi Chen, Xu-Cun Ma, and Qi-Kun Xue. Molecular-beam epitaxy and robust superconductivity of stoichiometric FeSe crystalline films on bilayer graphene. *Phys. Rev. B*, 84:020503, Jul 2011.
- [56] H. Okamoto. The Fe-Se (iron-selenium) system. *Journal of Phase Equilibria*, 12(3):383–389, 1991.
- [57] D. Braithwaite, B. Salce, G. Lapertot, F Bourdarot, C. Marin, D. Aoki, and M. Hanfland. Superconducting and normal phases of FeSe single crystals at high pressure. *Journal of Physics: Condensed Matter*, 21(23):232202, 2009.
- [58] E. Pomjakushina, K. Conder, V. Pomjakushin, M. Bendele, and R. Khasanov. Synthesis, crystal structure, and chemical stability of the superconductor FeSe_{1-x} . *Phys. Rev. B*, 80:024517, Jul 2009.
- [59] T. M. McQueen, Q. Huang, V. Ksenofontov, C. Felser, Q. Xu, H. Zandbergen, Y. S. Hor, J. Allred, A. J. Williams, D. Qu, J. Checkelsky, N. P. Ong, and R. J. Cava. Extreme sensitivity of superconductivity to stoichiometry in $\text{Fe}_{1+\delta}\text{Se}$. *Phys. Rev. B*, 79:014522, Jan 2009.

- [60] Ravhi S. Kumar, Yi Zhang, Stanislav Sinogeikin, Yuming Xiao, Sathish Kumar, Paul Chow, Andrew L. Cornelius, and Changfeng Chen. Crystal and electronic structure of FeSe at high pressure and low temperature. *The Journal of Physical Chemistry B*, 114(39):12597–12606, 2010.
- [61] S. B. Zhang, Y. P. Sun, X. D. Zhu, X. B. Zhu, B. S. Wang, G. Li, H. C. Lei, X. Luo, Z. R. Yang, W. H. Song, and J. M. Dai. Crystal growth and superconductivity of FeSe_x. *Superconductor Science and Technology*, 22(1):015020, 2008.
- [62] Rongwei Hu, Hechang Lei, Milinda Abeykoon, Emil S. Bozin, Simon J. L. Billinge, J. B. Warren, Theo Siegrist, and C. Petrovic. Synthesis, crystal structure, and magnetism of β -Fe_{1.00(2)}Se_{1.00(3)} single crystals. *Phys. Rev. B*, 83:224502, Jun 2011.
- [63] U. Patel, J. Hua, S. H. Yu, S. Avci, Z. L. Xiao, H. Claus, J. Schlueter, V. V. Vlasko-Vlasov, U. Welp, and W. K. Kwok. Growth and superconductivity of FeSe_x crystals. *Applied Physics Letters*, 94(8):082508, 2009.
- [64] Y. Hara, K. Takase, A. Yamasaki, H. Sato, N. Miyakawa, N. Umeyama, and S.I. Ikeda. Structural and physical properties of FeSe crystals fabricated by the chemical vapor transport method. *Physica C: Superconductivity*, 470, Supplement 1:S313 – S314, 2010. Proceedings of the 9th International Conference on Materials and Mechanisms of Superconductivity.
- [65] Dmitriy Chareev, Evgeniy Osadchii, Tatiana Kuzmicheva, Jiunn-Yuan Lin, Svetoslav Kuzmichev, Olga Volkova, and Alexander Vasiliev. Single crystal growth and characterization of tetragonal FeSe_{1-x} superconductors. *CrystEngComm*, 15:1989–1993, 2013.
- [66] A. E. Böhmer, F. Hardy, F. Eilers, D. Ernst, P. Adelman, P. Schweiss, T. Wolf, and C. Meingast. Lack of coupling between superconductivity and orthorhombic distortion in stoichiometric single-crystalline FeSe. *Phys. Rev. B*, 87:180505, May 2013.
- [67] A. E. Böhmer, V. Taufour, W. E. Straszheim, T. Wolf, and P. C. Canfield. Variation of transition temperatures and residual resistivity ratio in vapor-grown FeSe. *Phys. Rev. B*, 94:024526, Jul 2016.
- [68] Shigeru Kasahara, Tatsuya Watashige, Tetsuo Hanaguri, Yuhki Kohsaka, Takuya Yamashita, Yusuke Shimoyama, Yuta Mizukami, Ryota Endo, Hiroaki Ikeda, Kazushi Aoyama, Taichi Terashima, Shinya Uji, Thomas Wolf, Hilbert von Löhneysen, Takasada Shibauchi, and Yuji Matsuda. Field-induced superconducting phase of FeSe in the BCS-BEC cross-over. *Proc. Natl. Acad. Sci. USA*, 111(46):16309, 2014.
- [69] Mingwei Ma, Dongna Yuan, Yue Wu, Huaxue Zhou, Xiaoli Dong, and Fang Zhou. Flux-free growth of large superconducting crystal of FeSe by traveling-solvent floating-zone technique. *Superconductor Science and Technology*, 27(12):122001, 2014.
- [70] M.K. Wu, F.C. Hsu, K.W. Yeh, T.W. Huang, J.Y. Luo, M.J. Wang, H.H. Chang, T.K. Chen, S.M. Rao, B.H. Mok, C.L. Chen, Y.L. Huang, C.T. Ke, P.M. Wu, A.M. Chang, C.T. Wu, and T.P. Perng. The development of the superconducting PbO-type β -FeSe and related compounds. *Physica C: Superconductivity*, 469(9):340–349, 2009.
- [71] Yoshikazu Mizuguchi and Yoshihiko Takano. Review of Fe chalcogenides as the simplest Fe-based superconductor. *Journal of the Physical Society of Japan*, 79(10):102001, 2010.
- [72] David Joseph Singh. Superconductivity and magnetism in 11-structure iron chalcogenides in relation to the iron pnictides. *Science and Technology of Advanced Materials*, 13(5):054304, 2012.
- [73] Lorenzo Malavasi and Serena Margadonna. Structure-properties correlations in Fe chalcogenide superconductors. *Chem. Soc. Rev.*, 41:3897–3911, 2012.
- [74] Xu Liu, Lin Zhao, Shaolong He, Junfeng He, Defa Liu, Daixiang Mou, Bing Shen, Yong Hu, Jianwei Huang, and X J Zhou. Electronic structure and superconductivity of FeSe-related superconductors. *J. Phys.: Condens. Matter*, 27(18):183201, 2015.
- [75] Y. V. Pustovit and A. A. Kordyuk. Metamorphoses of electronic structure of FeSe-based superconductors (review article). *Low Temperature Physics*, 42:995, 2016.
- [76] A. I. Coldea and M. D. Watson. The key ingredients of the electronic structure of FeSe. *ArXiv*

- e-prints*, (Preprint 1706.00338), June 2017.
- [77] K. Kothapalli, A. E. Böhmer, W. T. Jayasekara, B. G. Ueland, P. Das, A. Sapkota, V. Taufour, Y. Xiao, E. E. Alp, S. L. Bud'ko, P. C. Canfield, A. Kreyssig, and A. I. Goldman. Strong cooperative coupling of pressure-induced magnetic order and nematicity in FeSe. *Nature Communications*, 7:12728, (Preprint 1603.04135), 2016.
- [78] A. E. Böhmer. (unpublished).
- [79] A. E. Böhmer, T. Arai, F. Hardy, T. Hattori, T. Iye, T. Wolf, H. v. Löhneysen, K. Ishida, and C. Meingast. Origin of the tetragonal-to-orthorhombic phase transition in FeSe: A combined thermodynamic and NMR study of nematicity. *Phys. Rev. Lett.*, 114:027001, Jan 2015.
- [80] S. Avci, O. Chmaissem, E. A. Goremychkin, S. Rosenkranz, J.-P. Castellan, D. Y. Chung, I. S. Todorov, J. A. Schlueter, H. Claus, M. G. Kanatzidis, A. Daoud-Aladine, D. Khalyavin, and R. Osborn. Magnetoelastic coupling in the phase diagram of $\text{Ba}_{1-x}\text{K}_x\text{Fe}_2\text{As}_2$ as seen via neutron diffraction. *Phys. Rev. B*, 83:172503, May 2011.
- [81] S. Karlsson, P. Strobel, A. Sulpice, C. Marcenat, M. Legendre, F. Gay, S. Pairis, O. Leynaud, and P. Toulemonde. Study of high-quality superconducting FeSe single crystals: crossover in electronic transport from a metallic to an activated regime above 350 K. *Superconductor Science and Technology*, 28(10):105009, 2015.
- [82] M. A. Tanatar, A. E. Böhmer, E. I. Timmons, M. Schütt, G. Drachuck, V. Taufour, K. Kothapalli, A. Kreyssig, S. L. Bud'ko, P. C. Canfield, R. M. Fernandes, and R. Prozorov. Origin of the resistivity anisotropy in the nematic phase of FeSe. *Phys. Rev. Lett.*, 117:127001, Sep 2016.
- [83] S.-H. Baek, D. V. Efremov, J. M. Ok, J. S. Kim, Jeroen van den Brink, and B. Büchner. Orbital-driven nematicity in FeSe. *Nature Materials*, 14:210–214, 2015.
- [84] M. A. Tanatar, E. C. Blomberg, A. Kreyssig, M. G. Kim, N. Ni, A. Thaler, S. L. Bud'ko, P. C. Canfield, A. I. Goldman, I. I. Mazin, and R. Prozorov. Uniaxial-strain mechanical detwinning of CaFe_2As_2 and BaFe_2As_2 crystals: Optical and transport study. *Phys. Rev. B*, 81:184508, May 2010.
- [85] S. Ishida, M. Nakajima, T. Liang, K. Kihou, C. H. Lee, A. Iyo, H. Eisaki, T. Kakeshita, Y. Tomioka, T. Ito, and S. Uchida. Anisotropy of the in-plane resistivity of underdoped $\text{Ba}(\text{Fe}_{1-x}\text{Co}_x)_2\text{As}_2$ superconductors induced by impurity scattering in the antiferromagnetic orthorhombic phase. *Phys. Rev. Lett.*, 110:207001, May 2013.
- [86] Hisashi Kotegawa, Satoru Masaki, Yoshiki Awai, Hideki Tou, Yoshikazu Mizuguchi, and Yoshihiko Takano. Evidence for unconventional superconductivity in arsenic-free iron-based superconductor FeSe: A ^{77}Se -NMR study. *J. Phys. Soc. Jpn.*, 77:113703, 2008.
- [87] T. Imai, K. Ahilan, F. L. Ning, T. M. McQueen, and R. J. Cava. Why does undoped FeSe become a high- T_c superconductor under pressure? *Phys. Rev. Lett.*, 102:177005, Apr 2009.
- [88] S.-H. Baek, D. V. Efremov, J. M. Ok, J. S. Kim, Jeroen van den Brink, and B. Büchner. Nematicity and in-plane anisotropy of superconductivity in β -FeSe detected by ^{77}Se nuclear magnetic resonance. *Phys. Rev. B*, 93:180502, May 2016.
- [89] P. S. Wang, S. S. Sun, Y. Cui, W. H. Song, T. R. Li, Rong Yu, Hechang Lei, and Weiqiang Yu. Pressure induced stripe-order antiferromagnetism and first-order phase transition in FeSe. *Phys. Rev. Lett.*, 117:237001, Nov 2016.
- [90] Q. Wang, Y. Shen, B. Pan, Y. Hao, M. Ma, F. Zhou, P. Steffens, K. Schmalzl, T. R. Forrest, M. Abdel-Hafiez, X. Chen, D. A. Chareev, A. N. Vasiliev, P. Bourges, Y. Sidis, H. Cao, and J. Zhao. Strong interplay between stripe spin fluctuations, nematicity and superconductivity in FeSe. *Nature Materials*, 15:159–163, 2016.
- [91] Fa Wang, Steven A. Kivelson, and Dung-Hai Lee. Nematicity and quantum paramagnetism in FeSe. *Nat. Phys.*, 11(11):959–963, Nov 2015. Article.
- [92] M. Chinotti, A. Pal, L. Degiorgi, A. E. Böhmer, and P. C. Canfield. Optical anisotropy in the electronic nematic phase of FeSe. *Phys. Rev. B*, 96:121112, Sep 2017.
- [93] Chih-Wei Luo, Po Chung Cheng, Shun-Hung Wang, Jen-Che Chiang, Jiunn-Yuan Lin, Kaung-Hsiung Wu, Jenh-Yih Juang, Dmitry A. Chareev, Olga S. Volkova, and Alexander N. Vasiliev.

- Unveiling the hidden nematicity and spin subsystem in FeSe. *npj Quantum Materials*, 2(1):32–, 2017.
- [94] M. He, L. Wang, F. Hardy, L. Xu, T. Wolf, P. Adelmann, and C. Meingast. Evidence for short-range magnetic order in the nematic phase of FeSe from anisotropic in-plane magnetostriction and susceptibility measurements. *ArXiv e-prints*, (Preprint 1709.03861), 2017.
- [95] Suguru Hosoi, Kohei Matsuura, Kousuke Ishida, Hao Wang, Yuta Mizukami, Tatsuya Watashige, Shigeru Kasahara, Yuji Matsuda, and Takasada Shibauchi. Nematic quantum critical point without magnetism in $\text{FeSe}_{1-x}\text{S}_x$ superconductors. *Proceedings of the National Academy of Sciences*, 113(29):8139–8143, 2016.
- [96] Pierre Massat, Donato Farina, Indranil Paul, Sandra Karlsson, Pierre Strobel, Pierre Toulemonde, Marie-Aude Méasson, Maximilien Cazayous, Alain Sacuto, Shigeru Kasahara, Takasada Shibauchi, Yuji Matsuda, and Yann Gallais. Charge-induced nematicity in FeSe. *Proceedings of the National Academy of Sciences*, 113(33):9177–9181, 2016.
- [97] Anna E. Böhrer and Christoph Meingast. Electronic nematic susceptibility of iron-based superconductors. *Comptes Rendus Physique*, 17:90 – 112, 2016. Iron-based superconductors / Supraconducteurs à base de fer.
- [98] Jiun-Haw Chu, Hsueh-Hui Kuo, James G. Analytis, and Ian R. Fisher. Divergent nematic susceptibility in an iron arsenide superconductor. *Science*, 337(6095):710–712, 2012.
- [99] Hsueh-Hui Kuo, Maxwell C. Shapiro, Scott C. Riggs, and Ian R. Fisher. Measurement of the elastoresistivity coefficients of the underdoped iron arsenide $\text{Ba}(\text{Fe}_{0.975}\text{Co}_{0.025})_2\text{As}_2$. *Phys. Rev. B*, 88:085113, Aug 2013.
- [100] Hsueh-Hui Kuo, Jiun-Haw Chu, Johanna C. Palmstrom, Steven A. Kivelson, and Ian R. Fisher. Ubiquitous signatures of nematic quantum criticality in optimally doped Fe-based superconductors. *Science*, 352(6288):958–962, 2016.
- [101] M. D. Watson, T. K. Kim, A. A. Haghighirad, N. R. Davies, A. McCollam, A. Narayanan, S. F. Blake, Y. L. Chen, S. Ghannadzadeh, A. J. Schofield, M. Hoesch, C. Meingast, T. Wolf, and A. I. Coldea. Emergence of the nematic electronic state in FeSe. *Phys. Rev. B*, 91:155106, Apr 2015.
- [102] G. A. Zvyagina, T. N. Gaydamak, K. R. Zhekov, I. V. Bilich, V. D. Fil, D. A. Chareev, and A. N. Vasiliev. Acoustic characteristics of FeSe single crystals. *EPL (Europhysics Letters)*, 101(5):56005, 2013.
- [103] R. M. Fernandes, L. H. VanBebber, S. Bhattacharya, P. Chandra, V. Keppens, D. Mandrus, M. A. McGuire, B. C. Sales, A. S. Sefat, and J. Schmalian. Effects of nematic fluctuations on the elastic properties of iron arsenide superconductors. *Phys. Rev. Lett.*, 105:157003, Oct 2010.
- [104] A. E. Böhrer, P. Burger, F. Hardy, T. Wolf, P. Schweiss, R. Fromknecht, M. Reinecker, W. Schranz, and C. Meingast. Nematic susceptibility of hole-doped and electron-doped BaFe_2As_2 iron-based superconductors from shear modulus measurements. *Phys. Rev. Lett.*, 112:047001, Jan 2014.
- [105] Y. Gallais, R. M. Fernandes, I. Paul, L. Chauvière, Y.-X. Yang, M.-A. Méasson, M. Cazayous, A. Sacuto, D. Colson, and A. Forget. Observation of incipient charge nematicity in $\text{Ba}(\text{Fe}_{1-x}\text{Co}_x)_2\text{As}_2$. *Phys. Rev. Lett.*, 111:267001, Dec 2013.
- [106] Yann Gallais and Indranil Paul. Charge nematicity and electronic Raman scattering in iron-based superconductors. *Comptes Rendus Physique*, 17(1-2):113 – 139, 2016.
- [107] M. D. Watson, T. K. Kim, L. C. Rhodes, M. Eschrig, M. Hoesch, A. A. Haghighirad, and A. I. Coldea. Evidence for unidirectional nematic bond ordering in FeSe. *Phys. Rev. B*, 94:201107, Nov 2016.
- [108] Y. Suzuki, T. Shimojima, T. Sonobe, A. Nakamura, M. Sakano, H. Tsuji, J. Omachi, K. Yoshioka, M. Kuwata-Gonokami, T. Watashige, R. Kobayashi, S. Kasahara, T. Shibauchi, Y. Matsuda, Y. Yamakawa, H. Kontani, and K. Ishizaka. Momentum-dependent sign inversion of orbital order in superconducting FeSe. *Phys. Rev. B*, 92:205117, Nov 2015.

- [109] Matthew D Watson, Amir A Haghighirad, Luke C Rhodes, Moritz Hoesch, and Timur K Kim. Electronic anisotropies revealed by detwinned angle-resolved photo-emission spectroscopy measurements of FeSe. *New Journal of Physics*, 19(10):103021, 2017.
- [110] K. K. Huynh, Y. Tanabe, T. Urata, H. Oguro, S. Heguri, K. Watanabe, and K. Tanigaki. Electric transport of a single-crystal iron chalcogenide fese superconductor: Evidence of symmetry-breakdown nematicity and additional ultrafast dirac cone-like carriers. *Phys. Rev. B*, 90:144516, Oct 2014.
- [111] S. Knöner, D. Zielke, S. Köhler, B. Wolf, Th. Wolf, L. Wang, A. Böhmer, C. Meingast, and M. Lang. Resistivity and magnetoresistance of FeSe single crystals under helium-gas pressure. *Phys. Rev. B*, 91:174510, May 2015.
- [112] Yue Sun, Tatsuhiko Yamada, Sunseng Pyon, and Tsuyoshi Tamegai. Structural-transition-induced quasi-two-dimensional Fermi surface in FeSe. *Phys. Rev. B*, 94:134505, Oct 2016.
- [113] Yue Sun, Sunseng Pyon, and Tsuyoshi Tamegai. Electron carriers with possible Dirac-cone-like dispersion in FeSe_{1-x}S_x ($x = 0$ and 0.14) single crystals triggered by structural transition. *Phys. Rev. B*, 93:104502, Mar 2016.
- [114] Taichi Terashima, Naoki Kikugawa, Shigeru Kasahara, Tatsuya Watashige, Yuji Matsuda, Takasada Shibauchi, and Shinya Uji. Magnetotransport study of the pressure-induced antiferromagnetic phase in FeSe. *Phys. Rev. B*, 93:180503, May 2016.
- [115] M. D. Watson, T. Yamashita, S. Kasahara, W. Knafo, M. Nardone, J. Béard, F. Hardy, A. McCollam, A. Narayanan, S. F. Blake, T. Wolf, A. A. Haghighirad, C. Meingast, A. J. Schofield, H. v. Löhneysen, Y. Matsuda, A. I. Coldea, and T. Shibauchi. Dichotomy between the hole and electron behavior in multiband superconductor FeSe probed by ultrahigh magnetic fields. *Phys. Rev. Lett.*, 115:027006, Jul 2015.
- [116] Y. A. Ovchencov, D. A. Chareev, V. A. Kulbachinskii, V. G. Kytin, D. E. Presnov, O. S. Volkova, and A. N. Vasiliev. Highly mobile carriers in iron-based superconductors. *Superconductor Science and Technology*, 30(3):035017, 2017.
- [117] L. C. Rhodes, M. D. Watson, A. A. Haghighirad, M. Eschrig, and T. K. Kim. Strongly enhanced temperature dependence of the chemical potential in FeSe. *Phys. Rev. B*, 95:195111, May 2017.
- [118] Y. S. Kushnirenko, A. A. Kordyuk, A. V. Fedorov, E. Haubold, T. Wolf, B. Büchner, and S. V. Borisenko. Anomalous temperature evolution of the electronic structure of FeSe. *Phys. Rev. B*, 96:100504, Sep 2017.
- [119] Taichi Terashima, Naoki Kikugawa, Anshika Kiswandhi, Eun-Sang Choi, James S. Brooks, Shigeru Kasahara, Tatsuya Watashige, Hiroaki Ikeda, Takasada Shibauchi, Yuji Matsuda, Thomas Wolf, Anna E. Böhmer, Frédéric Hardy, Christoph Meingast, Hilbert v. Löhneysen, Michi-To Suzuki, Ryotaro Arita, and Shinya Uji. Anomalous Fermi surface in FeSe seen by Shubnikov - de Haas oscillation measurements. *Phys. Rev. B*, 90:144517, 2014.
- [120] Alain Audouard, Fabienne Duc, Loïc Drigo, Pierre Toulemonde, Sandra Karlsson, Pierre Strobel, and André Sulpice. Quantum oscillations and upper critical magnetic field of the iron-based superconductor FeSe. *Europhys. Lett.*, 109(2):27003, 2015.
- [121] P. Zhang, T. Qian, P. Richard, X. P. Wang, H. Miao, B. Q. Lv, B. B. Fu, T. Wolf, C. Meingast, X. X. Wu, Z. Q. Wang, J. P. Hu, and H. Ding. Observation of two distinct d_{xz}/d_{yz} band splittings in FeSe. *Phys. Rev. B*, 91:214503, Jun 2015.
- [122] S. V. Borisenko, D. V. Evtushinsky, Z.-H. Liu, I. Morozov, R. Kappenberger, S. Wurmehl, B. Büchner, A. N. Yaresko, T. K. Kim, M. Hoesch, T. Wolf, and N. D. Zhigadlo. Direct observation of spin-orbit coupling in iron-based superconductors. *Nat Phys*, 12(4):311–317, April 2016.
- [123] Matthew D. Watson, Amir A. Haghighirad, Hitoshi Takita, Wumiti Mansuer, Hideaki Iwasawa, Eike F. Schwier, Akihiro Ino, and Moritz Hoesch. Shifts and splittings of the hole bands in the nematic phase of FeSe. *Journal of the Physical Society of Japan*, 86(5):053703, 2017.
- [124] A. Fedorov, A. Yaresko, T. K. Kim, Y. Kushnirenko, E. Haubold, T. Wolf, M. Hoesch, A. Grüneis, B. Büchner, and S. V. Borisenko. Effect of nematic ordering on electronic structure of FeSe.

- Scientific Reports*, 6:36834, 2016.
- [125] T. Shimojima, Y. Suzuki, T. Sonobe, A. Nakamura, M. Sakano, J. Omachi, K. Yoshioka, M. Kuwata-Gonokami, K. Ono, H. Kumigashira, A. E. Böhmer, F. Hardy, T. Wolf, C. Meingast, H. v. Löhneysen, H. Ikeda, and K. Ishizaka. Lifting of xz / yz orbital degeneracy at the structural transition in detwinned FeSe. *Phys. Rev. B*, 90:121111, Sep 2014.
- [126] K. Nakayama, Y. Miyata, G.N. Phan, T. Sato, Y. Tanabe, T. Urata, K. Tanigaki, and T. Takahashi. Reconstruction of band structure induced by electronic nematicity in an FeSe superconductor. *Phys. Rev. Lett.*, 113:237001, Dec 2014.
- [127] Laura Fanfarillo, Joseph Mansart, Pierre Toulemonde, Hervé Cercellier, Patrick Le Fèvre, François Bertran, Belen Valenzuela, Lara Benfatto, and Véronique Brouet. Orbital-dependent Fermi surface shrinking as a fingerprint of nematicity in FeSe. *Phys. Rev. B*, 94:155138, Oct 2016.
- [128] P. O. Sprau, A. Kostin, A. Kreisel, A. E. Böhmer, V. Taufour, P. C. Canfield, S. Mukherjee, P. J. Hirschfeld, B. M. Andersen, and J. C. Séamus Davis. Discovery of orbital-selective Cooper pairing in FeSe. *Science*, 357(6346):75–80, 2017.
- [129] Qisi Wang, Yao Shen, Bingying Pan, Xiaowen Zhang, K. Ikeuchi, K. Iida, A. D. Christianson, H. C. Walker, D. T. Adroja, M. Abdel-Hafiez, Xiaojia Chen, D. A. Chareev, A. N. Vasiliev, and Jun Zhao. Magnetic ground state of FeSe. *Nat. Comm.*, 7:12182, Jul 2016.
- [130] Hisashi Kotegawa and Masaki Fujita. Magnetic excitations in iron chalcogenide superconductors. *Science and Technology of Advanced Materials*, 13(5):054302, 2012.
- [131] M. C. Rahn, R. A. Ewings, S. J. Sedlmaier, S. J. Clarke, and A. T. Boothroyd. Strong $(\pi, 0)$ spin fluctuations in β -FeSe observed by neutron spectroscopy. *Phys. Rev. B*, 91:180501, May 2015.
- [132] Mingwei Ma, Philippe Bourges, Yvan Sidis, Yang Xu, Shiyang Li, Biaoyan Hu, Jiarui Li, Fa Wang, and Yuan Li. Prominent role of spin-orbit coupling in FeSe revealed by inelastic neutron scattering. *Phys. Rev. X*, 7:021025, May 2017.
- [133] David Vaknin. Magnetic nematicity: A debated origin. *Nat Mater*, 15(2):131–132, Feb 2016. News and Views.
- [134] A. Baum, H. N. Ruiz, N. Lazarević, Y. Wang, T. Böhm, R. Hosseinian Ahangharnejhad, P. Adelman, T. Wolf, Z. V. Popović, B. Moritz, T. P. Devereaux, and R. Hackl. Frustrated spin order and stripe fluctuations in FeSe. *ArXiv e-prints*, (Preprint 1709.08998), sep 2017.
- [135] W.-L. Zhang, S.-F. Wu, S. Kasahara, T. Shibauchi, Y. Matsuda, and G. Blumberg. Stripe quadrupole order in the nematic phase of FeSe $_{1-x}$ S $_x$. *ArXiv e-prints*, (Preprint 1710.09892), October 2017.
- [136] J. K. Glasbrenner, I. I. Mazin, H. O. Jeschke, P. J. Hirschfeld, R. M. Fernandes, and R. Valentí. Effect of magnetic frustration on nematicity and superconductivity in iron chalcogenides. *Nature Physics*, 11:953–958, 2015.
- [137] Taichi Terashima, Naoki Kikugawa, Shigeru Kasahara, Tatsuya Watashige, Takasada Shibauchi, Yuji Matsuda, Thomas Wolf, Anna E. Böhmer, Frédéric Hardy, Christoph Meingast, Hilbert v. Löhneysen, and Shinya Uji. Pressure-induced antiferromagnetic transition and phase diagram in FeSe. *Journal of the Physical Society of Japan*, 84(6):063701, 2015.
- [138] J. P. Sun, K. Matsuura, G. Z. Ye, Y. Mizukami, M. Shimozawa, K. Matsubayashi, M. Yamashita, T. Watashige, S. Kasahara, Y. Matsuda, J. Q. Yan, B. C. Sales, Y. Uwatoko, J. G. Cheng, and T. Shibauchi. Dome-shaped magnetic order competing with high-temperature superconductivity at high pressures in FeSe. *Nature Communications*, 7:12146, July 2016.
- [139] V. Svitlyk, M. Raba, V. Dmitriev, P. Rodière, P. Toulemonde, D. Chernyshov, and M. Mezouar. Complex biphasic nature of the superconducting dome of the FeSe phase diagram. *Phys. Rev. B*, 96:014520, Jul 2017.
- [140] Taichi Terashima, Naoki Kikugawa, Andhika Kiswandhi, David Graf, Eun-Sang Choi, James S. Brooks, Shigeru Kasahara, Tatsuya Watashige, Yuji Matsuda, Takasada Shibauchi, Thomas Wolf, Anna E. Böhmer, Frédéric Hardy, Christoph Meingast, Hilbert v. Löhneysen, and Shinya

- Uji. Fermi surface reconstruction in FeSe under high pressure. *Phys. Rev. B*, 93:094505, Mar 2016.
- [141] Rustem Khasanov, Zurab Guguchia, Alex Amato, Elvezio Morenzoni, Xiaoli Dong, Fang Zhou, and Zhongxian Zhao. Pressure-induced magnetic order in FeSe: A muon spin rotation study. *Phys. Rev. B*, 95:180504, May 2017.
- [142] P. Wiecki, M. Nandi, A. E. Böhmer, S. L. Bud'ko, P. C. Canfield, and Y. Furukawa. NMR evidence for static local nematicity and its cooperative interplay with low-energy magnetic fluctuations in FeSe under pressure. *Phys. Rev. B*, 96:180502, Nov 2017.
- [143] P. S. Wang, P. Zhou, S. S. Sun, Y. Cui, T. R. Li, Hechang Lei, Ziqiang Wang, and Weiqiang Yu. Robust short-range-ordered nematicity in FeSe evidenced by high-pressure NMR. *Phys. Rev. B*, 96:094528, Sep 2017.
- [144] J.-Y. Lin, Y. S. Hsieh, D. A. Chareev, A. N. Vasiliev, Y. Parsons, and H. D. Yang. Coexistence of isotropic and extended s -wave order parameters in FeSe as revealed by low-temperature specific heat. *Phys. Rev. B*, 84:220507, Dec 2011.
- [145] P. Bourgeois-Hope, S. Chi, D. A. Bonn, R. Liang, W. N. Hardy, T. Wolf, C. Meingast, N. Doiron-Leyraud, and Louis Taillefer. Thermal conductivity of the iron-based superconductor FeSe: Nodeless gap with a strong two-band character. *Phys. Rev. Lett.*, 117:097003, Aug 2016.
- [146] T. Watashige, Y. Tsutsumi, T. Hanaguri, Y. Kohsaka, S. Kasahara, A. Furusaki, M. Sigrist, C. Meingast, T. Wolf, H. v. Löhneysen, T. Shibauchi, and Y. Matsuda. Evidence for time-reversal symmetry breaking of the superconducting state near twin-boundary interfaces in FeSe revealed by scanning tunneling spectroscopy. *Phys. Rev. X*, 5:031022, Aug 2015.
- [147] Matevž Majcen Hrovat, Peter Jeglič, Martin Klanjšek, Takehiro Hatakeda, Takashi Noji, Yoichi Tanabe, Takahiro Urata, Khuong K. Huynh, Yoji Koike, Katsumi Tanigaki, and Denis Arčon. Enhanced superconducting transition temperature in hyper-interlayer-expanded FeSe despite the suppressed electronic nematic order and spin fluctuations. *Phys. Rev. B*, 92:094513, Sep 2015.
- [148] S. N. Rebec, T. Jia, C. Zhang, M. Hashimoto, D.-H. Lu, R. G. Moore, and Z.-X. Shen. Coexistence of replica bands and superconductivity in FeSe monolayer films. *Phys. Rev. Lett.*, 118:067002, Feb 2017.
- [149] Q.-Y. Wang, Z. Li, W.-H. Zhang, Z.-C. Zhang, J.-S. Zhang, W. Li, H. Ding, Y.-B. OU, P. Deng, K. Chang, J. Wen, C.-L. Song, K. He, J.-F. Jia, S.-H. Ji, Y.-Y. Wang, L.-L. Wang, X. Chen, X.-C. Ma, and Q.-K. Xue. Interface-induced high-temperature superconductivity in single unit-cell FeSe films on SrTiO₃. *Chin. Phys. Lett.*, 29:037402, 2012.
- [150] P. J. Hirschfeld, D. Altenfeld, I. Eremin, and I. I. Mazin. Robust determination of the superconducting gap sign structure via quasiparticle interference. *Phys. Rev. B*, 92:184513, Nov 2015.
- [151] Johannes H. J. Martiny, Andreas Kreisel, P. J. Hirschfeld, and Brian M. Andersen. Robustness of a quasiparticle interference test for sign-changing gaps in multiband superconductors. *Phys. Rev. B*, 95:184507, May 2017.
- [152] Lin Jiao, Sahana Rößler, Cevriye Koz, Ulrich Schwarz, Deepa Kasinathan, Ulrich K. Rößler, and Steffen Wirth. Impurity-induced bound states inside the superconducting gap of FeSe. *Phys. Rev. B*, 96:094504, Sep 2017.
- [153] S. Gerber, S.-L. Yang, D. Zhu, H. Soifer, J. A. Sobota, S. Rebec, J. J. Lee, T. Jia, B. Moritz, C. Jia, A. Gauthier, Y. Li, D. Leuenberger, Y. Zhang, L. Chaix, W. Li, H. Jang, J.-S. Lee, M. Yi, G. L. Dakovski, S. Song, J. M. Glowina, S. Nelson, K. W. Kim, Y.-D. Chuang, Z. Hussain, R. G. Moore, T. P. Devereaux, W.-S. Lee, P. S. Kirchmann, and Z.-X. Shen. Femtosecond electron-phonon lock-in by photoemission and x-ray free-electron laser. *Science*, 357(6346):71–75, 2017.
- [154] S. Kasahara, T. Yamashita, A. Shi, R. Kobayashi, Y. Shimoyama, T. Watashige, K. Ishida, T. Terashima, T. Wolf, F. Hardy, C. Meingast, H. v. Löhneysen, A. Levchenko, T. Shibauchi, and Y. Matsuda. Giant superconducting fluctuations in the compensated semimetal FeSe at

- the BCS-BEC crossover. *Nature Communications*, 7:12843, 2016.
- [155] Tatsuya Watashige, Stevan Arsenijević, Takuya Yamashita, Daiki Terazawa, Takafumi Onishi, Lars Opherden, Shigeru Kasahara, Yoshifumi Tokiwa, Yuichi Kasahara, Takasada Shibauchi, Hilbert von Löhneysen, Jochen Wosnitzer, and Yuji Matsuda. Quasiparticle excitations in the superconducting state of FeSe probed by thermal Hall conductivity in the vicinity of the BCS-BEC crossover. *Journal of the Physical Society of Japan*, 86(1):014707, 2017.
- [156] Y. Lubashevsky, E. Lahoud, K. Chashka, D. Podolsky, and A. Kanigel. Shallow pockets and very strong coupling superconductivity in $\text{FeSe}_x\text{Te}_{1-x}$. *Nature Physics*, 8:309–312, 2012.
- [157] K. Okazaki, Y. Ito, Y. Ota, Y. Kotani, T. Shimojima, T. Kiss, S. Watanabe, C.-T. Chen, S. Niitaka, T. Hanaguri, H. Takagi, A. Chainani, and S. Shin. Superconductivity in an electron band just above the Fermi level: possible route to BCS-BEC superconductivity. *Scientific Reports*, 4:4109, 2014.
- [158] M. Abdel-Hafiez, J. Ge, A. N. Vasiliev, D. A. Chareev, J. Van de Vondel, V. V. Moshchalkov, and A. V. Silhanek. Temperature dependence of lower critical field $H_{c1}(T)$ shows nodeless superconductivity in FeSe. *Phys. Rev. B*, 88:174512, Nov 2013.
- [159] Yu. G. Naidyuk, O. E. Kvitnitskaya, N. V. Gamayunova, D. L. Bashlakov, L. V. Tyutrina, G. Fuchs, R. Hühne, D. A. Chareev, and A. N. Vasiliev. Superconducting gaps in FeSe studied by soft point-contact Andreev reflection spectroscopy. *Phys. Rev. B*, 96:094517, Sep 2017.
- [160] Y. Sun, S. Kittaka, S. Nakamura, T. Sakakibara, K. Irie, T. Nomoto, K. Machida, J. Chen, and T. Tamegai. Gap structure of FeSe determined by field-angle-resolved specific heat measurements. *ArXiv e-prints*, (Preprint 1707.00547), July 2017.
- [161] Can-Li Song, Yi-Lin Wang, Ye-Ping Jiang, Lili Wang, Ke He, Xi Chen, Jennifer E. Hoffman, Xu-Cun Ma, and Qi-Kun Xue. Suppression of superconductivity by twin boundaries in FeSe. *Phys. Rev. Lett.*, 109:137004, Sep 2012.
- [162] Hsiang-Hsuan Hung, Can-Li Song, Xi Chen, Xucun Ma, Qi-kun Xue, and Congjun Wu. Anisotropic vortex lattice structures in the FeSe superconductor. *Phys. Rev. B*, 85:104510, Mar 2012.
- [163] Lin Jiao, Chien-Lung Huang, Sahana Rößler, Cevriye Koz, Ulrich K. Rößler, Ulrich Schwarz, and Steffen Wirth. Superconducting gap structure of FeSe. *Scientific Reports*, 7:44024 EP –, Mar 2017. Article.
- [164] Meng Li, N. R. Lee-Hone, Shun Chi, Ruixing Liang, W. N. Hardy, D. A. Bonn, E. Girt, and D. M. Broun. Superfluid density and microwave conductivity of FeSe superconductor: ultra-long-lived quasiparticles and extended s-wave energy gap. *New J. Phys.*, 18(8):082001, 2016.
- [165] S. Teknowijoyo, K. Cho, M. A. Tanatar, J. Gonzales, A. E. Böhmer, O. Cavani, V. Mishra, P. J. Hirschfeld, S. L. Bud’ko, P. C. Canfield, and R. Prozorov. Enhancement of superconducting transition temperature by pointlike disorder and anisotropic energy gap in FeSe single crystals. *Phys. Rev. B*, 94:064521, Aug 2016.
- [166] Liran Wang, Frédéric Hardy, Thomas Wolf, Peter Adelman, Rainer Fromknecht, Peter Schweiss, and Christoph Meingast. Superconductivity-enhanced nematicity and “s+d” gap symmetry in $\text{Fe}(\text{Se}_{1-x}\text{S}_x)$. *physica status solidi (b)*, 254(1):1600153–n/a, 2017.
- [167] Guan-Yu Chen, Xiyu Zhu, Huan Yang, and Hai-Hu Wen. Highly anisotropic superconducting gaps and possible evidence of antiferromagnetic order in FeSe single crystals. *Phys. Rev. B*, 96:064524, Aug 2017.
- [168] Yue Sun, Akiyoshi Park, Sunseng Pyon, Tsuyoshi Tamegai, and Hisashi Kitamura. Symmetry-unprotected nodes or gap minima in the s_{++} state of monocrystalline FeSe. *Phys. Rev. B*, 96:140505, Oct 2017.
- [169] Can-Li Song, Yi-Lin Wang, Peng Cheng, Ye-Ping Jiang, Wei Li, Tong Zhang, Zhi Li, Ke He, Lili Wang, Jin-Feng Jia, Hsiang-Hsuan Hung, Congjun Wu, Xucun Ma, Xi Chen, and Qi-Kun Xue. Direct observation of nodes and twofold symmetry in FeSe superconductor. *Science*, 332(6036):1410–1413, 2011.
- [170] H. C. Xu, X. H. Niu, D. F. Xu, J. Jiang, Q. Yao, Q. Y. Chen, Q. Song, M. Abdel-Hafiez, D. A.

- Chareev, A. N. Vasiliev, Q. S. Wang, H. L. Wo, J. Zhao, R. Peng, and D. L. Feng. Highly anisotropic and twofold symmetric superconducting gap in nematically ordered $\text{FeSe}_{0.93}\text{S}_{0.07}$. *Phys. Rev. Lett.*, 117:157003, Oct 2016.
- [171] S. Ran, S. L. Bud'ko, W. E. Straszheim, J. Soh, M. G. Kim, A. Kreyssig, A. I. Goldman, and P. C. Canfield. Control of magnetic, nonmagnetic, and superconducting states in annealed $\text{Ca}(\text{Fe}_{1-x}\text{Co}_x)_2\text{As}_2$. *Phys. Rev. B*, 85:224528, Jun 2012.
- [172] K. Y. Yip, Y. C. Chan, Q. Niu, K. Matsuura, Y. Mizukami, S. Kasahara, Y. Matsuda, T. Shibauchi, and Swee K. Goh. Weakening of the diamagnetic shielding in $\text{FeSe}_{1-x}\text{S}_x$ at high pressures. *Phys. Rev. B*, 96:020502, Jul 2017.
- [173] M. H. Fang, H. M. Pham, B. Qian, T. J. Liu, E. K. Vehstedt, Y. Liu, L. Spinu, and Z. Q. Mao. Superconductivity close to magnetic instability in $\text{Fe}(\text{Se}_{1-x}\text{Te}_x)_{0.82}$. *Phys. Rev. B*, 78:224503, Dec 2008.
- [174] P. Reiss, M. D. Watson, T. K. Kim, A. A. Haghighirad, D. N. Woodruff, M. Bruma, S. J. Clarke, and A. I. Coldea. Suppression of electronic correlations by chemical pressure from FeSe to FeS. *Phys. Rev. B*, 96:121103, Sep 2017.
- [175] T. Urata, Y. Tanabe, K. K. Huynh, Y. Yamakawa, H. Kontani, and K. Tanigaki. Superconductivity pairing mechanism from cobalt impurity doping in FeSe: Spin (s_{\pm}) or orbital (s_{++}) fluctuation. *Phys. Rev. B*, 93:014507, Jan 2016.
- [176] Nathalie C. Gresty, Yasuhiro Takabayashi, Alexey Y. Ganin, Martin T. McDonald, John B. Claridge, Duong Giap, Yoshikazu Mizuguchi, Yoshihiko Takano, Tomoko Kagayama, Yasuo Ohishi, Masaki Takata, Matthew J. Rosseinsky, Serena Margadonna, and Kosmas Prassides. Structural phase transitions and superconductivity in $\text{Fe}_{1+\delta}\text{Se}_{0.57}\text{Te}_{0.43}$ at ambient and elevated pressures. *Journal of the American Chemical Society*, 131(46):16944–16952, 2009.
- [177] S. Rößler, Dona Cherian, W. Lorenz, M. Doerr, C. Koz, C. Curfs, Yu. Prots, U. K. Rößler, U. Schwarz, Suja Elizabeth, and S. Wirth. First-order structural transition in the magnetically ordered phase of $\text{Fe}_{1.13}\text{Te}$. *Phys. Rev. B*, 84:174506, Nov 2011.
- [178] Cevriye Koz, Sahana Rößler, Alexander A. Tsirlin, Steffen Wirth, and Ulrich Schwarz. Low-temperature phase diagram of Fe_{1+y}Te studied using x-ray diffraction. *Phys. Rev. B*, 88:094509, Sep 2013.
- [179] M. Tegel, C. Löhnert, and D. Johrendt. The crystal structure of $\text{FeSe}_{0.44}\text{Te}_{0.56}$. *Solid State Communications*, 150(9-10):383 – 385, 2010.
- [180] Y. Mizuguchi, Y. Hara, K. Deguchi, S. Tsuda, T. Yamaguchi, K. Takeda, H. Kotegawa, H. Tou, and Y. Takano. Anion height dependence of T_c for the Fe-based superconductor. *Superconductor Science and Technology*, 23(5):054013, 2010.
- [181] K. Matsuura, Y. Mizukami, Y. Arai, Y. Sugimura, N. Maejima, A. Machida, T. Watanuki, T. Fukuda, T. Yajima, Z. Hiroi, K. Y. Yip, Y. C. Chan, Q. Niu, S. Hosoi, K. Ishida, K. Mukasa, S. Kasahara, J.-G. Cheng, S. K. Goh, Y. Matsuda, Y. Uwatoko, and T. Shibauchi. Maximizing T_c by tuning nematicity and magnetism in $\text{FeSe}_{1-x}\text{S}_x$ superconductors. *Nature Communications*, 8(1):1143–, 2017.
- [182] T. Urata, Y. Tanabe, K. K. Huynh, H. Oguro, K. Watanabe, and K. Tanigaki. Non-Fermi liquid behavior of electrical resistivity close to the nematic critical point in $\text{Fe}_{1-x}\text{Co}_x\text{Se}$ and $\text{FeSe}_{1-y}\text{S}_y$. *ArXiv e-prints*, page 1608.01044, 2016.
- [183] M. Abdel-Hafiez, Y. J. Pu, J. Brisbois, R. Peng, D. L. Feng, D. A. Chareev, A. V. Silhanek, C. Krellner, A. N. Vasiliev, and Xiao-Jia Chen. Impurity scattering effects on the superconducting properties and the tetragonal-to-orthorhombic phase transition in FeSe. *Phys. Rev. B*, 93:224508, Jun 2016.
- [184] M. D. Watson, T. K. Kim, A. A. Haghighirad, S. F. Blake, N. R. Davies, M. Hoesch, T. Wolf, and A. I. Coldea. Suppression of orbital ordering by chemical pressure in $\text{FeSe}_{1-x}\text{S}_x$. *Phys. Rev. B*, 92:121108, Sep 2015.
- [185] A. I. Coldea, S. F. Blake, S. Kasahara, A. A. Haghighirad, M. D. Watson, W. Knafo, E. S. Choi, A. McCollam, P. Reiss, T. Yamashita, M. Bruma, S. Speller, Y. Matsuda, T. Wolf, T. Shibauchi,

- and A. J. Schofield. Evolution of the Fermi surface of the nematic superconductors $\text{FeSe}_{1-x}\text{S}_x$. *ArXiv e-prints*, (Preprint 1611.07424), 2016.
- [186] S. Kasahara, T. Shibauchi, K. Hashimoto, K. Ikada, S. Tonegawa, R. Okazaki, H. Shishido, H. Ikeda, H. Takeya, K. Hirata, T. Terashima, and Y. Matsuda. Evolution from non-Fermi- to Fermi liquid transport via isovalent doping in $\text{BaFe}_2(\text{As}_{1-x}\text{P}_x)_2$ superconductors. *Phys. Rev. B*, 81:184519, 2010.
- [187] Y. Nakai, T. Iye, S. Kitagawa, K. Ishida, H. Ikeda, S. Kasahara, H. Shishido, T. Shibauchi, Y. Matsuda, and T. Terashima. Unconventional superconductivity and antiferromagnetic quantum critical behavior in the isovalent-doped $\text{BaFe}_2(\text{As}_{0.67}\text{P}_{0.33})_2$. *Phys. Rev. Lett.*, 105:107003, 2010.
- [188] Kenichiro Hashimoto, Yuta Mizukami, Ryo Katsumata, Hiroaki Shishido, Minoru Yamashita, Hiroaki Ikeda, Yuji Matsuda, John A. Schlueter, Jonathan D. Fletcher, Antony Carrington, Daniel Gnida, Dariusz Kaczorowski, and Takasada Shibauchi. Anomalous superfluid density in quantum critical superconductors. *Proceedings of the National Academy of Sciences*, 110(9):3293–3297, 2013.
- [189] C. Putzke, P. Walmsley, J. D. Fletcher, L. Malone, D. Vignolles, C. Proust, S. Badoux, P. See, H. E. Beere, D. A. Ritchie, S. Kasahara, Y. Mizukami, T. Shibauchi, Y. Matsuda, and A. Carrington. Anomalous critical fields in quantum critical superconductors. *Nature Communications*, 5:5679, 2014.
- [190] Ian M. Hayes, Ross D. McDonald, Nicholas P. Breznay, Toni Helm, Philip J. W. Moll, Mark Wartenbe, Arkady Shekhter, and James G. Analytis. Scaling between magnetic field and temperature in the high-temperature superconductor $\text{BaFe}_2(\text{As}_{1-x}\text{P}_x)_2$. *Nat Phys*, 12:916–919, 2016.
- [191] T. Hanaguri, K. Iwaya, Y. Kohsaka, T. Machida, T. Watashige, S. Kasahara, T. Shibauchi, and Y. Matsuda. Two distinct superconducting pairing states divided by the nematic end point in $\text{FeSe}_{1-x}\text{S}_x$. *ArXiv e-prints*, (Preprint 1710.02276), 2017.
- [192] Y. Sato, S. Kasahara, T. Taniguchi, X. Z. Xing, Y. Kasahara, Y. Tokiwa, T. Shibauchi, and Y. Matsuda. Highly anisotropic superconducting gap in nematically ordered and tetragonal phases of $\text{FeSe}_{1-x}\text{S}_x$. *ArXiv e-prints*, (Preprint 1705.09074), 2017.
- [193] Christopher K. H. Borg, Xiuquan Zhou, Christopher Eckberg, Daniel J. Campbell, Shanta R. Saha, Johnpierre Paglione, and Efrain E. Rodriguez. Strong anisotropy in nearly ideal tetrahedral superconducting FeS single crystals. *Phys. Rev. B*, 93:094522, Mar 2016.
- [194] U. Pachmayr, N. Fehn, and D. Johrendt. Structural transition and superconductivity in hydrothermally synthesized FeX (X = S, Se). *Chem. Commun.*, 52:194–197, 2016.
- [195] Hai Lin, Yufeng Li, Qiang Deng, Jie Xing, Jianzhong Liu, Xiyu Zhu, Huan Yang, and Hai-Hu Wen. Multiband superconductivity and large anisotropy in FeS crystals. *Phys. Rev. B*, 93:144505, Apr 2016.
- [196] Xiong Yang, Zengyi Du, Guan Du, Qiangqiang Gu, Hai Lin, Delong Fang, Huan Yang, Xiyu Zhu, and Hai-Hu Wen. Strong-coupling superconductivity revealed by scanning tunneling microscope in tetragonal FeS. *Phys. Rev. B*, 94:024521, Jul 2016.
- [197] T. P. Ying, X. F. Lai, X. C. Hong, Y. Xu, L. P. He, J. Zhang, M. X. Wang, Y. J. Yu, F. Q. Huang, and S. Y. Li. Nodal superconductivity in FeS: Evidence from quasiparticle heat transport. *Phys. Rev. B*, 94:100504, Sep 2016.
- [198] Jie Xing, Hai Lin, Yufeng Li, Sheng Li, Xiyu Zhu, Huan Yang, and Hai-Hu Wen. Nodal superconducting gap in tetragonal FeS. *Phys. Rev. B*, 93:104520, Mar 2016.
- [199] S. Hohenstein, U. Pachmayr, Z. Guguchia, S. Kamusella, R. Khasanov, A. Amato, C. Baines, H.-H. Klauss, E. Morenzoni, D. Johrendt, and H. Luetkens. Coexistence of low-moment magnetism and superconductivity in tetragonal FeS and suppression of T_c under pressure. *Phys. Rev. B*, 93:140506, Apr 2016.
- [200] Haoran Man, Jiangan Guo, Rui Zhang, Rico Schönemann, Zhiping Yin, Mingxuan Fu, Matthew B. Stone, Qingzhen Huang, Yu Song, Weiyi Wang, David J. Singh, Felix Lochner,

- Tilman Hickel, Ilya Eremin, Leland Harriger, Jeffrey W. Lynn, Collin Broholm, Luis Balicas, Qimiao Si, and Pengcheng Dai. Spin excitations and the Fermi surface of superconducting FeS. *npj Quantum Materials*, 2(1):14–, 2017.
- [201] Li Xiang, Udhara S. Kaluarachchi, Anna E. Böhmer, Valentin Taufour, Makariy A. Tanatar, Ruslan Prozorov, Sergey L. Bud’ko, and Paul C. Canfield. Dome of magnetic order inside the nematic phase of sulfur-substituted FeSe under pressure. *Phys. Rev. B*, 96:024511, Jul 2017.
- [202] Udhara S. Kaluarachchi, Valentin Taufour, Anna E. Böhmer, Makariy A. Tanatar, Sergey L. Bud’ko, Vladimir G. Kogan, Ruslan Prozorov, and Paul C. Canfield. Nonmonotonic pressure evolution of the upper critical field in superconducting FeSe. *Phys. Rev. B*, 93:064503, Feb 2016.
- [203] Ji-Hoon Kang, Soon-Gil Jung, Sangyun Lee, Eunsung Park, Jiunn-Yuan Lin, Dmitriy A Chareev, Alexander N. Vasiliev, and Tuson Park. Pressure dependence of upper critical fields in FeSe single crystals. *Superconductor Science and Technology*, 29(3):035007, 2016.
- [204] Rui-Qi Xing, Laura Classen, Maxim Khodas, and Andrey V. Chubukov. Competing instabilities, orbital ordering, and splitting of band degeneracies from a parquet renormalization group analysis of a four-pocket model for iron-based superconductors: Application to FeSe. *Phys. Rev. B*, 95:085108, Feb 2017.
- [205] Andrey V. Chubukov, M. Khodas, and Rafael M. Fernandes. Magnetism, superconductivity, and spontaneous orbital order in iron-based superconductors: Which comes first and why? *Phys. Rev. X*, 6:041045, Dec 2016.
- [206] Helmut Eschrig and Klaus Koepernik. Tight-binding models for the iron-based superconductors. *Phys. Rev. B*, 80:104503, Sep 2009.
- [207] Takashi Miyake, Kazuma Nakamura, Ryotaro Arita, and Masatoshi Imada. Comparison of ab initio low-energy models for LaFePO, LaFeAsO, BaFe₂As₂, LiFeAs, FeSe, and FeTe: Electron correlation and covalency. *Journal of the Physical Society of Japan*, 79(4):044705, 2010.
- [208] Alaska Subedi, Lijun Zhang, D. J. Singh, and M. H. Du. Density functional study of FeS, FeSe, and FeTe: Electronic structure, magnetism, phonons, and superconductivity. *Phys. Rev. B*, 78:134514, Oct 2008.
- [209] J. Maletz, V. B. Zabolotnyy, D. V. Evtushinsky, S. Thirupathaiyah, A. U. B. Wolter, L. Harnagea, A. N. Yaresko, A. N. Vasiliev, D. A. Chareev, A. E. Böhmer, F. Hardy, T. Wolf, C. Meingast, E. D. L. Rienks, B. Büchner, and S. V. Borisenko. Unusual band renormalization in the simplest iron-based superconductor FeSe_{1-x}. *Phys. Rev. B*, 89:220506, Jun 2014.
- [210] Markus Aichhorn, Silke Biermann, Takashi Miyake, Antoine Georges, and Masatoshi Imada. Theoretical evidence for strong correlations and incoherent metallic state in FeSe. *Phys. Rev. B*, 82:064504, Aug 2010.
- [211] Z. P. Yin, K. Haule, and G. Kotliar. Kinetic frustration and the nature of the magnetic and paramagnetic states in iron pnictides and iron chalcogenides. *Nat. Mater.*, 10(12):932, Dec 2011.
- [212] Daniel Guterding, Steffen Backes, Milan Tomić, Harald O. Jeschke, and Roser Valentí. Ab initio perspective on structural and electronic properties of iron-based superconductors. *physica status solidi (b)*, 254(1):1600164–n/a, 2017. 1600164.
- [213] Kristjan Haule and Gheorghe L. Pascut. Forces for structural optimizations in correlated materials within a DFT+embedded DMFT functional approach. *Phys. Rev. B*, 94:195146, Nov 2016.
- [214] D. V. Evtushinsky, M. Aichhorn, Y. Sassa, Z.-H. Liu, J. Maletz, T. Wolf, A. N. Yaresko, S. Biermann, S. V. Borisenko, and B. Büchner. Direct observation of dispersive lower Hubbard band in iron-based superconductor FeSe. *ArXiv e-prints*, (Preprint 1612.02313), December 2016.
- [215] Matthew D. Watson, Steffen Backes, Amir A. Haghighirad, Moritz Hoesch, Timur K. Kim, Amalia I. Coldea, and Roser Valentí. Formation of Hubbard-like bands as a fingerprint of strong electron-electron interactions in FeSe. *Phys. Rev. B*, 95:081106, Feb 2017.

- [216] Z. P. Yin, K. Haule, and G. Kotliar. Spin dynamics and orbital-antiphase pairing symmetry in iron-based superconductors. *Nat. Phys.*, 10(11):845, Nov 2014.
- [217] Youichi Yamakawa, Seiichiro Onari, and Hiroshi Kontani. Nematicity and magnetism in FeSe and other families of Fe-based superconductors. *Phys. Rev. X*, 6:021032, Jun 2016.
- [218] Zhentao Wang, Wen-Jun Hu, and Andriy H. Nevidomskyy. Spin ferroquadrupolar order in the nematic phase of FeSe. *Phys. Rev. Lett.*, 116:247203, Jun 2016.
- [219] Rong Yu and Qimiao Si. Antiferroquadrupolar and Ising-nematic orders of a frustrated bilinear-biquadratic Heisenberg model and implications for the magnetism of FeSe. *Phys. Rev. Lett.*, 115:116401, Sep 2015.
- [220] Seiichiro Onari and Hiroshi Kontani. In-plane anisotropy of transport coefficients in electronic nematic states: Universal origin of nematicity in Fe-based superconductors. *Phys. Rev. B*, 96:094527, Sep 2017.
- [221] Daniel D. Scherer, A. C. Jacko, Christoph Friedrich, Ersoy Şaşıoğlu, Stefan Blügel, Roser Valentí, and Brian M. Andersen. Interplay of nematic and magnetic orders in FeSe under pressure. *Phys. Rev. B*, 95:094504, Mar 2017.
- [222] Kai Liu, Zhong-Yi Lu, and Tao Xiang. Nematic antiferromagnetic states in bulk FeSe. *Phys. Rev. B*, 93:205154, May 2016.
- [223] Brian Busemeyer, Mario Dagrada, Sandro Sorella, Michele Casula, and Lucas K. Wagner. Competing collinear magnetic structures in superconducting FeSe by first-principles quantum Monte Carlo calculations. *Phys. Rev. B*, 94:035108, Jul 2016.
- [224] Wei Li, Yan Zhang, Peng Deng, Zhilin Xu, S.-K. Mo, Ming Yi, Hao Ding, M. Hashimoto, R. G. Moore, D.-H. Lu, Xi Chen, Z.-X. Shen, and Qi-Kun Xue. Stripes developed at the strong limit of nematicity in FeSe film. *Nat Phys*, advance online publication, Jul 2017. Letter.
- [225] A. Kreisel, Shantanu Mukherjee, P. J. Hirschfeld, and Brian M. Andersen. Spin excitations in a model of FeSe with orbital ordering. *Phys. Rev. B*, 92:224515, Dec 2015.
- [226] Shantanu Mukherjee, A. Kreisel, P. J. Hirschfeld, and Brian M. Andersen. Model of electronic structure and superconductivity in orbitally ordered FeSe. *Phys. Rev. Lett.*, 115:026402, Jul 2015.
- [227] S. L. Skornyakov, V. I. Anisimov, D. Vollhardt, and I. Leonov. Effect of electron correlations on the electronic structure and phase stability of FeSe upon lattice expansion. *Phys. Rev. B*, 96:035137, Jul 2017.
- [228] Shou-Shu Gong, W. Zhu, D. N. Sheng, and Kun Yang. Possible nematic spin liquid in spin-1 antiferromagnetic system on the square lattice: Implications for the nematic paramagnetic state of FeSe. *Phys. Rev. B*, 95:205132, May 2017.
- [229] W.-J. Hu, H.-H. Lai, S.-S. Gong, R. Yu, A. H. Nevidomskyy, and Q. Si. Frustrated magnetism and quantum transitions of nematic phases in FeSe. *ArXiv e-prints*, (Preprint 1606.01235), June 2016.
- [230] X. Wu, Y. Liang, H. Fan, and J. Hu. Nematic orders and nematicity-driven topological phase transition in FeSe. *ArXiv e-prints*, (Preprint 1603.02055), March 2016.
- [231] Andrey V. Chubukov, Rafael M. Fernandes, and Joerg Schmalian. Origin of nematic order in FeSe. *Phys. Rev. B*, 91:201105, May 2015.
- [232] Carsten Honerkamp. Nematic and superconducting order in a three-band model for the iron superconductors. *physica status solidi (b)*, 254(1):1600151–n/a, 2017. 1600151.
- [233] Laura Classen, Rui-Qi Xing, Maxim Khodas, and Andrey V. Chubukov. Interplay between magnetism, superconductivity, and orbital order in 5-pocket model for iron-based superconductors: Parquet renormalization group study. *Phys. Rev. Lett.*, 118:037001, Jan 2017.
- [234] L. Fanfarillo, L. Benfatto, and B. Valenzuela. Orbital mismatch boosting nematic instability in iron-based superconductors. *ArXiv e-prints*, (Preprint 1706.08953), June 2017.
- [235] Seiichiro Onari, Youichi Yamakawa, and Hiroshi Kontani. Sign-reversing orbital polarization in the nematic phase of FeSe due to the C_2 symmetry breaking in the self-energy. *Phys. Rev.*

- Lett.*, 116:227001, Jun 2016.
- [236] Liang Yi, Wu Xian-Xin, and Hu Jiang-Ping. Electronic structure properties in the nematic phases of FeSe. *Chin. Phys. Lett.*, 32(11):117402, 2015.
- [237] Seiichiro Onari, Youichi Yamakawa, and Hiroshi Kontani. Sign-reversing orbital polarization in the nematic phase of fese due to the C_2 symmetry breaking in the self-energy. *Phys. Rev. Lett.*, 116:227001, Jun 2016.
- [238] Kun Jiang, Jiangping Hu, Hong Ding, and Ziqiang Wang. Interatomic Coulomb interaction and electron nematic bond order in FeSe. *Phys. Rev. B*, 93:115138, Mar 2016.
- [239] Andreas Kreisell, Brian M. Andersen, P. O. Sprau, A. Kostin, J. C. Séamus Davis, and P. J. Hirschfeld. Orbital selective pairing and gap structures of iron-based superconductors. *Phys. Rev. B*, 95:174504, May 2017.
- [240] J.-H. She, M. J. Lawler, and E.-A. Kim. Mechanism for nematic superconductivity in FeSe. *ArXiv e-prints*, (Preprint 1701.07813), January 2017.
- [241] Jian Kang and Rafael M. Fernandes. Superconductivity in FeSe thin films driven by the interplay between nematic fluctuations and spin-orbit coupling. *Phys. Rev. Lett.*, 117:217003, Nov 2016.
- [242] Can-Li Song, Hui-Min Zhang, Yong Zhong, Xiao-Peng Hu, Shuai-Hua Ji, Lili Wang, Ke He, Xu-Cun Ma, and Qi-Kun Xue. Observation of double-dome superconductivity in potassium-doped FeSe thin films. *Phys. Rev. Lett.*, 116:157001, Apr 2016.
- [243] L. de Medici. *Weak and Strong Correlations in Fe Superconductors in Iron-Based Superconductivity* Peter D. Johnson, Guangyong Xu, and Wei-Guo Yin (Editors). Springer Series in Materials Science. Springer, 2015.
- [244] Elena Bascones, Belén Valenzuela, and Maria José Calderón. Magnetic interactions in iron superconductors: A review. *C. R. Phys.*, 17(1-2):36, 2016. Iron-based superconductors / Supraconducteurs à base de fer.
- [245] Ambroise van Roekeghem, Pierre Richard, Hong Ding, and Silke Biermann. Spectral properties of transition metal pnictides and chalcogenides: Angle-resolved photoemission spectroscopy and dynamical mean-field theory. *C. R. Phys.*, 17(1-2):140, 2016. Iron-based superconductors / Supraconducteurs à base de fer.
- [246] Yu Li, Zhiping Yin, Xiancheng Wang, David W. Tam, D. L. Abernathy, A. Podlesnyak, Chenglin Zhang, Meng Wang, Lingyi Xing, Changqing Jin, Kristjan Haule, Gabriel Kotliar, Thomas A. Maier, and Pengcheng Dai. Orbital selective spin excitations and their impact on superconductivity of $\text{LiFe}_{1-x}\text{Co}_x\text{As}$. *Phys. Rev. Lett.*, 116:247001, Jun 2016.
- [247] Subhasish Mandal, Peng Zhang, Sohrab Ismail-Beigi, and K. Haule. How correlated is the FeSe/SrTiO₃ system? *Phys. Rev. Lett.*, 119:067004, Aug 2017.
- [248] Z. R. Ye, Y. Zhang, F. Chen, M. Xu, J. Jiang, X. H. Niu, C. H. P. Wen, L. Y. Xing, X. C. Wang, C. Q. Jin, B. P. Xie, and D. L. Feng. Extraordinary doping effects on quasiparticle scattering and bandwidth in iron-based superconductors. *Phys. Rev. X*, 4:031041, Sep 2014.
- [249] Naoya Arakawa and Masao Ogata. Orbital-selective superconductivity and the effect of lattice distortion in iron-based superconductors. *J. Phys. Soc. Jpn.*, 80(7):074704, 2011.
- [250] Rong Yu, Jian-Xin Zhu, and Qimiao Si. Orbital-selective superconductivity, gap anisotropy, and spin resonance excitations in a multiorbital t - J_1 - J_2 model for iron pnictides. *Phys. Rev. B*, 89:024509, Jan 2014.